# Kent Academic Repository

# Performance Evaluation of In-Building DAS for High Data Rate Wireless Transmission

by

## Temitope Toba Alade

A thesis submitted in fulfillment of the requirements for the degree of
Doctor of Philosophy in Electronic Engineering,
The University of Kent, 2012.

UE 7

# Supervisor

Professor Jiangzhou Wang

# Abstract

In wireless systems, providing high data rate services is a major challenge, particularly for mobile terminals (MTs) in multi-floor buildings. The system performance is impaired by path loss, and co-channel interference due to the need to reuse the limited available spectrum. One way to achieve high data rates and better signal quality in this environment is by getting the transmitter and the receiver closer to each other through the use of distributed antenna systems (DASs). DAS reduces the overall transmit power (and hence co-channel interference) and achieves better link reliability by exploiting spatial diversity of multiple antennas. Currently, DASs are designed primarily to provide good coverage in outdoor environments. However, high quality indoor reception and high data rates may not be guaranteed if the system is not deployed within the building. Indoor environments can be very complex, and an insight into the design, and a thorough understanding of the performance of DASs inside the building is required.

In this thesis, the performance of an in-building DAS employing frequency reuse is examined, where remote antenna units (RAUs) are deployed on each floor throughout the building and connected to a central unit (CU) where received signals are processed. The impact of co-channel interference on system performance is investigated by using a propagation channel model derived from multi-floor in-building path loss values retrieved from measurement results.

System performance is investigated in terms of location-specific spectral efficiency and bit error rate (BER) which are analysed for a range of potential MT locations and various in-building propagation characteristics. The potential benefits of location based antenna selection and deployment options are also investigated. Co-channel interference cancellation where CUs cooperate through joint signal processing in order to reduce the impact of co-channel interference is considered. Results obtained suggest that the proposed scheme can facilitate better use of the available radio spectrum, and provide high data rates for indoor MTs.

iii

# Dedication

To my parents, Olu and Dupe Alade, for your unparalleled love and support.

# Acknowledgments

First and foremost I would like to express my sincere gratitude to my supervisor, Professor Jiangzhou Wang, for his insightful contributions and discussions during the course of this PhD studies. His valuable feedback and enthusiasm for research made the journey very challenging and successful.

I would also like to acknowledge:

- Doctor Huiling for her immeasurable guidance in all aspects of this journey. Thank you for sharing many inspiring insights and ideas that contributed to the success of this research.

- Hassan for his valuable comments and contributions. His advice, constructive criticism and endless jokes assisted this work in various ways. I am very grateful.

- Blessing Ojede for her unfailing love and support over the years. Thanks for being there for me always. I love and cherish you.

- Mimi for all her never ceasing support and encouragement throughout this journey. No words can ever express how grateful I am for your unconditional love. Thanks for always believing in me.

- Members of the broadband and wireless communications research group, especially Nikos, L. Wu and Tunde who have provided assistance. I will always remember the times we spent in the lab.

Finally, I would like to thank my dad and mum, Busola and Bunmi for their unconditional love and support throughout the course. I will always be in your debt.

Temitope Alade

December 2011

# List of publications

1. T. Alade, H.Zhu, H. Osman, "Performance Evaluation of DAS for Inter-floor Wireless Communications," *to appear in Proc. IEEE ICC. Canada.*, 2012.

2. T. Alade, H.Zhu, H. Osman, "Performance Evaluation of In-Building DAS for High Data Rate Wireless Transmission," *to appear in Proc. IEEE WCNC. Paris - France.*, 2012.

3. T. Alade, H.Zhu, H. Osman, "In-Building DAS for High Data Rate Indoor Mobile Communication," *to appear in Proc. IEEE Veh. Technol. Conf.* (VTC '12 (Spring, Yokohama, Japan))., 2012.

4. T. Alade, H.Zhu, H. Osman, J.Wang, "Performance Evaluation of In-Building DAS for High Data Rate Wireless Transmission," *Submitted, IEEE, Trans. Wireless Commun.*, 2011.

5. T. Alade, H.Zhu, H. Osman, "Spectral Efficiency Analysis of Distributed Antenna System for In-Building Mobile Communication," *in Proc. IEEE, Globecom Commun. Conf., Houston Texas*, 2011.

6. T. Alade, H.Zhu, H. Osman, "Performance Analysis of Distributed Antenna System for High Building Wireless Communication," *in Proc. IEEE Veh. Technol. Conf.* (VTC '11 (Spring)), pp. 1-5, May 2011.

7. H. Osman, H. Zhu, T. Alade, D. Toumpakaris and J. Wang, "Capacity Evaluation of In-Building Distributed Antenna Systems," submitted to *IEEE Trans. Commun.*

8. T. Alade, H.Zhu, H. Osman, "Spectral Efficiency Analysis of Distributed Antenna System for In-Building Wireless Communication," *in Proc. IEEE Veh. Technol. Conf.* (VTC '11 (Fall) San Francisco, pp. 1-5, Sept. 2011.

9. T. Alade, H.Zhu, H. Osman, "Perfromance Evaluation of Distributed Antenna System for High Data Rate Wireless Communication," *in Proc. IEEE PIMRC Conf.* Toronto, Canada, pp. 1-5, Sept. 2011.

10. H. Osman, H. Zhu, T. Alade and D. Toumpakaris, "Capacity of Distributed Antenna Systems in Multi-Floor Buildings," Workshop *Golbecom Houston*, 2011.

11. H. Osman, H. Zhu and T. Alade, "Wireless Distributed Antenna Systems in High Buildings," *in Proc. IEEE Veh. Technol. Conf.* (VTC '11 (Fall) San Francisco, pp. 1-5, Sept. 2011.

12. H. Osman, H. Zhu and T. Alade, "Distributed Antenna Systems With Frequency Reuse," *in Proc. IEEE PIMRC Conf.* Toronto, Canada, pp. 1-5, Sept. 2011.

13. H. Osman, H. Zhu, T. Alade and J. Wang, "Downlink Transmission of Distributed Antenna Systems in High Building Environments," *in Proc. IEEE ICC Kyoto*, pp. 1-5, 2011.

14. H. Osman, H. Zhu and T. Alade, "Deployment of Distributed Antenna Systems in High Buildings," *in Proc. IEEE Veh. Technol. Conf.* (VTC '11 (Spring)), pp. 1-5, May 2011.

15. T. Alade, H.Zhu, J.Wang, "Uplink Co-Channel Interference Analysis and Cancellation in Femtocell Based Distributed Antenna System," *in Proc. IEEE ICC. Capetown* pp. 1-5, 2010.

16. T. Alade, H.Zhu, J.Wang, "Joint Signal Processing in Femtocell Based Distributed Antenna Systems in High Buildings ," *in Proc. IEEE Veh. Technol. Conf., Ottawa* (VTC '11 (Fall)), pp. 1-5, Sept. 2010.

# Contents

1

2

# List of Figures

4

# List of Tables

# List of Abbreviations and Acronyms

| | |
|---|---|
| 1G | First Generation |
| 2G | Second Generation |
| 3G | Third Generation |
| 4G | Fourth Generation |
| 2D | Two-dimensional |
| 3D | Three-dimensional |
| AWGN | Additive White Gaussian Noise |
| BER | Bit Error Rate |
| BS | Base Station |
| BPSK | Binary Phase Shift Keying |
| CLT | Central Limit Theorem |
| CU | Central Unit |
| DAS | Distributed Antenna System |
| DS-CDMA | Direct Sequence Code Division Multiple Access |
| FAF | Floor Attenuation Factor |
| FDTD | Finite-Difference Time-Domain |
| FFR | Fractional Frequency Reuse |
| GSM | Global System for Mobile Communication |
| GTD | Geometrical Theory of Diffraction |
| ISI | Intersymbol Interference |
| ISM | Industrial, Scientific and Medical |
| ITU | International Telecommunication Union |
| LOS | Line Of Sight |
| LTE | Long Term Evolution |
| MCN | Multi-hop Cellular Networks |

MGF       Moment Generating Function

MQAM      Multi-level Quadrature Amplitude Modulation

MRC       Maximum Ratio Combining

MIMO      Multiple Input Multiple Output

MMSEC     Minimum Mean Square Error Combining

MSE       Mean Square Error

MT        Mobile Terminal

NLOS      Non Line Of Sight

OFDM      Orthogonal Frequency Division Multiplexing

PDF       Probability Density Function

RAU       Remote Antenna Unit

RF        Radio Frequency

RRM       Radio Resource Management

RS        Relay Station

RV        Random Variable

SINR      Signal to Interference plus Noise Ratio

SIR       Signal to Interference Ratio

SNR       Signal to Noise Ratio

WAF       Wall Attenuation Factor

WIMAX     Worldwide Interoperability for Microwave Access

WiFi      Wireless Fidelity

WLAN      Wireless Local Area Networks

# List of symbols

$b_u[(i)]$     Transmitted symbol

$\hat{b}_u(t)$     Estimate of the desired transmitted symbol

$d$     Distance between transmitter and receiver

$d_o$     Reference distance

$\hat{d}_1$     Distance between MT and the window

$\hat{d}_2$     Distance between the reference building and the adjacent building

$\hat{d}_3$     Length of the reflected path from the adjacent building

$\hat{d}_4$     Distance between the RAU and the window

$\bar{d}_1$     Diffracted distance between MT and the window

$\bar{d}_2$     Distance between co-channel window and reference floor's window

$\hat{d}_3$     Distance between the RAU on the reference floor and the window

$d_{u,n}$     Distance between transmitter and receiver through direct path

$\hat{d}_{u,n}$     Distance between transmitter and receiver through reflected path

$\bar{d}_{u,n}$     Distance between transmitter and receiver through diffracted path

$D^2(\alpha_i)$     Diffraction coefficient

$|E|^2$     Electric field strength of the direct path

$\left|\hat{E}\right|^2$     Electric field strength of the diffracted path

$E_s$     Total symbol energy

$E\{x\}$     Expected value of $x$

$f_c$     Frequency carrier

$F$     Inter-floor spacing

$h_{u,n}(t)$     Impulse response of the channel

$h'_{u,n}(t)$     Impulse response of the direct path

$\hat{h}_{u,n}(t)$     Impulse response of the reflected path

$\bar{h}_{u,n}(t)$     Impulse response of the diffracted path

| | |
|---|---|
| $I$ | Co-channel interference signal |
| $I_{u,n}$ | Co-channel interference received by the $n$th RAU |
| $I_u$ | Total co-channel interference |
| $j$ | Number of bits per symbol |
| $k$ | Number of intervening floors |
| $m$ | Nakagami fading value |
| $m_n$ | Nakagami fading value of the $n$th RAU |
| $M_{\gamma(x_u,y_u)}$ | MGF for the SINR |
| $M_j$ | Modulation order |
| $n$ | Number of walls |
| $N$ | Number of RAUs |
| $N'$ | Strongest RAUs |
| $N_0/2$ | Noise power spectral density |
| $N_F$ | Number of floors between transmitter and receiver |
| $p$ | Number of soft partitions |
| $p_{\bar{\alpha}}$ | PDF of lognormal distributed $\bar{\alpha}$ |
| $p_\alpha(\alpha)$ | PDF of $\alpha$ |
| $P_{\gamma(x_u,y_u)}(\gamma)$ | PDF of SINR |
| $P_e(\gamma)$ | Conditional BER |
| $\bar{P}_e(\rho_1,\rho_2)$ | Conditional BER for a given position |
| $P_e$ | Radiated power |
| $\hat{P}_e(x_u,y_u)$ | Average BER |
| $\hat{P}_e(u)$ | BER before interference cancellation |
| $PL(d_o)$ | Path loss measured at a specified distance $d_o$ |
| $PL(dB)$ | Path loss in dB |
| $\hat{P}_0$ | Target BER |

| | |
|---|---|
| $P_s$ | Transmit power |
| $q$ | Number of concrete walls |
| $Q(x)$ | Gaussian Q function |
| $r_{u,n}(t)$ | Uplink received signal |
| $\bar{r}_{u,n}(t)$ | Uplink received signal before interference cancellation |
| $Re[x]$ | Real part of $x$ |
| $S$ | Desired received signal |
| $S_n$ | Desired received signal received by the $n$th RAU |
| $T_s$ | Symbol duration |
| $T_u(x_u, y_u)$ | Average spectral efficiency |
| $u'$ | Desired user |
| $u$ | Co-channel user |
| $U$ | Number of CUs in the building |
| $v$ | Distance between a MT and the floor |
| $\text{WAF}_{\text{concrete}}$ | Concrete wall attenuation factor |
| $\text{WAF}_{\text{soft}}$ | Soft partitions attenuation factor |
| $W_n$ | Optimum weight |
| $\hat{x}_u(t)$ | Transmitted signal |
| $x_u(t)$ | Complex representation of the transmitted signal |
| $x_n$ | x coordinate of the $\text{RAU}_{u,n}$ |
| $x_u$ | x coordinate of the $\text{MT}_{u,n}$ |
| $(x, y)$ | Floor dimension |
| $y_n$ | y coordinate of the $\text{RAU}_{u,n}$ |
| $y_u$ | y coordinate of the $\text{MT}_{u,n}$ |
| $Y$ | Demodulated signal |
| $Y_n$ | Demodulated signal before interference cancellation |

| | |
|---|---|
| $\hat{Y}_n$ | Received signal after interference cancellation |
| $Z_o$ | Free space impedance |
| $Z_0$ | Desired signal decision variable |
| $Z_n$ | Demodulated signal |
| $\alpha$ | Amplitude of the channel fading |
| $\alpha_i$ | Wave bending angle |
| $\bar{\alpha}$ | Mean of the fast fading voltage |
| $\delta(t)$ | Dirac delta function |
| $\Delta_{I_u}$ | Residual interference |
| $\Gamma(\cdot)$ | Gamma function |
| $\Omega$ | Average fading power of the received signal |
| $\Omega_n$ | Average fading power of the received signal from $RAU_n$ |
| $\rho_{T_s}(t)$ | Pulse waveform |
| $\vartheta$ | Phase of the channel fading |
| $\lambda$ | Path loss exponent |
| $\lambda_w$ | Wave length |
| $\eta_n(t)$ | AWGN |
| $\phi$ | Angle of a diffracted path |
| $\rho_n$ | Variance of the interfering signal plus background noise |
| $\sigma^2_{I_u}$ | Variance of the co-channel interference |
| $\sigma^2_\eta$ | Variance of the noise |
| $\tau$ | Time delay |
| $\sigma$ | Standard deviation |
| $\sigma^2$ | Mean power |
| $\sigma^2_{\Delta_{I_u}}(u)$ | Variance of residual interference |

| | |
|---|---|
| $\gamma_j$ | Adaptive modulator switching threshold |
| $\gamma$ | SINR before interference cancellation |
| $\gamma(x_u, y_u)$ | SINR |
| $\gamma_n(x_u, y_u)$ | SINR per RAU |
| $\bar{\gamma}(x_u, y_u)$ | Average SINR |
| $\varphi_{u,n}$ | Penetration loss through a single floor |
| $\hat{\varphi}_{u,n}$ | Reflection loss |
| $\ddot{\varphi}_{u,n}$ | Transmission loss through the glass windows |

# Chapter 1

# Introduction

## Contents

## 1.1 Trends in Wireless Communication Systems

The wireless communication industry is currently experiencing a period of tremendous growth with no foreseeable decline in the near future. As of the end of 2005, there were approximately 2 billion wireless subscribers worldwide, and this number is expected to increase to approximately 7.2 billion by the end of 2015 [1]. This has led to explosive increases in data usage, and the demand for high data rate services due to the advent of smart phones, ipads and various handheld units. Cisco(2010), reported in its Visual Networking Index [2] that, there was approximately 0.09 exabytes of data traffic on the world's mobile networks each month. By the end of this year, the figure will have more than doubled to 0.2 exabytes. When

you consider that one exabyte is the equivalent of one billion gigabytes, the short term implications for the network are immediately apparent. This is a huge challenge for the industry and it is clear that new wireless technologies are needed sooner rather than later, especially as the trend for data consumption is set to rocket to 3.6 exabytes by 2015 [2].

New wireless technologies have appeared approximately every 10th year (as illustrated in Figure 1.1) since the first generation (1G) of wireless mobile communication systems (based on analog technology) were introduced in the 1980s [3, pp. 563-567]. In the 1990s, the second generation (2G) digital mobile systems with improved spectral efficiency and voice quality were rolled out [4, pp. 12-13]. The third generation (3G) mobile service networks were developed in the early 2000s to satisfy the requirements of data transmission and quality for multimedia services [5, pp. 23-29]. More recently in 2010, possible candidates of fourth generation (4G) mobile service networks (developed from current pre-4G networks) such as the Long Term Evolution (LTE) and Worldwide Interoperability for Microwave Access (WiMAX)
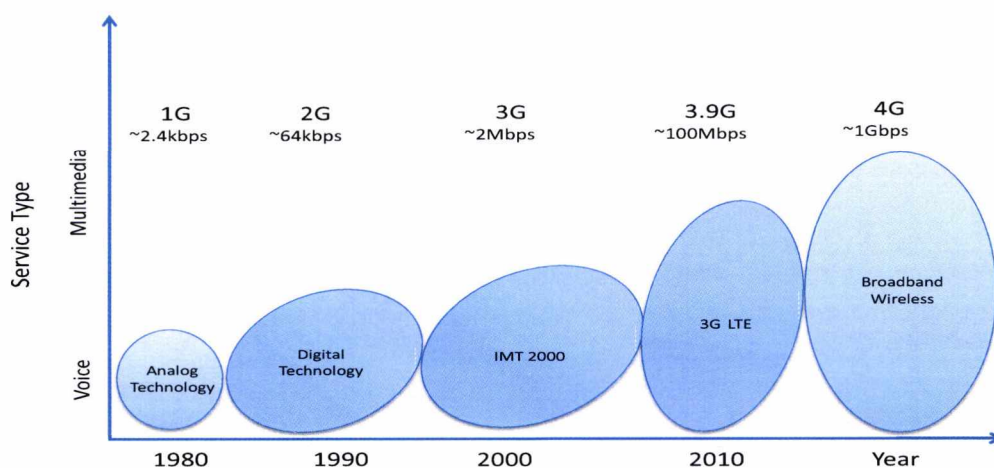


Figure 1.1: Mobile network evolution.

have been deployed in many countries to further improve the transmission speed and provide mobile broadband connectivity across cities [5, pp. 229-252]. The LTE-Advanced is a further evolution of the LTE, offering vastly higher capacity and more spectral efficiency gains. The LTE-Advanced will address the market needs of the next decade, with data rate of up to 1Gbps. It is expected that the technology will first be commercially available in 2012, with wider deployments by 2015 [6, 7].

The advancements in wireless systems have been enhanced by the proliferation of wireless computer networks operating in unlicensed portions of the spectrum. Wireless Local Area Networks (WLAN) are often deployed to provide wireless connectivity to existing networks or the internet to mobile users within buildings [5, pp. 30-40]. The current generation of WLANs are based on the IEEE 802.11 family of standards, and were originally introduced in the 1990s. Successive improvements such as the IEEE 802.11b (CDMA, 2.45 GHz), 802.11a (OFDM, 5.8 GHz), 802.11g (OFDM, 2.45 GHz) and 802.11n (OFDM/MIMO, 2.45 GHz) have seen a promising increase in performance. The marketing of Wi-Fi (wireless fidelity) has also been crucial in the success of these WLAN systems for ensuring interoperability of WLAN equipment from different vendors. The Wi-Fi standard is currently experiencing a major growth, although in contrast to contemporary wired networks, the maximum achievable data rates are still relatively low [5, pp. 30-35]. The presence of walls and floor inside buildings also limits the achievable rate. Thus, the consideration of mobile data offload through Wi-Fi networks as a solution to the unprecedented increase in mobile data traffic, cannot guarantee high data rate transmission. Furthermore, systems operating in the unlicensed frequency bands are prone to co-channel interference from other systems operating in close proximity. Such interference may not only degrade the system performance causing packet losses and throughput reductions, but may also compromise the system's security and privacy [5, pp. 30-35]. Therefore, it is essential to develop techniques that allow systems to operate well in the presence of interference.

16

## 1.2 Motivation and Challenges

Although new wireless technologies will continue to emerge to fulfill the demand for high data rate services, the radio systems engineer is faced with a number of challenges when designing wireless systems. Amongst these is the provision of high data rate wireless service to an unlimited number of users (thus requiring more frequency spectrum), but allocated frequency spectrum is limited. It is expected that the unlicensed and the licensed bands will soon be overcrowded due to the increasing number of users, especially in high user-density areas (such as urban/metropolitan areas and within buildings) [8]. Optimal allocation of frequency channels particularly in these environments remain a challenge for modern cellular systems. In order to increase the efficiency of spectrum utilisation, frequency reuse is indispensable; however, interference between users competing for spectrum will become the limiting factor to performance. Thus, wireless systems often encounter conflicting requirements between either providing reliable communication or obtaining higher spatial reuse of spectrum. Therefore, the design of the wireless systems that supports high data rates for limited bandwidth requires spectrally efficient schemes especially for indoor communication systems [9].

In addition to the above limiting factor, transmission power is limited. In conventional macrocellular systems (providing a wide area coverage for rural, suburban and urban environments typically of the order of a kilometer or more), providing reliable wireless performance - for example, a guaranteed minimum data rate for a given transmit power is difficult because of path losses, the random wireless channel fluctuations (known as fading), and most seriously, co-channel interference from neighboring base-station (BS) transmissions. To achieve peak data rate of up to 1Gbps (as expected of 4G systems), greater power level is required if the same communication distance between the BS and the mobile terminal (MT) in conventional macrocellular systems is maintained. On the other hand, if the transmission power

is kept the same as in the conventional macrocellular systems, the communication range will significantly shrink. Consequently, gigabit wireless services may only be available near the BS [10].

In many countries, 60-80% of users are indoors. A study by Japan's NTT DoCoMo found that more than 70% of mobile traffic in a 3G system, originates from or terminates inside buildings [11]. Mobile data is mostly consumed from inside buildings; however, delivering high data rate wireless services inside buildings is a tough challenge for the macro network, particularly in high-rise residential and office buildings, factories, airports, shopping malls, and other indoor environments with high concentrations of mobile users. Many 3G networks deployed to date have been designed primarily to provide good coverage in outdoor environments not inside buildings. Only serving macro BS within a few hundred meters of a building can
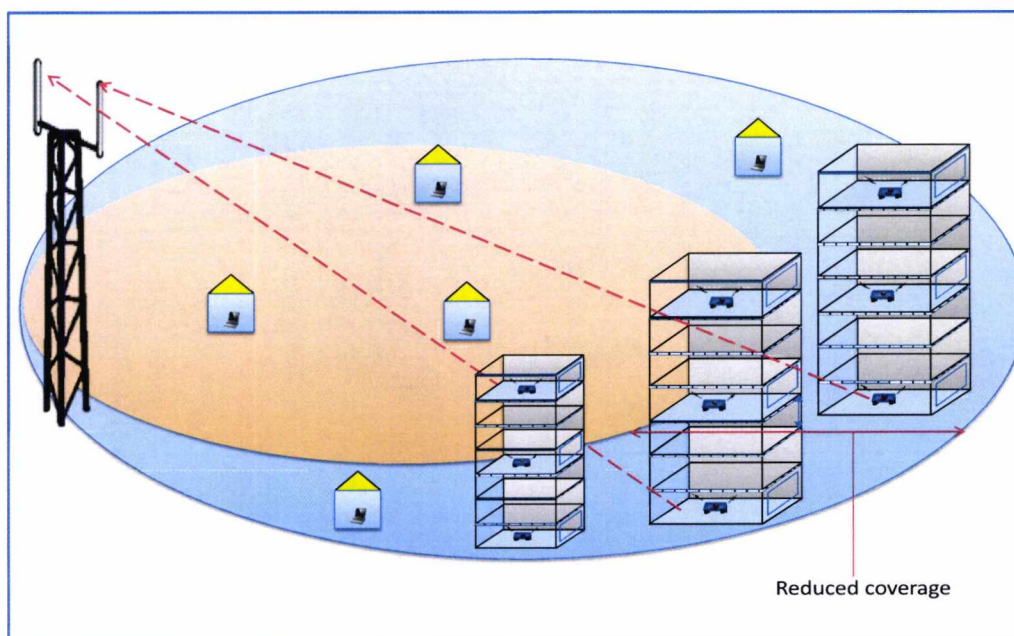


Figure 1.2: Reduced coverage due to long radio propagation distance.

18

provide sufficient level of radio frequency (RF) signal to support indoor voice/data services. In reality, only a few buildings will fall into this category. The coverage problem is essentially due to the long radio propagation distance between the BS and the indoor MTs (Figure 1.2), and the electromagnetic shielding of wireless signals from the outdoor macrocell network, by the floors and walls inside the building, resulting in lower bit rates for data services, lower capacity and, in some instances, complete loss of signal [12]. Achieving adequate coverage and reliable system performance within buildings is therefore very crucial.

A promising approach to resolve the above technical issues is by getting the transmitter and receiver closer to each other. This technique creates the benefits of higher-quality links, lower transmission power (hence lower co-channel interference), and more spatial reuse. There are existing technologies capable of reducing the radio transmission distance between the transmitter and the receiver. Amongst these are relays, microcells and distributed antenna systems.

**Relays.** Relays are operator deployed infrastructure points which route the data between the source and destination via multiple hops and routes, thereby enhancing the overall end-to-end performance. An illustration of a multi-hop relay system is depicted in Figure 1.3. The use of relaying techniques is currently the focus of intense research in the area of cooperative communications [13, 14] as well as in upcoming deployments of multi-hop cellular networks (MCN) - for example, the IEEE 802.16j, the multi-hop relay specification for the IEEE 802.16e (WiMAX) wireless standard. Relays are used to fill coverage holes in existing cellular systems (at the cell-edge, at tunnels/subways/railways), or end-user deployed in poor coverage areas, or even provide temporary coverage (for example, during public events). The application of the multi-hop concept to cellular networks, however, raises many technical issues, such as the best positions for the BS and relay stations (RSs), the number of RSs, spectrum allocation and multiplexing between the BS and RSs, scheduling and handover [15, 16].

19

**Microcells.** Microcells are operator installed radio networks that improve outdoor coverage in urban areas experiencing poor reception. In the microcellular system, a conventional large cell (macrocell) is split into a number of small cells (microcells) [17-19]. Each microcell has a BS and a user can communicate directly with the closest BS. An illustration of microcellular system is depicted in Figure 1.4. Typically, the radio range of a microcell is less than a kilometer wide and the antennas are usually mounted at street level [20]. Since the service area of a microcell is reduced greatly with respect to that of a macrocell, the radio transmission distance between the user and the BS is reduced significantly and higher data rate can be achieved for a given transmit power. The disadvantage associated with microcells are the high costs associated with installation and maintenance of new cell BSs. Furthermore, microcells do not guarantee reliable indoor coverage.

**Distributed antenna systems (DASs).** In DASs, a macrocell is divided into a number of sectors. In contrast to the conventional collocated antenna system where the antenna units are centrally collocated, remote antenna units (RAUs) in DAS are geographically distributed in the macrocell so that the radio transmission distances from a MT to the surrounding RAUs are reduced and high data rates can be achieved for a given transmit power and bandwidth [21]. An illustration of the DAS is depicted in Figure 1.5. DAS is able to achieve an improved spectral efficiency without using the extra frequency bandwidth through all RAUs since they are typically connected to the BS or a central unit (CU) via dedicated wires such as optical fibres or coaxial cables. RAUs in the DAS are only simple antenna units carrying out transmission and reception for its CU unlike in microcellular systems. Saleh [22] originally introduced DAS to simply cover the dead spots in environments hostile to radio propagation, such as in mines or tunnels and indoors; however, DASs have drawn considerable attention in recent years due to their enormous improvement in terms of signal quality, power efficiency and data rates [23]. Relative to deploying more BSs, DAS is becoming increasingly popular with vendors as an inexpensive way

20
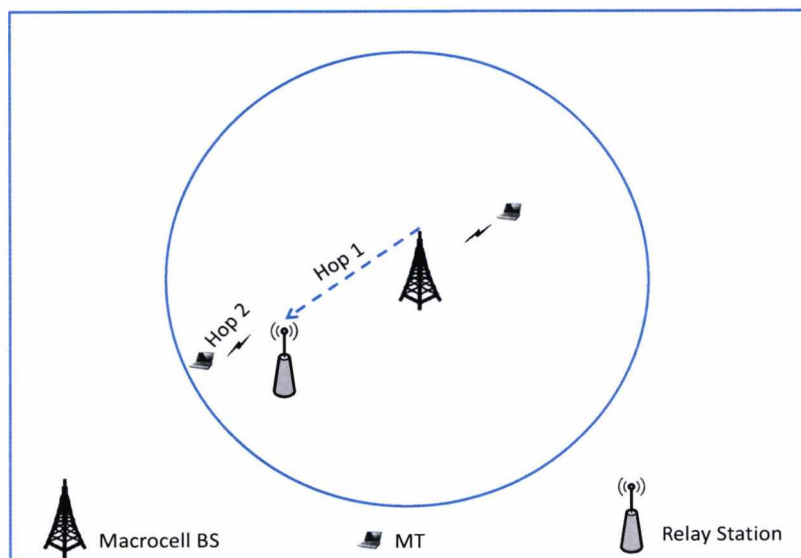
Figure 1.3: An illustration of a relay system.
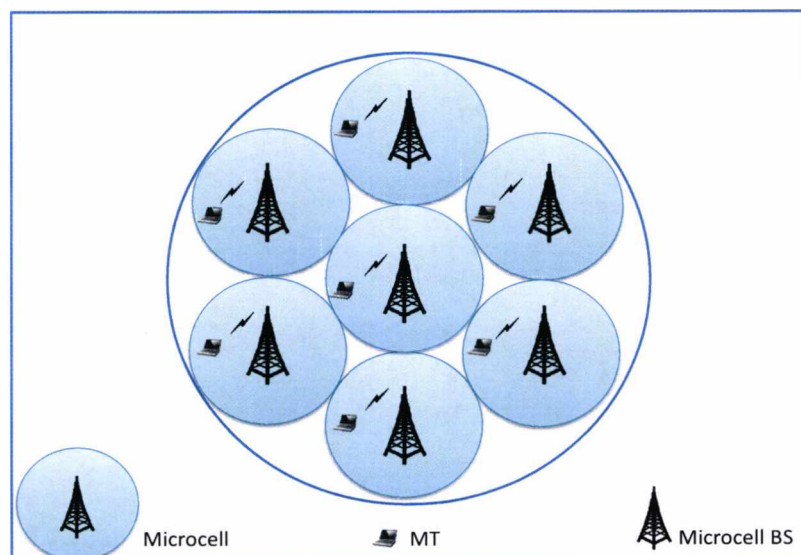


Figure 1.4: An illustration of a microcellular system.
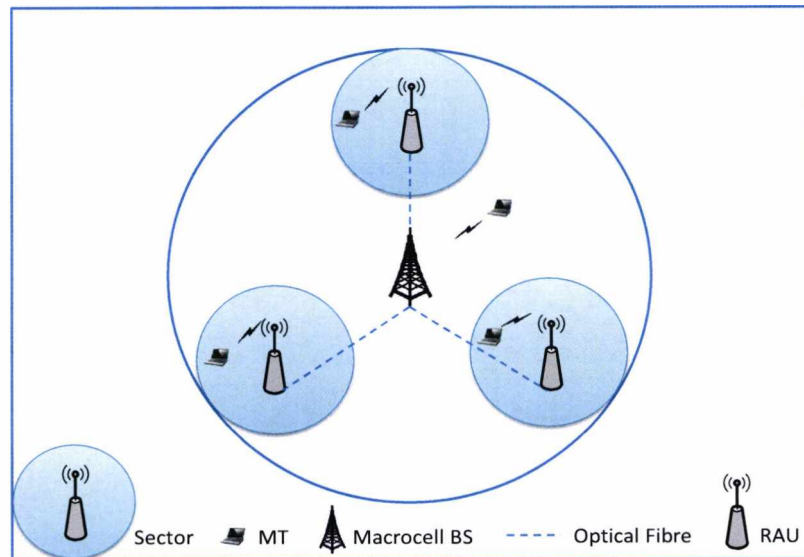
Figure 1.5: An illustration of a DAS.

to increase coverage and date rate.

The common problem associated with the each of the above technologies is that they have all been designed primarily to provide good coverage in outdoor environments with cell sizes generally within hundreds of meters. Indoor regions with high traffic density (e.g. train-stations and airports) are not well served. Since a great portion of mobile communication service users are likely to be located within buildings, providing high data rate services for those users by traditionally distributing antennas within sectors of a macrocell or via the use of relays could be very difficult to achieve, particularly in multi-floor buildings. Although the users are relatively stationary, the traffic density can be extremely high. Furthermore, because the RAUs are generally located outside, large penetration losses are often encountered when propagating the signal into the building. A better strategy to provide additional capacity and coverage for indoor users is to install a dedicated in-building DAS within the building. This is described in the following section.

## 1.3 The Concept of In-Building DAS

The in-building DAS is a dedicated wireless distribution system where RAUs are deployed on each floor throughout the building to distribute the RF signal with sufficient strength to provide 3G voice and high speed data services for MTs within the building. An illustration of an in-building DAS is depicted in Figure 1.6. In this setup, the wall penetration loss provides isolation between the outdoor macro cellular layer and the indoor radio system. Furthermore, the in-building DAS exploits the power falloff due to penetration of the signal through the floors in order to reuse the same spectrum in spatially separated floors, which increases system spectral efficiency and also reduces co-channel interference.
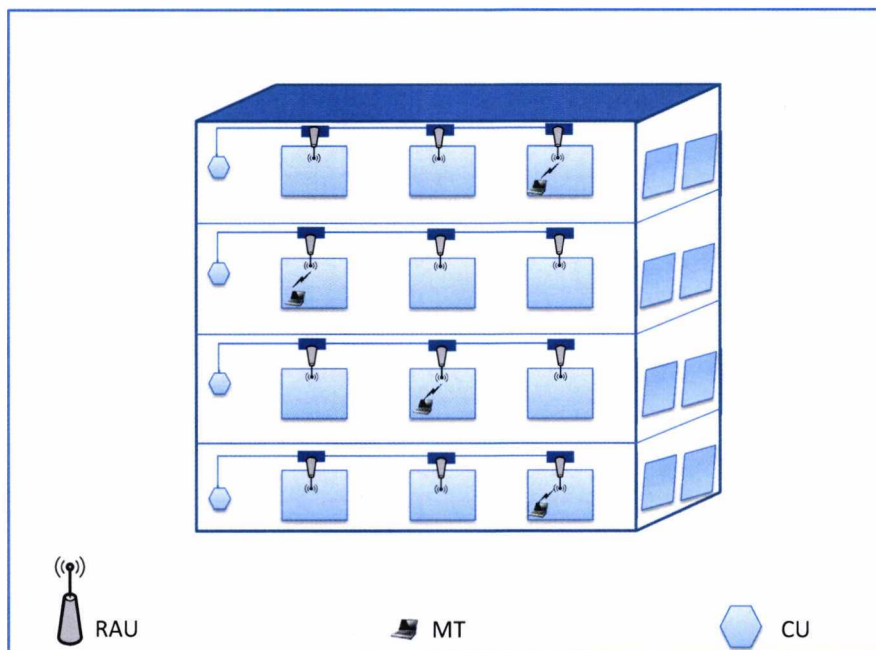


Figure 1.6: An illustration of an in-building DAS

In contrast to the conventional DAS, Wi-Fi and other techniques for increasing system capacity, the radio signal is confined to a smaller area, generally within a few

meters. Consequently, the path loss of the transmitted signal is much smaller, which implies that data rate is likely to be a great deal higher in the in-building DAS. The indoor reception is improved, and the subscriber is happy with the higher data rates and reliability. The operator can reduce the amount of traffic on their expensive macrocell network, and can then redirect its resources to provide better coverage for other mobile users, leading to efficient spatial reuse of the limited spectrum. The enhanced coverage and data rate provided by in-building DAS will reduce the motivation for mobile users to switch carriers.

On the other hand, the in-building mobile communication systems are likely to face a critical problem of interference. This is mainly because the in-building communication system introduces a markedly different propagation environment characterized by a complex mix of strong line of sight (LOS) and non LOS (NLOS) propagation, which are affected by factors including, but not limited to, the walls, floors, building partition, floor plan, building layout and possible nearby buildings in dense urban environments. The multipath generated by reflection from nearby buildings and transmission from other floors within the building may increase the level of interference, which may greatly diminish the advantages of DAS if the same frequency channels are reused - for example, in adjacent floors of high-rise buildings [24].

Due to these differences, channel modelling and performance analysis of in-building DAS may not be carried out using existing tools for conventional DAS and different mathematical tools are needed. Thus, in order to analyse and design multi-floor in-building wireless systems with acceptable performance, it is necessary to explore the characteristics of the indoor propagation channel and develop a propagation channel model which accounts for inter-floor interference caused by the effect of the building structure and its terrain. This exploration is also important when deploying indoor femtocell system which is one of the technologies planned for future in-building mobile communication system [25].

## 1.3.1 Objectives and Contributions

The aim of this thesis is to investigate the performance of an in-building wireless communication system employing DAS for high data rate indoor communication in the presence of co-channel interference. Of particular importance in this thesis is propagation processes in the indoor radio channel. Among various building types, multi-storey buildings are a common feature in many cities and are expected to exhibit the most demand for high capacity and high data rate wireless services. Therefore, this thesis focuses on radio propagation and performance analysis in a multi-storey building environment. The outcome of this thesis contributes toward appropriate channel modelling, and subsequently gives an insight into the design and the potential uplink system performance of DAS in multi-storey buildings.

The primary objectives of this research have been:

1. to investigate the three dimensional (3D) radio channel propagation characteristics in indoor high-rise buildings,

2. to formulate indoor propagation channel models from path loss values retrieved from measurement data,

3. to evaluate the impact of co-channel interference on the performance of in-building DAS using the system models,

4. to analyse location-specific performance of in-building DAS,

5. to determine the effect of the building structure and its terrain on performance,

6. to compare and contrast the performance for different RAU deployment options,

7. to investigate interference avoidance strategy where a subset of $N'$ strongest RAUs out of $N$ available RAUs is selected for combining, and the resulting impact on the performance of system,

8. to investigate in-building DAS in the context of joint processing, where the CUs cooperatively reduce the impact of co-channel interference and improve performance of the system.

In order to achieve these objectives, the uplink transmission in and around a multi-storey building has been examined. The same set of spectrum is assumed to be reused on each floor. The levels of interfering signals from vertically located co-channel MTs have been quantified and the system performance has been evaluated. System performance has been evaluated in terms of location-specific spectral efficiency and BER which are analysed for a range of potential MT locations and various in-building propagation characteristics. Two RAU deployment options have been investigated and their impact on performance evaluated.

## 1.4 The Structure of this Thesis

This thesis is comprised of seven chapters, and the related publications to this research are shown on pages vi-vii of this thesis. As a foundation for the subsequent investigations presented in this thesis, the characteristics of indoor propagation environments are examined in Chapter 2. The key propagation mechanisms, the received signal variations and the typical behaviour in indoor propagation channel are discussed. To provide a review of the research activities concerning in-building propagation, previous related research on indoor environments is also surveyed.

Chapter 3 overviews the investigation. Along with the underlying philosophy of the investigation, it also provides the essential details of the propagation model and the system model which are used in conducting the investigation.

Chapter 4 evaluates the uplink spectral efficiency achievable in the in-building DAS based on the channel and system models developed in Chapter 3. The adaptive multi-level quadrature amplitude modulation is applied. Location-specific spectral efficiency under a specified BER constraint is analysed. Location-specific antenna

selection via interference avoidance and the impact on the achievable spectral efficiency is investigated via simulation. The impact of RAU deployment options on system performance is also presented. A range of representative numerical results are provided to develop insights into the design of in-building DAS. To the author's knowledge, this is the first study of uplink in-building DAS performance in high-rise building that uses measured propagation data and considers co-channel interference emanating from vertically located MTs. The outcome of this chapter is a set of guidelines for deploying in-building DAS.

Chapter 5 quantifies the performance of in-building DAS in terms of achievable BER for various in-building characteristics. The developed models in Chapter 3 are utilized, mathematical formulas are derived to compute the BER, and hence used to quantify the gains due to the integration of DASs inside the building. A range of representative numerical results are provided.

Chapter 6 introduces co-channel interference cancellation of the received signal among co-channel receivers, where each CU can cooperate through joint signal processing for all cells in order to estimate the received signal, reduce co-channel interference introduced by frequency reuse among the floors, and maintain high spectral efficiency. A range of representative numerical results are provided. This chapter also overviews previous studies on interference mitigation and shows that no previous research has been published relating interference cancellation to in-building DAS via joint processing.

Chapter 7 presents the key conclusions from this thesis and suggests directions for future developments.

Appendix A details the derivation of the variance of co-channel interference discussed in Chapter 3

Appendix B presents the generation of Rayleigh and Nakagami random variables discussed in Chapter 5.

# Chapter 2

# In-Building Radio Propagation and Modelling Techniques

## Contents

## 2.1 Introduction

A common feature of many urban environments is the presence of multi-storey buildings (Figure 2.1). They are built not just for economy of space but also considered symbols of a city's economic power. As discussed in chapter 1, mobile data is mostly ➤

Figure 2.1: Multi-storey buildings, a common feature of many urban cities

consumed from inside buildings, thus the design of wireless systems that provide high data rates inside buildings is of primary concern in this thesis. In order to achieve this objective, a general understanding of radio propagation inside the building is required. Therefore, the aim of this chapter is to explore radiowave propagation characteristics in indoor wireless environment, particularly in multi-floor buildings. The possible propagation paths in an indoor environment are outlined and this is extended in chapter 3, where indoor propagation channel models are formulated from path loss values retrieved from measurement results in order to evaluate the performance of the system. Section 2.2 describes the phenomena influencing the propagation of radio signals inside the building. The received signal variation due to small-scale fading, large-scale fading and distance dependence are explained. Section 2.3 presents a literature review on in-building propagation modelling, and it has been divided into two parts. The first part surveys the case where the transmitter and the receiver are both located on the same floor, and the second, propagation models for multi-floor buildings. Significant findings and their implications for propagation

modelling are discussed. Finally, Section 2.4 summarises the chapter.

## 2.2 In-Building Radio Propagation

In the development of mobile radio communication systems, extensive research has been performed for the understanding of propagation characteristics of radio waves in outdoor environments [26-30]. While the fundamentals of radio wave propagation remain the same in indoor environments, indoor radio channels differ from outdoor channels in three important aspects, namely; (a)the indoor environments are inherently 3D in topology, (b) the propagation distances are typically much smaller, and (c) the physical variation of the environment is much greater for a much smaller range of transmitter-receiver separation distances [31]. Indoor propagation is complicated and strongly influenced by local features, such as floor layout and building construction materials for walls, floors and ceilings, and possible nearby buildings in dense urban environments [32]. An understanding of radio propagation inside buildings has been made possible through numerous experimental measurements and ray tracing techniques. Site specific propagation predictions were presented in [33, 34], which included measured path loss due to obstructions such as walls, soft partitions and floors. Furthermore, ray-tracing techniques were used in [35] to predict in-building propagation characteristics with reasonable accuracy. A few major propagation mechanisms govern the propagation of these rays inside the building. For example, when a ray strikes a flat surface such as an internal wall, the incident ray generates two rays, the reflected ray and the transmitted ray. This is further discussed in Section 2.2.1.

### 2.2.1 In-Building Radio Propagation Phenomena

In any given location within the building, the received signal is usually comprised of several components which propagate along different paths. Figure 2.2 illustrates the

30

radio propagation phenomena which have been represented as rays in a hypothetical high-rise building environment. The signal component propagates through the following paths [36, p78]:

**Direct path.** - This is the most basic path for radio propagation, in which radio signals travel along the shortest path between the transmitter and receiver. In Figure 2.2 the direct path (coloured green) can include a LOS path with no intervening obstacle, and a NLOS path with obstacles (e.g. floors, walls) between the transmitter and the receiver. The transmitted signals are likely to experience attenuation when passing through the obstacles. Therefore, appropriate methods for estimating the transmission loss through obstacles are required for accurate propagation modelling in indoor environments.

**Reflected path.** This path occurs when a propagating electromagnetic wave strikes an object which is large compared with the wavelength of the propagating wave, and then reflects towards the opposite direction of the incident wave. Reflection is generally regarded as an important propagation process which has been found to contribute significantly to the received signal strength [36, pp. 78-79]. The strength of this path depends on the electrical and physical properties of the object. If the incident wave impinges on a dielectric object, then part of the energy is transmitted through, part of the energy is reflected back, and part of the energy is absorbed. The material properties, wave polarisation, angle of incidence, and frequency are the parameters which can influence the extent of energy reflection/transmission. Reflections typically occur at walls, floors and nearby buildings in close proximity as illustrated in Figure 2.2 (coloured red). The reflected paths are potential dominant energy paths and may need to be considered.

**Diffracted path.** This path occurs when the direct path between the transmitter and receiver is obstructed by obstacles with abrupt changes such as a sharp edge or a corner [36, pp. 90-91]. Diffraction can occur from the corners of corridor, the window edges or the vertical edges of the walls inside a building. When the

direct path is obstructed and significantly attenuated, the radio signal can reach the receiver via a diffracted path (coloured brown), as illustrated in Figure 2.2, and may be the major contributor to the received signal strength.

**Scattered path.** This path occurs when the propagating waves travel through a medium consisting of obstacles that are small compared to the wavelength and then scatters in several different non specular directions. For example, scattered paths can result when a radio wave impinges on a door knob and then propagates to the receiving terminal [36, pp. 100-101]. Scattering is expected where a large amount of clutter such as furniture and office equipment is present.
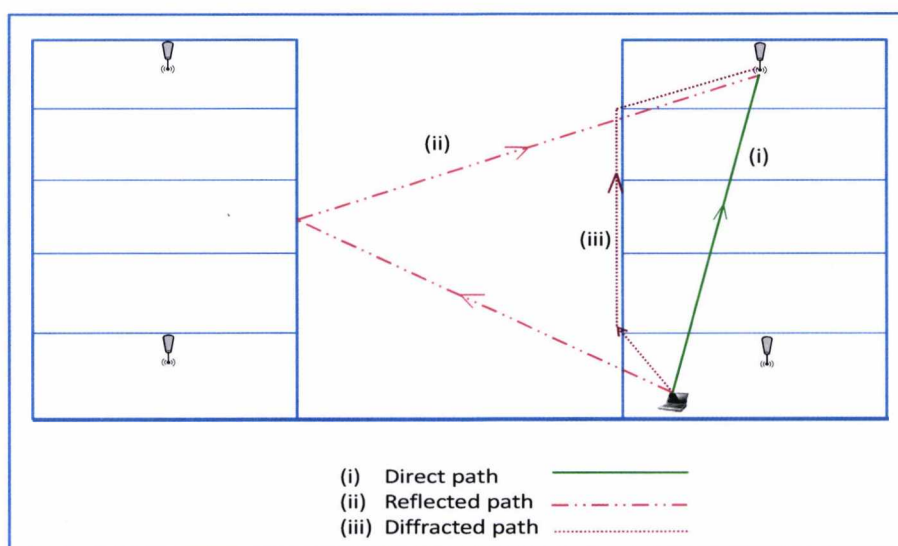


Figure 2.2: A hypothetical high-rise building environment showing possible propagation paths

## 2.2.2 Multipath Fading

Multipath fading is a feature that needs to be taken into account when designing or developing an in-building radio communications system, this is of particular im-

portance in this thesis. As signals propagate from a transmitter through the indoor environment via different propagation mechanisms, the received signal arrives at the receiver not only via the direct path, but via other paths as a result of reflections from objects such as buildings, walls furniture, etc that are adjacent to the main path as discussed in Section 2.2. The received signal envelope at the receiver tends to vary as a function of distance and time. The overall signal at the radio receiver is a summation of the variety of signals being received. As they all have different path lengths, the signals will add and subtract from the total depending on their relative phases. Three scales of signal fluctuation can be identified [26, pp. 67-69], namely small-scale fading, large-scale fading and distance-dependent path loss.

**Small-scale fading.** Small-scale fading is used to describe the rapid fluctuation of the amplitude of a radio signal over a short distance (in the order of half a wavelength) [26, pp. 67-69]. Fading is caused by interference between multiple versions of the transmitted signal that arrive at the receiver at slightly different times [36, pp. 139-141]. These multipath waves combine vectorially at the receiver resulting in a signal that can vary widely in amplitude and phase.

The Rayleigh distribution is commonly used to model the envelope (in volts) of multipath signals in wireless systems when there is NLOS between the transmitter and receiver. The probability density function (PDF) for a Rayleigh distributed received signal $\alpha$ (in volts) can be expressed as [36, pp. 172-174]

$$p(\alpha) = \begin{cases} \frac{\alpha}{\sigma^2} \exp\left(-\frac{\alpha^2}{2\sigma^2}\right) \ , & \alpha \geq 0 \\ 0 & , \quad \text{otherwise} \end{cases} \tag{2.1}$$

where $\sigma^2$ is the mean power (in watts) of the multipath signal.

The Nakagami-$m$ fading distribution was first introduced by Nakagami [37] for modelling ionospheric and troposheric fast fading channels. The Nakagami-$m$ distribution provides a very good fit for measured data in a variety of fading environments and has been widely adopted for multipath modelling in wireless communications

due to its good accuracy and versatility. This distribution is useful for the modelling of radiowave propagation in environments where there is a LOS or specular signal component in addition to other multipath (Rayleigh) components. The PDF for a Nakagami distributed signal $\alpha$ (in volts) is given by [38, p. 329]

$$p(\alpha) = \begin{cases} \frac{2}{\Gamma(m)} \left(\frac{m}{\Omega}\right)^m \alpha^{2m-1} \exp\left(-\frac{m\alpha^2}{\Omega}\right) , & \alpha \geq 0 \\ 0 \quad , & \text{otherwise} \end{cases} \tag{2.2}$$

where $\Gamma(\cdot)$ is the gamma function defined by $\Gamma(x) = \int_0^\infty t^{x-1} e^{-t} dt$, $m$ is a parameter accounting for the fading severity thereby having a significant impact on the error performance of the system, and $\Omega$ is the average fading power of the received signal. The parameters $\Omega$ and $m$ can be expressed as

$$\Omega = E\left\{\alpha^2\right\} \tag{2.3}$$

$$m = \frac{\Omega^2}{E\left\{(\alpha^2 - \Omega)^2\right\}}, \quad m \geq \frac{1}{2} \tag{2.4}$$

The notation $E\{x\}$ denotes the expected value of $x$. The Nakagami-$m$ distribution relates to other distributions through some simple formulae. For example, the Rayleigh distribution is a special case of the Nakagami distribution when $m = 1$. The Nakagami-$m$ distribution can closely approximate a Rician distribution also [38, pp. 329-330].

**Large-scale fading.** Large-scale fading is used to describe the long-term fluctuation of the received signals when small-scale fading is averaged out over a localised area of the order of tens of wavelengths [26, pp. 67-69]. This type of signal fluctuation is due to the presence of large obstacles in the propagation path, hence it is also known as shadowing. The Lognormal distribution is commonly used to model this scale of fading [30, p. 155]. The PDF for a lognormal distributed signal $\alpha$ (in

volts) can be expressed as [30, pp. 232-233]

$$p(\bar{\alpha}) = \begin{cases} \frac{20}{\bar{\alpha}\sigma \ln 10 \sqrt{2\pi}} \exp\left(-\frac{(20\log \bar{\alpha} - v)^2}{2\sigma^2}\right), & \bar{\alpha} \geq 0 \\ 0 & , & \text{otherwise} \end{cases} \tag{2.5}$$

where $v$(dB) and $\sigma$(dB) are the mean and standard deviation of the slow fading component respectively. $\bar{\alpha}$ is the mean of the fast fading voltage.

**Distance-dependent path loss.** This is the third and largest scale of signal variation which describes the attenuation of the received signal as the distance between the transmitter and receiver increases. This scale of signal variation is due to the spatial divergence of the radiowaves in space over the given environment [26, pp. 67-69]. Figure 2.3 shows the linear relationship between the received signal (in dB) and the distance from the transmitter (in logarithmic units), in which small and large scale fading have been averaged out. The distance-dependent path loss determines the area mean [26, p 22]. In outdoor environments, the area mean normally follows an inverse exponent law with the distance $d$ between the transmitter and the receiver, in the form of $\frac{1}{d^\lambda}$ [26, pp. 24-26]. The path loss exponent $\lambda$ determines the rate of
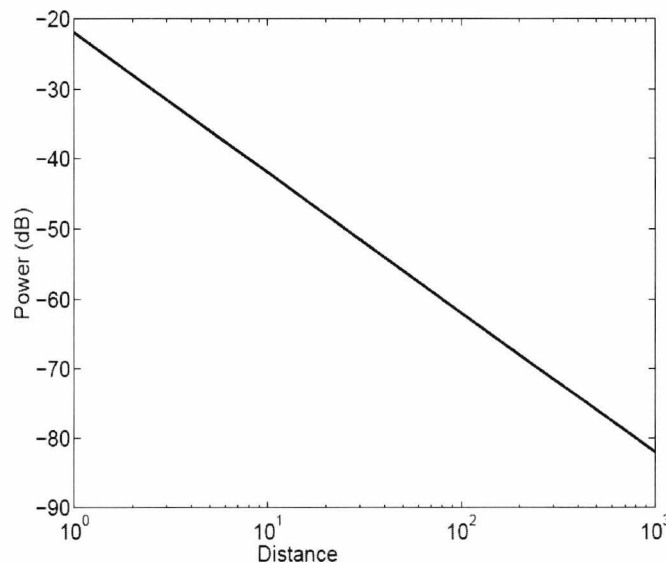


Figure 2.3: Distance-dependent mean power variation

decay of the received signal with respect to the separation between the transmitter and the receiver, and can typically take a value between 2 to 6 depending on the propagation environment. In indoor environment, the value $\lambda$ can be smaller than 2 for propagation down corridors, or larger than 2 for propagation through rooms and walls [39]. This will be discussed in greater details in Section 2.3.

## 2.3  In-Building Radio Propagation Modelling

Extensive radio propagation measurements have been conducted in a wide variety of buildings in order to understand radio propagation behaviour inside the building [40-54]. To differentiate in-building propagation phenomena, researchers often classify buildings by the following categories: residential homes in suburban areas, residential homes in urban areas, traditional older office buildings with fixed walls (hard partitions), open-plan buildings with movable wall panels (soft partitions), factory buildings, grocery stores, retail stores, and sports arenas. Hard partitions describe obstructions within the building which cannot be easily moved such as existing walls and corridors, while soft partitions describe movable obstructions such as office furniture, which have a height less than the ceiling height. Within a building, propagation geometry may be classified as LOS where the transmitter and receiver are visible to one another or obstructed (NLOS), where objects within the building block a direct propagation path. Physical similarities often exist between different types of buildings. For example, factory buildings and grocery stores both contain a large amount of metal inventory and often have few hard partitions within the building. Traditional office buildings, with many walls made of plaster and metal lathe, often have similar propagation characteristics to large residential homes or retails stores that contain many partitions. Although predicting radio coverage between floors of a multi-storey buildings has proven to be difficult, measurements have shown that there are general rules-of-thumb that apply.

Numerous propagation models have been developed to predict radio propagation behaviour to enable the efficient planning of wireless communication systems. A variety of methods have been used to develop these propagation models. This include *Empirical* and *Site-Specific* models. Empirical/statistical models are usually a set of equations that are derived from experimental measurements. These equations are simple and can be used to predict the received signal strength efficiently. Predictions from these models have been compared with measured propagation data to assess their accuracy. **Alexander** [40] first found that the mean path loss, PL (dB) between transmitter and receiver of separation distance, $d$ could be represented by a power law and given by

$$PL(d) = \lambda \cdot \log_{10}(d) \tag{2.6}$$

where $\lambda$ is the gradient parameter used to indicate the signal decay rate in the building. This model is simple and can be easily applied to an indoor environment with a single input parameter (i.e. the transmitter and receiver separation distance, $d$). However, the prediction accuracy is greatly dependent on the gradient parameter $\lambda$ derived from each building construction type through measurements. As a result, a series of measurements in different commercial buildings and houses is required.

On the other hand, site-specific models are based on electromagnetic methods such as the ray-tracing and finite-difference time-domain (FDTD) methods. Hybrid models which combine more than one electromagnetic models have recently emerged as another promising indoor propagation modelling approach [41]. The purpose of this section is to evaluate relevant propagation models reported in the literature and then formulate a propagation model for use in this thesis. The formulated propagation model is then used to estimate the mean path loss between the transmitter and the receiver. For a system within multi-floor buildings (as considered in this thesis) with transmitters and receivers located inside the building, it is important to model the path loss within a floor of interest (intra-floor) as well as between floors

(inter-floor). Propagation modelling approaches for both of these cases are discussed in the following sections.

## 2.3.1 Intra-Floor Propagation Modelling

Modelling radio signal propagation within a floor of interest is required for cases where the transmitter and receiver are on the same floor (e.g. single floor buildings). Previous research has shown that the mean received signal strength is generally found to decay with the distance between the transmitter and receiver. The log-distance propagation model is a common model which predicts the mean path loss, $PL(d)$(dB), between a transmitter and receiver separated by a distance $d$ as [42]

$$PL(d) = PL(d_o) + 10\lambda \log_{10}\left(\frac{d}{d_o}\right) \tag{2.7}$$

where $d$ is the distance between the transmitter and the receiver, $PL(d_o)$ is the mean path loss (dB) measured at a specified distance, $d_o$, and $\lambda$ is the path loss exponent. The path loss exponent $\lambda$ determines the rate of decay of the received signal with respect to the 3D separation between the transmitter and the receiver, and can typically take a value between 2 to 6 depending on the propagation condition (the variation can be attributed to the physical layout and type of building, as summarized in Table 2.1). Experimentally obtained values of $\lambda$ for indoor environments vary considerably depending on the presence of a LOS or a NLOS propagation path. For example, if there is LOS propagation path between a transmitter and receiver in an open space (e.g. a large room or corridor), values for $\lambda$ are reported in the literature [43] to vary from $1.8 \leq \lambda \leq 3$. For NLOS cases (e.g. between rooms separated by several partitions), values for $\lambda$ are reported in the literature to vary from $2.45 \leq \lambda \leq 6.5$ [43]. In indoor environments, a reference distance (selected so that it lies in the far field of the transmitting antenna) of $d_o = 1$m is typically used.

Several researchers have attempted to modify (2.7) in order to obtain a better fit to their measured data for different indoor environments. The lack of accuracy in

Table 2.1: Path Loss Exponent Measured in Different Buildings [43].

| Building | Path Loss Exponent, $\lambda$ |
|---|---|
| Grocery store | 1.8 |
| Retail store | 2.2 |
| Open-plan Factories | 1.4 - 3.3 |
| Suburban office building open-plan | 2.4 - 2.6 |
| Suburban office building with soft partition | 2.8 - 3.8 |
| Office building with hard partition | 3.0 |

the above model occurs because it is only a function of distance and the impact of specific propagation environment features (e.g. the intervening walls and partitions) between the transmitter and the receiver are not accounted for.

**Seidel** *et at.* [44] have subsequently considered the impact of intervening walls and obstacles by adding relevant attenuation factors (wall attenuation factor) to the distance-dependent path loss model. This models assume that the signal attenuates as in free space ($\lambda = 2$) and attributes all additional path loss directly to intervening soft partitions and concrete walls. The mean path loss predicted by the wall attenuation factor (WAF) model can be represented as

$$PL(d) = PL(d_o) + 10\lambda \, (\text{freespace}) \log_{10}\left(\frac{d}{d_o}\right) + p \cdot \text{WAF}_{\text{soft}} + q \cdot \text{WAF}_{\text{concrete}} \quad (2.8)$$

where $p$ and $q$ are the number of soft partitions and concrete walls between the transmitter and receiver, respectively. $\text{WAF}_{\text{soft}}$ and $\text{WAF}_{\text{concrete}}$ are respectively soft partitions and concrete walls attenuation factors derived from experimental measurements. Typical values for $\text{WAF}_{\text{soft}}$ and $\text{WAF}_{\text{concrete}}$ are 1.4 dB/partition and 2.4 dB/wall, respectively [44]. By including the wall attenuation factor in (2.8), it is shown that more accurate mean path loss predictions than from the distance-dependent models represented by (2.6) and (2.7) can be achieved. However, additional input information is required regarding the types of intervening walls.

## 2.3.2 Inter-Floor Propagation Modelling

Modelling radio signal propagation between floors is required when the transmitter and receiver are on different floors of a building as illustrated in the representation of the high-rise building shown in Figure 2.4. The intervening floors between the transmitter and receiver are likely to have a significant influence on the mean path loss. There have been numerous experimental studies of the indoor radio channel in multi-storey office buildings, and this section outlines several relevant, noteworthy empirical propagation models developed to predict signal strengths within the buildings.
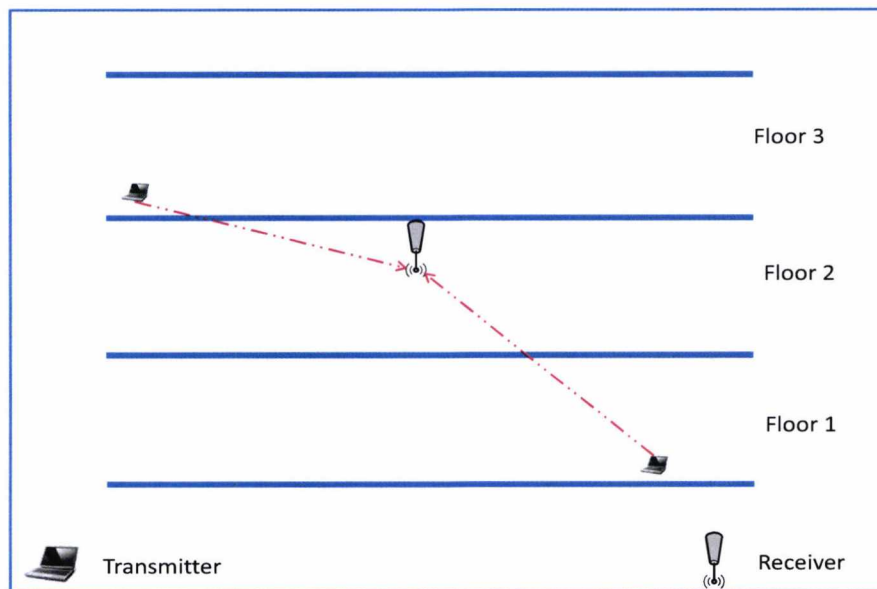


Figure 2.4: Generalised depiction of inter-floor propagation in multi-storey building

**Motley and Keenan's** [45] model is based on experimental measurements of the received signal strength/path-loss in a multi-storey office building at 900 and 1700 MHz. Similar to Seidel's model for intervening walls within a single floor (2.8), the path loss was observed to follow a logarithmic relationship with distance but includes

an additional attenuation factor accounting for each intervening floor between the transmitter and the receiver. The path loss can be represented as

$$PL(d) = PL(d_o) + 10\lambda \log_{10}\left(\frac{d}{d_o}\right) + k \cdot F \tag{2.9}$$

where $F$ (dB) is the loss encountered propagating through a single floor and $k$ represents the number of penetrated floors in the transmission path between the transmitter and the receiver. $\lambda$ is the path loss exponent. At 900 MHz the parameters $\lambda$ and $F$ were found to be 4.0 and 10 dB respectively; whereas at 1700 MHz, $\lambda = 3.5$ and $F = 16dB$ [45]. It is noted that higher losses are predicted at 1700 MHz, and for the limited number of floors considered in [45], the path loss was observed to increase linearly with the number of floors penetrated. However, propagation measurements conducted by several researchers have shown that for a large number of floors, the incremental attenuation of each additional floor decreases with an increasing number of floors between a transmitter and receiver [46-47].

Based on experimental measurements in two multi-storey university buildings (containing a mix of laboratories, offices and classrooms) at 917 MHz, **LaFortune and Lecours** [46] attempted to modify Motley and Keenan's model. The measurement set was divided into a number of canonical regions such as propagation in corridors, penetration through soft and hard internal partitions and propagation to adjacent floors. Models to predict the mean path loss were fitted to the measurements. When the transmitter and receiver are located on different floors, the loss in excess of free space can be represented as [46]

$$PL(dB) = -1.5n - 10.7 \log_{10} 10d - 23.8 - 41.7 \log_{10} 10p \tag{2.10}$$

where $n$ and $p$ are the number of (internal, soft partitioned) walls and concrete floors in the transmission path between the transmitter and the receiver respectively, and $d$ is the distance between the transmitter and the receiver. In contrast to the model proposed in (2.9), the floor attenuation is observed to decrease as more floors separate the transmitter and receiver.

In [47], **Bertoni** *et al.* developed a theoretical model, based on the geometrical theory of diffraction (GTD), which explains the propagation between a transmitter and a receiver located on different floors of a building. It was observed that depending on the structure of the building and the location of antennas, either direct ray propagation through floors or diffraction outside the building would determine the propagation characteristics and strength of the signal. The direct paths through the floors may include multiple reflections between semi-transparent walls, floors and ceilings. The electromagnetic field strength of this path at the receiver can be represented as [47]

$$|E|^2 = \frac{Z_o P_e}{4\pi L^2} \prod_m T^2_{\text{floor,m}} \prod_n T^2_{\text{wall,n}} \tag{2.11}$$

where $Z_o$ is the free space wave impedance, $P_e$ is the effective radiated power, and $L$ is the distance between transmitting and receiving antennas the radio wave penetrates through the floors. $T^2_{\text{floor,m}}$ and $T^2_{\text{wall,n}}$ accounts for losses due to each floor and wall respectively.

The diffracted paths involve transmission outside the building through windows and diffraction into paths that run along side the face of the building and propagate back through another window into a different floor. The electromagnetic field strength at the receiver via such diffracted path can be represented as [47]

$$\left|\hat{E}\right|^2 = \frac{Z_o P_e}{4\pi L^2} \frac{\prod_i D^2(\alpha_i) \prod_j T^2_{\text{glass,j}} \prod_k T^2_{\text{wall,k}}}{\sum_n L_{nm} \prod_n L_{nm}} \tag{2.12}$$

where $L_{nm}(n = 1, 2, 3; m = 1, 2)$ are the lengths of the diffracted paths, $T^2_{\text{glass,j}}$ and $T^2_{\text{wall,k}}$ accounts for the losses through glass and interior walls in the transmission paths between the transmitter and the receiver. In (2.12), $D(\alpha_i)$ is the diffraction coefficient for a propagating wave bending through angle $\alpha_i$. Depending on the construction of the building and window frame, different choices may be made for the diffraction coefficient. The coefficient for an absorbing wedge obtained by Keller's diffraction theory [48], was used in investigating the relative strength of the total field associated with the direct path through the floors and the diffracted path. The

coefficient can be expressed as

$$D(\alpha_i) = \frac{1}{2\pi k} \left[ \frac{1}{2\pi + \alpha_i} - \frac{1}{\alpha_i} \right] \tag{2.13}$$

where $k = 2\pi/\lambda$ is the wave number and $\lambda$ is the wavelength. Typical values of $T_{\text{wall}}$, $T_{\text{glass}}$ and $T_{\text{floor}}$ from experiment measurements and the knowledge of the material are 2.2dB, 0.25dB and 13.0dB respectively. This model offers complete physical calculations which are suitable for different kind of buildings in order to further improve the accuracy of empirical propagation models.

The models proposed by **Seidel and Rappaport** [49] are based on experimental measurements made in two multi-storey buildings. The measurements were conducted at 914 MHz; however, it was suggested the model could be generally extended to the low microwave bands (1.0-5.0 GHz). Seidel and Rappaport proposed a distance-dependent model and a floor attenuation factor model. The path loss models for multi-storey buildings can be represented as [49]

1. Distance-dependent path loss model

$$PL(d) = PL(d_o) + 10\lambda(\text{multi-floor}) \log_{10}\left(\frac{d}{d_o}\right) \tag{2.14}$$

This model is similar to the model described by (2.7), except that the mean path loss exponent is a function of the number of floors between transmitter and receiver. Larger value of $\lambda$ (typically between 4-5.5 for one to three floors [49]) is chosen to account for the increased attenuation by intervening floors. The values of $\lambda(\text{multi-floor})$ are given in Table 2.2.

2. Floor attenuation factor path loss model

$$PL(d) = PL(d_o) + 10\lambda(\text{same floor}) \log_{10}\left(\frac{d}{d_o}\right) + FAF \tag{2.15}$$

43

where $\lambda$ is the (constant) path loss exponent from data measured when the transmitter and the receiver are on the same floor (given in Table 2.2), and $FAF$ is the floor attenuation factor representing losses encountered while propagating though a number of floors. $FAF$ is a function of the building type, and number of floors between

Table 2.2: Experimental Values of Path Loss Exponent, $\lambda$ Through Floors of Two Multi-Storey Buildings [49].

| Building | $\lambda$ |
|---|---|
| **All buildings:** | |
| All locations | 3.14 |
| Same floor | 2.76 |
| Through 1 floor | 4.19 |
| Through 2 floors | 5.04 |
| Through 3 floor3 | 2.22 |
| **Office building 1** | |
| Entire building | 3.54 |
| Same floor | 3.27 |
| **Office building 2** | |
| Entire building | 4.33 |
| Same floor | 3.25 |

the transmitter and the receiver. The values of the floor attenuation factor is given in Table 2.3. It is noted that the $FAF$s shown in Table 2.3 are not a linear function of the number of floors between the transmitter and receiver. Since all floors in the buildings examined are identical, if penetration through the floors was the only dominant propagation path, the $FAF$ should increase linearly. However, the incremental $FAF$ decreases as more floors are penetrated, suggesting there may be other factors such as multipath reflections from neighbouring buildings that affect the path loss.

Since the publication of the Seidel model in 1992, various improvements have been suggested [50-52], but the model remains widely used and forms the basis of the International Telecommunications Union (ITU) model for mean path-loss prediction in multi-storey buildings [53].

Table 2.3: Experimental Values of $FAF$ in Two Office Buildings [49].

| Building | $FAF$ (dB) |
|---|---|
| **Office building 1** | |
| Through 1 floor | 12.9 |
| Through 2 floor | 18.7 |
| Through 3 floor | 24.4 |
| Through 4 floor | 27.0 |
| **Office building 2** | |
| Through 1 floor | 16.2 |
| Through 2 floor | 27.5 |
| Through 3 floor | 31.6 |

The **ITU** model is based on a number of experimental studies conducted in a wide range of buildings throughout the world at various frequencies. The mean path-loss is given by [53]

$$PL(dB) = 20 \log_{10} f + N_t \log_{10} d + L_f(k) - 28 \tag{2.16}$$

where $N_t$ is the distance power loss coefficient that expresses the loss of signal power with distance. This coefficient is an empirical one with some values provided in Table 2.4. $f$ is frequency (in MHz), $d$ is the distance between the transmitter and the receiver, $L_f$ is the floor penetration loss, and $k$ is the number of floors separating the transmitter and receiver. Table 2.4 shows values for $N_t$ and $L_f$ at typical operating frequencies, although it is suggested that a better performance can often be obtained

Table 2.4: ITU Model: Distance-Dependent Exponents and $FAF$s [53].

| Frequency (GHz) | Distance Dependent, $N_t$ | Floor Attenuation, $L_f(dB)$ |
|:---:|:---:|:---:|
| 0.9 | 33 | 9 (1 floor) |
| | | 19 (2 floors) |
| | | 24 (3 floors) |
| 1.8-2.0 | 30 | $15 + 4(N_t - 1)$ |
| 5.2 | 31 | 16 (1 floor) |

if the model is tuned by incorporating experimental measurements for $N_t$ and $L_f$ from the buildings of interest.

In addition to these findings, **Austin** *et al.* [54] have developed mechanistic models to characterise the indoor radio channel, particularly focusing on inter-floor propagation using FDTD method in order to identify the dominant mechanisms governing propagation within buildings.

The models proposed by **Austin** *et al.* [54] are based on FDTD implementation in two reinforced concrete multi-floor buildings surrounded by multi-storey buildings. The results presented indicate the power arriving on adjacent floors in a multi-storey building is dominated by the component penetrating through the floors and the component reflected by adjacent buildings. Based on the Friis equation [36, pp. 70-73], the model consists of two components which can be expressed as

$$PL = \left(\frac{\lambda_w}{4\pi d_d}\right)^2 k^{2n} + \sum_{b=1}^{B} \left(\frac{\lambda_w}{4\pi d_b}\right)^2 \prod |\Gamma|^2 \prod |\tau|^2 \ (\text{W}) \tag{2.17}$$

In the first component, $d_d$ is the distance between the transmitter and receiver when the radio wave penetrates through the floors, $n$ is the number of intervening floors in the transmission path between the transmitter and the receiver and $k$ is the (linear) attenuation through a single floor. The second component is the strength of the reflected path which reflected back from the surrounding buildings, where $B$ denotes

the number of adjacent buildings parallel to an external face, $d_b$ is the distance between the transmitter and receiver when the radio wave reflects from surrounding building $b$, $\Gamma$ is the reflection coefficient at the building face and $\tau$ is the transmission coefficient through the glass windows. $\lambda_w$ is the wave length. Transmission through two sets of glass windows and reflection at a glass fronted building reduces the received power by 18 dB and can be modelled by reflection and transmission coefficients of 0.5 in [54]. The results have also indicated that double-reflections and edge diffraction can increase the received power; however their contribution is inconsequential enough to be excluded from consideration in the mechanistic model.

### 2.3.3 Propagation Modelling Approach in This Thesis

Sections 2.3.1 and 2.3.2 reviewed the approaches for modelling mean path loss variations in single and multi-floor buildings. In this thesis, a floor by floor analysis of an in-building wireless communication system employing DAS is presented. All of the models used in this thesis are based on an understanding of the key propagation mechanism(s) in multi-storey buildings and relate the radio propagation to the specific layout of the buildings considered; however, in-building path loss values are retrieved from measurement results in multi-storey high-rise buildings [49-54]. These types of models are well suited to the analyses presented in this thesis where the performance over an entire floor is of interest. The common propagation paths assumed include, LOS from the transmitter to the receiver, diffraction at the window frame, and reflections from adjacent buildings; and in most circumstances one or two components dominate the mean received power. The parameters fitted to the models used in this thesis, include the distance between the transmitter and the receiver, $d$, propagation exponent, $\lambda$, and the penetration loss, $\varphi$, the reflection loss, $\hat{\varphi}$, the diffraction loss, $\bar{\varphi}_{u,n}$ and the transmission loss through the glass window, $\ddot{\varphi}_{u,n}$. The detailed in-building propagation channel models are described and formulated

in chapter 3 and used to evaluate the performance of the in-building DAS.

## 2.4 Summary

Indoor wireless systems pose one of the biggest design challenges to wireless communication system designers. Reflection, diffraction and scattering cause signal variations and propagation losses. The propagation environment is considerably more complex than outdoor environments. Multi-storey buildings often encourages 3D deployment strategies, with frequency channels often reused on adjacent (or nearly adjacent) floors. Furthermore, the path between a transmitter and a receiver inside a building may vary from having complete LOS with no intervening obstacles to NLOS with one or more different obstacles between and around them. Therefore understanding how radio waves propagate within buildings, and give rise to co-channel interference, is important in order to analyse and design in-building wireless systems with acceptable performance. This chapter has presented the commonly observed in-building propagation phenomena, and the received signal variations due to small-scale fading, large-scale fading, and distance-dependence. Various modelling techniques that are used to predict propagation behaviour in indoor environments have been reviewed. These include models for the case where the transmitter and the receiver are both located on the same floor, and propagation models for the case where the transmitter and the receiver are located on different floors. If the characteristics of the propagation channel is predicted accurately, radio frequency engineers can confidently predict the coverage area, evaluate system performance and design indoor wireless systems so that interference is minimised and system capacity is maximised. One of the major contributions of this thesis is an evaluation of the performance of in-building DAS based on a propagation channel model which accounts for inter-floor interference caused by the effect of the building structure and its terrain.

# Chapter 3

# In-Building Distributed Antenna System

## Contents

## 3.1 Introduction

Future wireless systems will need to provide gigabit wireless data services to a large number of users. The 4G systems are expected to provide broadband packet data services with peak data rate of about 100Mb - 1Gbps [55]. However, there are

important technical issues to be addressed. Amongst them are limited bandwidth and limited transmit power. In December 2007, ITU allocated the spectrum for 4G systems as follows [56]: 450-470MHz (20MHz), 790-806MHz (16MHz), 2.3-2.4GHz (100MHz) and only 3.4-3.6GHz for Global use. 200MHz bandwidth in the global frequency band must be shared by several operators (at least 2) and reused everywhere. The frequency spectrum allocations are limited while gigabit data services are increasingly demanded. Furthermore, the received signal quality degrades due to long radio transmission distance between the transmitter and the receiver. This leads to path and shadowing losses, since the transmit power is limited. Thus, for high rate transmission, a huge transmit power is required if the same communication range in distance as in the present cellular systems is kept. On the other hand if the transmit power is kept the same as in the present systems, high data rate services may only be available near the BS [57]. Therefore, a fundamental change is necessary in wireless access network architecture. One promising solution to solve the problems arising from limited bandwidth and limited transmit power is DASs.

This chapter introduces DASs and provides the essential details of the channel and system models which are used in conducting the analysis of the in-building DAS. The difference between the conventional DAS and the in-building DAS in the context of co-channel interference is discussed in Section 3.2. Section 3.3 presents the in-building DAS system models, and the impact of the building layout and its terrain on system performance is examined. The path loss between the MTs and each RAU, and the received signal-to-interference-plus-noise ratio (SINR) are also formulated.

## 3.2 Distributed Antenna Systems

DASs, which employ multiple RAUs connected to a CU have drawn considerable attention in recent years due to their enormous improvement in terms of signal

quality, coverage of dead spots, power efficiency and data rates [58]. Early proposals on the use of distributed antennas were simply to cover dead spots in environments hostile to radio propagation, such as in tunnels, mines and indoor environments. In such environments, the propagation loss encountered by the signal may render the use of a single central antenna ineffective [22]. RAUs in the DAS are geographically distributed so that the radio transmission distances from a MT to the surrounding RAUs are reduced and high data rates can be achieved for a given transmit power and bandwidth [59-63]. There is no additional signal processing needed at the RAUs except for amplifiers and down-converters. DAS increases the spectral efficiency without using extra bandwidth through all RAUs since they are typically connected to the CU via dedicated wires such as optical fibres.

However, most of the recent work on the conventional DAS have been focused on outdoor environments with cell sizes generally within hundreds of meters. In [59] and [60], it has been shown that DAS reduces co-channel interference in a multicell environment, and hence significantly improves system performance and capacity, particularly for MTs near cell boundaries. A similar study was considered in [61] for outdoor systems, where the authors argue that the DAS always achieves higher capacity than any corresponding multi-antenna system using colocated antennas. However, the results provided in these previous studies cannot be applied directly to 3D in-building multi-floor propagation environments. Since the demand for high data rate services is predominantly from mobile users who are relatively stationary in cafés, restaurants, offices, hotels, shopping centers, bars, pubs, subways, gyms, train stations, airports, homes, and other in-building environments, providing good signal quality which is needed for high data rate services, through distributed antennas is crucial, especially in multi-storey building environments.

An alternative solution proposed in this thesis is in-building DAS, where each floor of multi-storey buildings is treated as a cell and multiple RAUs are distributed on every floor throughout the building, to provide dedicated in-building coverage.

The RAUs are spatially distributed so that they are always visible from a MT within every floor of the building. Each RAU is connected to a CU by means of optical fibre links. The distributed antennas creates the following potential benefits:

- Higher received signal strength due to reduced propagation distance between the transmitter (MT) and the receiver (RAU),

- lower transmit power and hence lower co-channel interference,

- increased spectral efficiency due to more spatial reuse in spatially separated floors,

- hence, higher data rates.

On the other hand, the in-building DAS is likely to face a critical problem of interference between co-channel cells which can severely limit the system capacity and performance.

## 3.2.1 Co-channel Interference

In order to meet the increasing demand for wireless communication services, the same frequency channels are reused within different cells due to the limited available spectrum. Frequency reuse causes co-channel interference, which is detrimental to system performance, reducing the reliability, data rate and the number of users that can be supported. Frequency reuse is widely used in outdoor mobile communication systems, but the resulting co-channel interference from neighbouring BSs can be reduced with careful deployment strategies [62, pp. 16-19]. However, reducing co-channel interference for systems operating indoors is a challenge because the reuse distances indoors are typically much smaller, and all transceivers are located in close physical proximity.

### 3.2.2 Inter-Floor Interference

Unlike two dimensional (2D) planar frequency reuse strategies developed for outdoor cellular systems employing DAS, multi-storey buildings encourage a 3D approach to system analysis and design. The in-building environment is considerably more compact and the propagation inside buildings has a more complex multipath structure than that of the outdoor mobile radio channel. The multipath generated by reflection from nearby buildings and transmission from other floors within the building may increase the level of interference, which may greatly diminish the advantages of DAS if the same frequency channels are reused in adjacent floors of high-rise buildings [63]. The shorter the distance between co-channel floors, the greater the influence of co-channel interference. Although the floors form natural boundaries, signals can leak onto adjacent floors of the building via mulitpaths. Estimating inter-floor interference in indoor environments is complicated by the large variability in building layout, architectural styles, and building materials. In dense urban environments, nearby buildings in close proximity can potentially reflect strong co-channel signals back onto other floors, further complicating the problem. This phenomenon is also significant when deploying indoor femtocell system which is another wireless technology planned for indoor environments [64]. Therefore, to analyse and design multi-floor in-building wireless systems with acceptable performance, it is necessary to develop a propagation channel model which accounts for inter-floor interference caused by the effect of the building structure and its terrain.

Therefore, this thesis explores the performance of in-building DAS for high data rate indoor communication in the presence of co-channel interference. Radio channel propagation characteristics in indoor high-rise buildings, with full frequency reuse among floors, and the resulting impact on system performance is studied. The quality of service provided to the users will depend on the strength of the desired signal and the relative strength of the interfering signal. The ratio between the

desired and interfering signal powers is termed the signal-to-interference ratio (SIR). However, due to multipath fading on the desired and interfering propagation paths, the instantaneous SIR will fluctuate and consequently lead to a higher BER. It should be noted that achieving adequate coverage (i.e. sufficient desired signal strength at the RAU) for in-building DAS is usually not an issue, as the distances between the MTs and RAUs are considerably shorter, rather it is interference (typically from vertically located co-channel systems) that constrains performance [65].

## 3.3 In-Building DAS Modelling

In this section the system models which are the necessary prerequisites for the following chapters of this thesis are presented. To be able to analyse and evaluate the performance of in-building DAS, models for signals and channel are needed. The mathematical technique to evaluate the SINR of the in-building DAS is also presented.

### 3.3.1 System Description and Channel Model

The uplink transmission model in a multi-storey building is shown in Figure 3.1, where each floor represents a cell equipped with evenly spaced, multiple ceiling mounted RAUs, which are located in the same position on every floor, to serve all MTs on each floor. The RAUs are connected to a CU where received signals are constructively processed. Each floor of the building has a similar construction with an open office interior floor plan and the same frequencies are assumed to be reused on each floor. However, frequency reuse within the same floor is avoided in order to reduce co-channel interference, which implies that co-channel interference can only emanate from nearby floors.

In the building, it is assumed there are a total of $U$ CUs, one on each floor and each CU connects to $N$ RAUs. For a simple analysis, it is assumed that the floors
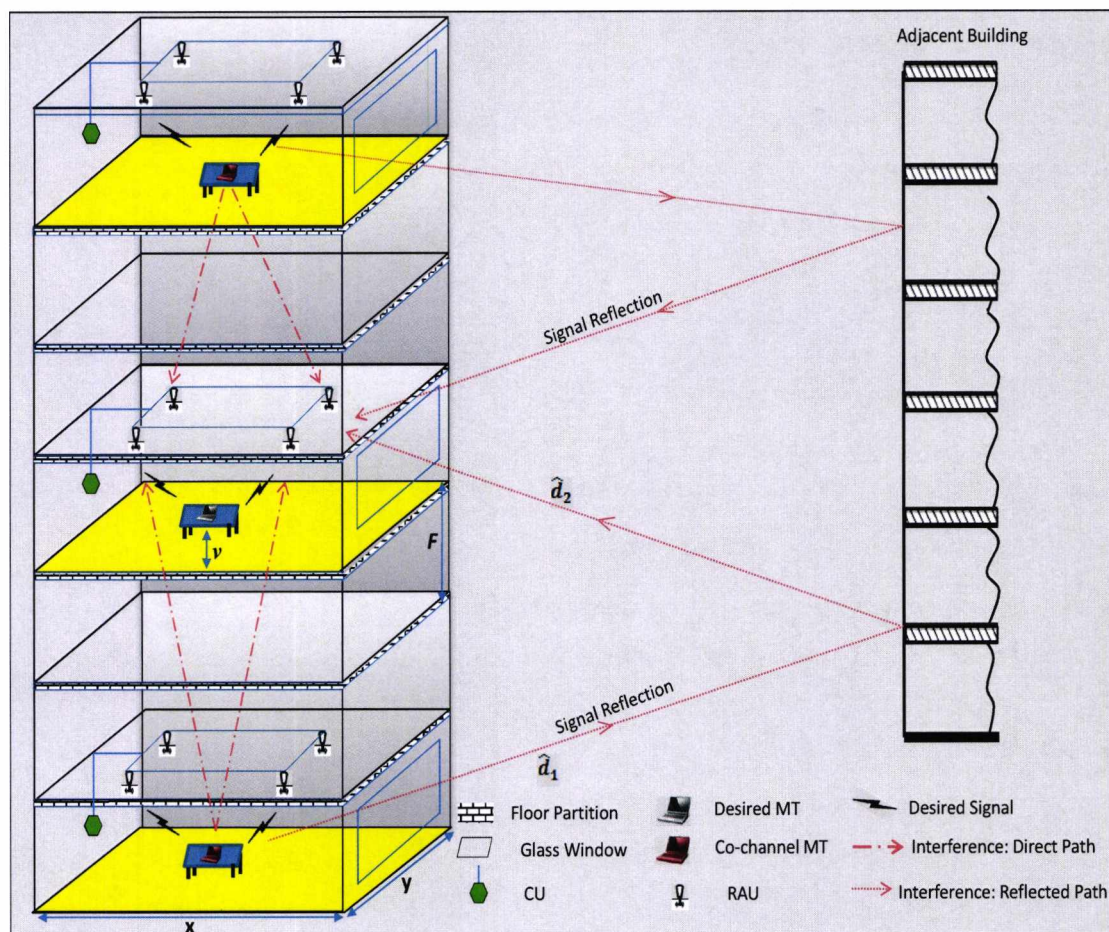
Figure 3.1: An illustration of in-building DAS with frequency reuse on every floor.

are shaped as cuboids with a common inter-floor spacing of $F$ meters and that there is one active MT evenly located across each floor at a height of $v$ meters. The MT of interest, $u'$, is located on the middle floor (reference floor) of the building. It is also assumed that there is a multi-storey building located a few meters away from the reference building.

In radio propagation between floors of high-rise buildings, experimental results have shown that there are two likely possible sources of interference. Depending on the structure of the building, and the location of the transmitter and the receiver, co-channel interference could emanate from [54]:

1. direct signal transmission through the floor partitions, which may include multiple reflections between the walls, floors and ceilings;

2. transmissions that involve signal reflections and scattering from nearby buildings that propagate back into the reference floor.

Although the dominant propagation path is via penetration through the floors, the reflection paths are largely free space and consequently may carry higher power, relative to paths penetrating through the floors after 2-3 floor separations. Thus, in the uplink transmission of the DAS considered in this chapter, the impact of co-channel interference from the direct and the reflected paths is studied. In this case, a RAU will receive a desired signal from a MT on the reference floor, and co-channel interfering signals from other MTs on co-channel floors via direct signal penetration through the floors and reflections from a nearby building.

The transmitted signal by MT-$u$ to the $n$-th RAU can be expressed as

$$\hat{x}_u(t) = Re\left[x_u(t)\right] = Re\left[\sqrt{P_s}\sum_{i=-\infty}^{\infty} b_u\left[i\right]\rho_{T_s}(t - iT_s)e^{j2\pi f_c t}\right] \tag{3.1}$$

where $Re[x]$ represents the real part of $x$, $x_u(t)$ is the complex representation of the transmitted signal, $P_s$ is the transmit power which is assumed to be the same for all MTs, $b_u[i]$ is the transmitted symbol with $E[b_u] = 0$ and $E[b_u \cdot b_u^*] = 1$, where $*$ represents the complex conjugate. $T_s$ represents the symbol duration, $\rho_{T_s}(t)$ is a pulse waveform defined as $\rho_{T_s}(t) = 1$ for $0 \leq t \leq T_s$ and $\rho_{T_s}(t) = 0$ otherwise and $f_c$ is the carrier frequency.

The channel from MT-$u$ to the $n$-th RAU on the reference floor is modelled as the sum of low pass equivalent impulse responses of the individual paths which can be expressed as

$$h_{u,n}(t) = h'_{u,n}(t) + \hat{h}_{u,n}(t) \tag{3.2}$$

where $h'_{u,n}(t)$ and $\hat{h}_{u,n}(t)$ are the impulse response for the paths that run through the floors (direct path) and the reflected paths from a neighbouring building, respectively.

The complex low pass equivalent impulse response for $h'_{u,n}(t)$ is expressed as

$$h'_{u,n}(t) = (d_{u,n})^{-\lambda/2} \cdot \varphi_{u,n}^{k/2} \cdot \alpha_{u,n} \cdot e^{j\theta_{u,n}} \cdot \delta(t - \tau_{u,n}) \tag{3.3}$$

where $(d_{u,n})^{-\lambda}$ is the distance dependent path loss when the signal propagates through the floors. $d_{u,n}$ is the distance between MT-$u$ and the $n$-th RAU on the reference floor. $\lambda$ is the path loss exponent of propagation and typically takes a value between 2 to 6 depending on the propagation condition (the variation can be attributed to the physical layout and type of building, as summarized in [49]). $\varphi_{u,n}$ is the penetration loss through a single floor and $k = u - u'$ represents the number of penetrated floors in the transmission path between MT-$u$ and the $n$-th RAU on the reference floor. The penetration loss introduced by each floor depends on the thickness and conductivity of the floor material. The reported penetration loss for floors made of concrete were found to be 10dB to 15dB per floor while those made of concrete over corrugated steel exhibit penetration loss as large as 26dB at 1700MHz (measurement values of penetration loss for different floor materials are summarized in [66]). It should be noted that, over the frequency range of interest (1.0-2.5 GHz) assumed in this thesis, the electromagnetic properties of typical materials encountered within buildings can be modelled as frequency independent [45]. In (3.3), $d_{u,n}$ is determined by the locations of the MT and the RAU. Assuming a $(x, y, z)$ Cartesian coordinate system, let $(x_u, y_u)$ denote the coordinate of the MT-$u$, and $(x_n, y_n)$ represents the coordinate of the $n$-th RAU on the reference floor. Then the MT-RAU distance in 3D space is given as

$$d_{u,n} = \sqrt{(x_u - x_n)^2 + (y_u - y_n)^2 + [Fk + (v - F)]^2} \tag{3.4}$$

Note that the number of intervening floors between the desired MT and its target RAU on the reference floor is zero (i.e. $k = 0$). $\alpha_{u,n}$, $\theta_{u,n}$ and $\tau_{u,n}$ in (3.3) are the channel fading coefficient, the path phase, and the path delay. It is assumed that transmission channels for all MTs are independent such that $\alpha_{u,n}$, $\theta_{u,n}$ and $\tau_{u,n}$ are

statistically independent. $\delta(t)$ denotes the Dirac delta function. It is assumed that $\theta_{u,n}$ and $\tau_{u,n}$ are uniformly distributed over $[0, 2\pi]$ and $[0, T_s]$ respectively.

Correspondingly, the complex low pass equivalent impulse response for $\hat{h}_{u,n}(t)$ in (3.2) can be expressed as

$$\hat{h}_{u,n}(t) = \left(\hat{d}_{u,n}\right)^{-\lambda/2} \cdot \hat{\varphi}_{u,n}^{1/2} \cdot \ddot{\varphi}_{u,n} \cdot \hat{\alpha}_{u,n} \cdot e^{j\hat{\theta}_{u,n}} \cdot \delta(t - \hat{\tau}_{u,n}) \quad (3.5)$$

where $\hat{d}_{u,n}$ denotes the distance between MT-$u$ and the $n$-th RAU on the reference floor when the signal is reflected by a neighbouring building as illustrated in Figure 3.1. $\hat{d}_{u,n}$ can be approximated as

$$\hat{d}_{u,n} = \hat{d}_1 + \hat{d}_2 \quad (3.6)$$

where $\hat{d}_1$ is the distance between MT-$u$ and the neighbouring building, and $\hat{d}_2$ is the length of the reflected path from the neighbouring building to the $n$-th RAU on the reference floor. In (3.5), $\hat{\varphi}_{u,n}$ is the reflection coefficient at the building surface and $\ddot{\varphi}_{u,n}$ is the transmission loss through the glass windows. $\hat{\alpha}_{u,n}$, $\hat{\theta}_{u,n}$ and $\hat{\tau}_{u,n}$ are the channel fading coefficient, the path phase and the channel delay of the reflected path respectively. The distribution of $\hat{\alpha}_{u,n}$ can be approximated as Rayleigh distribution since a LOS condition does not exist in the reflected signal path. $\hat{\theta}_{u,n}$ and $\hat{\tau}_{u,n}$ tend to have the same distribution as $\theta_{u,n}$ and $\tau_{u,n}$ respectively. The small delay spread relative to long symbol interval is assumed as in modulation schemes like orthogonal frequency division multiplex (OFDM) [67]. Hence, the effect of intersymbol interference (ISI) on the bit error rate (BER) performance is negligible.

Thus, in the examined building, when the MT and the RAUs are within the same floor of interest, intra-floor propagation is modelled as $(d_{u,n})^{-\lambda/2}$, however when the MT and the RAUs are on different floors, inter-floor propagation is modelled as $(d_{u,n})^{-\lambda/2} \cdot \varphi_{u,n}^{k/2} + \left(\hat{d}_{u,n}\right)^{-\lambda/2} \cdot \hat{\varphi}_{u,n}^{1/2} \cdot \ddot{\varphi}_{u,n}$ as indicated in (3.3) and (3.5).

### 3.3.2 Uplink Received Signal

The uplink received signal by the $n$-th RAU on the reference floor includes components from the desired MT-$u'$, co-channel interfering MT-$u$ from other floors of the building, and channel noise. This can be represented by its complex low-pass equivalent as

$$r_{u,n}(t) = x_{u'}(t) \otimes h_{u',n}(t) + \sum_{u=1,u\neq u'}^{U} x_u(t) \otimes h_{u,n}(t) + \eta_n(t)$$

$$= (d_{u',n})^{-\lambda/2} \cdot \alpha_{u',n} \cdot e^{j\theta_{u',n}} \cdot x_{u'}(t - \tau_{u',n})$$

$$+ \sum_{u=1,u\neq u'}^{U} (G_d + Q_r) \cdot x_u(t - \tau_{u,n}) + \eta_n(t) \qquad (3.7)$$

where $G_d = (d_{u,n})^{-\lambda/2} \cdot \varphi_{u,n}^k \cdot \alpha_{u,n} \cdot e^{j\theta_{u,n}}$, $Q_r = (\hat{d}_{u,n})^{-\lambda/2} \cdot \hat{\varphi}_{u,n}^{1/2} \cdot \ddot{\varphi}_{u,n} \cdot \hat{\alpha}_{u,n} \cdot e^{j\hat{\theta}_{u,n}}$ and $\eta_n(t)$ is the background additive white Gaussian noise (AWGN) at the $n$-th RAU, with zero mean and a double sided power spectral density $N_0/2$. The notation $\otimes$ denotes the convolution operation.

In [68], channel measurements were performed to determine channel characteristics in and around office and factory buildings where a LOS is present. The measurements showed that the propagation follows a Nakagami-$m$ fading distribution, where the received signal consists of several specular components plus several Rayleigh fading components. The Nakagami-$m$ distribution provides a very good fit for measured data in a variety of fading environments. Accordingly, the envelope of the desired signal is modelled by Nakagami-$m$ distribution. Hence, $\alpha_{u',n}^2$ is Gamma distributed with the PDF expressed as [69]

$$p_{\alpha_{u',n}^2}(\alpha_{u',n}^2) = \left(\frac{m_n}{\Omega_n}\right)^{m_n} \frac{(\alpha_{u',n}^2)^{m_n-1}}{\Gamma(m_n)} \exp\left(-\frac{m_n}{\Omega_n}\alpha_{u',n}^2\right), \qquad \alpha_{u',n} \leq 0 \qquad (3.8)$$

where $\Gamma(\cdot)$ is the gamma function defined by $\Gamma(x) = \int_0^\infty t^{x-1}e^{-t}dt$, $m_n$ is a parameter accounting for the fading severity and $\Omega_n$ is the average fading power of the received signal. The parameters $\Omega_n$ and $m_n$ may be expressed as $\Omega_n = E[\alpha_{u',n}^2]$ and $m_n =$

59

$\frac{\Omega_n^2}{E[(\alpha_{u',n}^2 - \Omega_n)^2]}$, $m_n \geq \frac{1}{2}$, respectively. It is assumed that interfering signals from other floors of the building have no specular component; therefore, the envelope of the interfering signal is Rayleigh distributed with mean square $E[\alpha_{u,n}^2] = 1$. The PDF of the instantaneous interfering signal power in a Rayleigh fading channel can be obtained by letting $m_n = 1$.

Assuming the phase and the path delay are known at the receiver and the receiver has a perfect timing synchronisation with the MT-$u'$ i.e., $\tau_{1,n} = 0$, the demodulated signal of MT-$u'$ over one symbol period $T_s$ is given by

$$Z_n = Re\left\{\frac{1}{T_s}\int_0^{T_s} r_{u,n}(t) \cdot e^{-j2\pi f_c t} \cdot e^{-j\theta_{u',n}} \, dt\right\} = Re\left[S_n + \sum_{u \neq u'}^{U} I_{u,n}\right] + \eta_n \quad (3.9)$$

where $S_n$ is the desired signal component received by the $n$-th RAU on the reference floor, expressed as

$$S_n = \frac{1}{T_s}\int_0^{T_s} (d_{u',n})^{-\lambda/2} \cdot \alpha_{u',n} \cdot e^{j\theta_{u',n}} \cdot x_{u'}(t) \cdot e^{-j\theta_{u',n}} \cdot e^{-j2\pi f_c t} dt$$

$$= \sqrt{P_s} \cdot \left(d_{u',n}\right)^{-\lambda/2} \cdot b_{u'} \cdot \alpha_{u',n} \quad (3.10)$$

$I_{u,n}$ is the interfering signal component received from other floors by the $n$-th RAU on the reference floor, expressed as

$$I_{u,n} = \frac{1}{T_s}\int_0^{T_s}\left(G_d \cdot x_u(t - \tau_{u,n}) \cdot e^{-j\theta_{u,n}} + Q_r \cdot x_u(t - \hat{\tau}_{u,n}) \cdot e^{-j\hat{\theta}_{u,n}}\right) dt$$

$$= \frac{\hat{G}_d}{T_s}\left(\int_0^{\tau_{u,n}} b_u[i] + \int_{\tau_{u,n}}^{T_s} b_u[i+1]\right) dt + \frac{\hat{Q}_r}{T_s}\left(\int_0^{\tau_{u,n}} b_u[i] + \int_{\tau_{u,n}}^{T_s} b_u[i+1]\right) dt$$

$$= \frac{\hat{G}_d}{T_s}\left[b_u[i] \cdot (\tau_{u,n}) + b_u[i+1] \cdot (T_s - \tau_{u,n})\right] + \frac{\hat{Q}_r}{T_s}\left[b_u[i] \cdot (\hat{\tau}_{u,n}) + b_u[i+1] \cdot (T_s - \hat{\tau}_{u,n})\right]$$

$$(3.11)$$

where $\hat{G}_d = (d_{u,n})^{-\lambda/2} \cdot \varphi_{u,n}^k \cdot \alpha_{u,n} \cdot e^{j(\theta_{u,n} - \theta_{u',n})}$ and $\hat{Q}_r = (\hat{d}_{u,n})^{-\lambda/2} \cdot \hat{\varphi}_{u,n}^{1/2} \cdot \ddot{\varphi}_{u,n} \cdot \hat{\alpha}_{u,n} \cdot e^{j(\hat{\theta}_{u,n} - \theta_{u',n})}$. $b_u[i]$ and $b_u[i+1]$ are the previous and current symbols transmitted by the MT-$u$ within $[0, T_s]$ respectively. The total co-channel interference term received

60

by the $n$-th RAU on the reference floor, denoted by $I_u$, is written as

$$I_u = \sum_{u=1,u\neq u'}^{U} I_{u,n} \tag{3.12}$$

The expectation of $I_u$ can be easily derived as $E[I_u] = 0$ and the variance denoted by $\sigma_{I_u}^2$ is derived in Appendix A as

$$\sigma_{I_u}^2 = \frac{P_s}{3} \sum_{u\neq u'}^{U} [(d_{u,n})^{-\lambda}\varphi_{u,n}^k + (\hat{d}_{u,n})^{-\lambda}\hat{\varphi}_{u,n}\ddot{\varphi}_{u,n}^2] \tag{3.13}$$

Since the number of interfering sources is sufficiently large and interfering sources are independent of each other, the total co-channel interference term $I_u$, can be approximated as a zero mean Gaussian distributed random variable by invoking the central limit theorem (CLT) [69]. The assumption that the multiple access interference is Gaussian distributed is valid for a large number of interferers, and when the interference emanates from a sufficiently large number of independent components.

If there are only a small number of mobiles in the system, the Gaussian Approximation has been shown to underestimate the BER. An improved Gaussian approximation has been developed by Morrow and Lehnert [70] to yield more accurate predictions. However, this technique requires significantly more computational effort than the standard Gaussian approximation. In this thesis, multiple floors are considered, and each floor has more than one RAU, thus sufficiently large number of independent interfering components are assumed and for this reason the standard Gaussian approximation is considered to be sufficiently accurate. This assumption has since been the basis of the many studies investigating the performance of wireless systems in the presence of co-channel interference [60-62, 67, 71-77].

In (3.9), $\eta_n$ is the noise component with zero mean and a variance of $\sigma_\eta^2 = N_0/(2T_s)$, which is assumed to be equal for all RAUs.

61

### 3.3.3  Minimum Mean Square Error Combining

At the receiver, the minimum mean square error combining (MMSEC) is applied, where the received signal by the $n$-th RAU, given in (3.9), is multiplied by a controllable weight (Figure 3.2) in order to achieve spatial diversity.
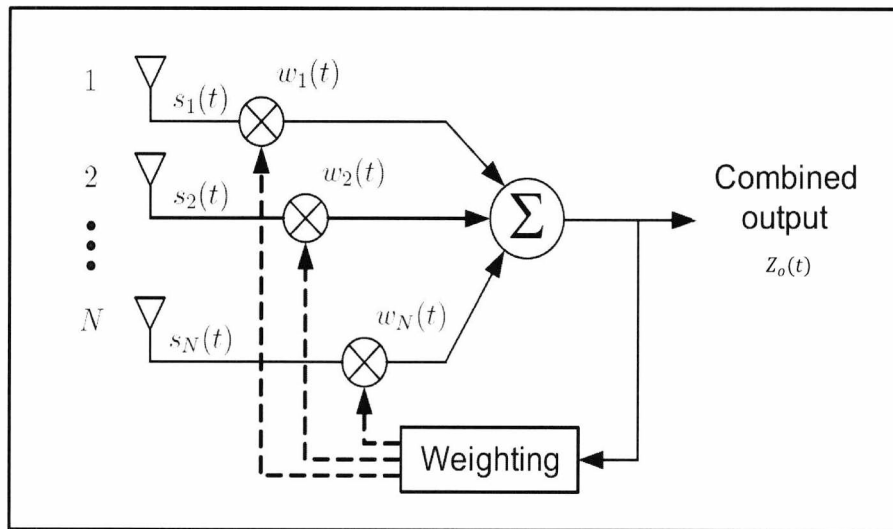


Figure 3.2: Diagram of MMSEC diversity scheme.

In the MMSEC spatial diversity scheme [71, p 437], the combiner output used for the detection is a linear combination of the weighted signals of all RAUs. The decision variable for detecting the desired signal on the reference floor using MMSEC is given by

$$Z_0 = W_n \cdot Z_n = \sum_{n=1}^{N} \left( W_n \cdot S_n + W_n \cdot \sum_{u \neq u'}^{U} I_{u,n} + W_n \cdot \eta_n \right) \qquad (3.14)$$

where $W_n$ is the optimum weight which maximizes the SINR. In the presence of co-channel interference, MMSEC spatial diversity is used not only to combat the fading of the desired signal (as with maximal ratio combining - MRC, which is the optimal combiner in a noise only system) but also to suppress the power of the interfering signals at the receiver. However, when there is no interference, MMSEC maximizes

62

the output signal-to-noise ratio (SNR) and its performance is then equivalent to that of MRC. For comprehensive discussions of various diversity schemes and the derivation of corresponding weight vectors, the reader is referred to [71, pp. 363-412]. The optimum weight $W_n$ in (3.14) is expressed as [72]

$$W_n = \frac{\alpha_{u'n}}{\rho_n} \tag{3.15}$$

where $\alpha_{u'n}$ is the channel fading coefficient of the desired signal and $\rho_n$ is the variance of the interfering signal plus background noise at the $n$-th RAU on the reference floor. $\rho_n$ is written as

$$\rho_n = E\left[I_u \cdot I_u^*\right] + \sigma_\eta^2 \tag{3.16}$$

Substituting $E\left[I_u \cdot I_u^*\right]$ with (A.4) as derived in Appendix A into (3.16), $\rho_n$ is rewritten as

$$\rho_n = \frac{P_s}{3} \sum_{u \neq u'}^{U} [(d_{u,n})^{-\lambda}\varphi_{u,n}^k + (\hat{d}_{u,n})^{-\lambda}\hat{\varphi}_{u,n}\ddot{\varphi}_{u,n}^2] + \sigma_\eta^2 \tag{3.17}$$

Therefore the optimum weight $W_n$ is expressed as

$$W_n = \frac{\alpha_{u',n}}{\frac{P_s}{3} \sum_{u \neq u'}^{U} [(d_{u,n})^{-\lambda}\varphi_{u,n}^k + (\hat{d}_{u,n})^{-\lambda}\hat{\varphi}_{u,n}\ddot{\varphi}_{u,n}^2] + \sigma_\eta^2} \tag{3.18}$$

Correspondingly, given the location $(x_u, y_u)$ of the desired MT-$u'$, the instantaneous SINR may be obtained as

$$\gamma(x_u, y_u) = \sum_{n=1}^{N} \gamma_n(x_u, y_u) = \frac{\left(\sum_{n=1}^{N} W_n S_n\right)^2}{\sum_{n=1}^{N} W_n^2 \sigma_{I_u}^2 + \sum_{n=1}^{N} W_n^2 \sigma_\eta^2} = \sum_{n=1}^{N} \frac{A_n^2}{\rho_n} \alpha_{u',n}^2 \tag{3.19}$$

where $\gamma_n(x_u, y_u)$ is the SINR per RAU and $A_n^2 = P_s(d_{u',n})^{-\lambda}$. The average SINR, defined as the ratio of the average received desired signal power to the average received interfering signal power plus noise power, can be expressed as

$$\bar{\gamma}(x_u, y_u) = \sum_{n=1}^{N} \frac{P_s \cdot (d_{u',n})^{-\lambda}}{\frac{P_s}{3} \sum_{u=1, u \neq u'}^{U} [D_u + R_u] + \frac{N_0}{2T_s}} \cdot \Omega_n$$

$$= \sum_{n=1}^{N} \frac{\frac{2E_s}{N_0} \cdot (d_{u',n})^{-\lambda}}{\frac{2}{3} \cdot \frac{E_s}{N_0} \sum_{u=1, u \neq u'}^{U} [D_u + R_u] + 1} \cdot \Omega_n \tag{3.20}$$

where $D_u = (d_{u,n})^{-\lambda} \varphi_{u,n}^k$ and $R_u = (\hat{d}_{u,n})^{-\lambda} \hat{\varphi}_{u,n} \ddot{\varphi}_{u,n}^2$. $\frac{E_s}{N_0}$ is the ratio of the transmit symbol energy to noise power density at the MT, where $E_s$ is expressed as

$$E_s = P_s \cdot T_s \tag{3.21}$$

Since $\alpha_{u'n}^2$ is Gamma distributed, the PDF of the instantaneous SINR, $\gamma(x_u, y_u)$, in (3.19), for arbitrary values of the Nakagami fading parameters is then obtained as [73]

$$P_{\gamma(x_u,y_u)}(\gamma) = \frac{1}{\pi} \int_0^\infty \frac{\cos\left[\sum_{n=1}^N m_n \tan^{-1}\left(\frac{t}{\beta_n}\right) - t\gamma\right]}{\prod_{n=1}^N \left(1 + \left(\frac{t}{\beta_n}\right)^2\right)^{m_n/2}} dt \tag{3.22}$$

where $\beta_n = m_n / \bar{\gamma}_n(x_u, y_u)$. In the case where $\alpha_{u'n}^2$ is assumed to be Rayleigh distributed, $P_{\gamma(x_u,y_u)}(\gamma)$ is obtained by letting $m_n = 1$. The SINR is largely a function of the propagation environment, the number and the specific location of the MTs.

## 3.4 Summary

This chapter has extended the propagation studies considered in Chapter 2 to analyse the performance of in-building DAS in the presence of co-channel interference in a multi-storey building. Unlike the propagation studies in 2D outdoor DASs, this thesis is unique in that it considers a 3D approach to investigate inter-floor propagation between floors of a generalised multi-storey building, and the impact of a neighbouring building is studied. In the building examined, co-channel inference could emanate from paths penetrating through the floors, and signal reflections from a neighboring building. Propagation channel models and techniques for evaluating the performance of in-buidling DAS were presented. The considered building is simple, but broadly representative for many modern building environments, and serves as a good starting point for inter-floor performance analysis of wireless systems employing DAS. The resulting system model is the basis for the subsequent system performance analyses discussed in Chapters 4, 5 and 6.

# Chapter 4

# Achievable Spectral Efficiency Performance of In-Building DAS

## Contents

## 4.1 Introduction

As discussed in the thesis introduction, the radio spectrum available for wireless services is extremely scarce, while high data rate services are increasingly demanded particularly within buildings. Hence, spectral efficiency is of primary concern in the design of future indoor wireless communication systems. The performance of the systems is largely limited by interference from other systems (MTs) operating over the same frequency bands. In order to evaluate the system performance in the presence of interference, the desired and interfering signal power from transceivers

operating within the building are required as investigated in Chapter 3, based on the underlying propagation and channel model for the building structure and its terrain. Accordingly, the effects of different system parameters on the performance of the in-building DAS is investigated in this chapter using the system models. The spectral efficiency achievable is used as the metric to measure the performance of the system, which is evaluated for different possible MT locations evenly spaced across the entire floor of the building. For each MT location, the achievable spectral efficiency is computed under a specified BER constraint in order to determine the achievable data rate. Section 4.2 derives location-specific spectral efficiency and discusses a location-specific RAU selection strategy. A range of representative numerical results are presented in Section 4.3 and a summary of the findings in this chapter is presented in Section 4.4.

## 4.2  Achievable Spectral Efficiency

In this section, the location-specific uplink spectral efficiency achievable in the in-building DAS is defined. The adaptive multi-level quadrature amplitude modulation (MQAM) which dynamically determines the modulation level based on the received SINR is applied to maximize spectral efficiency while keeping the BER under a target value [74-76]. This is essential since most applications require a certain maximum BER. During a good channel condition, a higher order modulation level is used, while during a poor channel condition, a lower modulation level is used. The relationship between BER and SINR, $\gamma$, under a certain modulation level $M_j = 2^j$ for MQAM can be approximated as [77]

$$\hat{P}_e(\gamma) = \frac{1}{5} \exp\left[\frac{-3\gamma}{2(2^j - 1)}\right] \tag{4.1}$$

where $j$ (an even number) is the number of bits per symbol. Given a target instantaneous BER equal to $\hat{P}_0$, the region boundaries (or adaptive modulator switching

thresholds) $\gamma_j$ for switching across the modulation levels can be solved from (4.1) and may be expressed as

$$\gamma_j = -\frac{2}{3}\ln(5\hat{P}_0)(2^j - 1); \quad j = 0, 2, 4, \cdots, J \tag{4.2}$$

The average spectral efficiency with unit of bits per second per Hertz, is the sum of the data rates $\log_2(M_j) = j$ weighted by the probability that the $j$-th modulation constellation is assigned to MT-$u'$. Given the location of MT-$u'$, this can be expressed as

$$T_u(x_u, y_u) = \sum_{j=1}^{J} \log_2(M_j) \int_{\gamma_j}^{\gamma_{j+1}} P_{\gamma(x_u,y_u)}(\gamma)d\gamma \tag{4.3}$$

where the values of $\gamma_j$ and $\gamma_{j+1}$ are obtained respectively according to (4.2), for a given $\hat{P}_0$. Note that $\gamma_{J+1} = +\infty$. By substituting (3.22) in Chapter 3 into (4.3), interchanging the order of integration and simplifying trigonometric identities, $T_u$ is rewritten as

$$\begin{aligned}
T_u(x_u, y_u) = \sum_{j=1}^{J} \log_2(M_j) \\
\times \frac{1}{\pi} \int_0^{\infty} -\frac{\sin(B_1(t) - t\gamma_{j+1}) - \sin(B_1(t) - t\gamma_j)}{tB_2(t)} dt
\end{aligned} \tag{4.4}$$

where $B_1 = \sum_{n=1}^{N} m_n \cdot \tan^{-}1(\frac{t}{\beta_n})$ and $B_2 = \prod_{n=1}^{N}(1 + (\frac{t}{\beta_n})^2)^{m_n/2}$. In general, the integral in (4.4) can be computed numerically using computer software such as MATLAB.

## 4.2.1 Location-Specific Antenna Selection

In this section, a location-specific antenna selection strategy, where a subset of $N'$ strongest RAUs out of $N$ available RAUs is selected for combining, is investigated in the in-building DAS.

Due to the range of geometric arrangements possible with MTs and RAUs in uplink transmission analysis, it is observed that there is the potential for a co-channel MT located directly above the reference floor, to get very close to a RAU located on

the reference floor, such that the distance between the co-channel MT and the desired RAU on the reference floor is less than the distance between the desired MT and reference RAUs on the reference floor, i.e. $d_{u,n} < d_{u',n}$. Accordingly, the achievable spectral efficiency is found to depend not only on the proximity of the desired MT to its RAU, but also very much on the location of the co-channel MT within the building because the path loss of the interfering signal can be much smaller than that of the desired signal in some locations across the floor. This finding is significant in terms of the number of RAUs to be selected for combining from $N$ diversity branches.

For various geometric arrangements of MTs described by Figure 4.1, $N$ RAUs are deployed on each floor and the performance of the system is evaluated with the system model, in order to show the effect of location of the desired MT and the co-channel MTs on the selection of RAUs. Figure 4.1(a) and (b) show two types of layouts for RAU deployment on each floor, (a) is the single line configuration, and (b), the square configuration. The achievable spectral efficiency is obtained by moving both the desired MT on the reference floor and the co-channel MTs on the co-channel floors over a large number of locations across the entire floor. Although an increase in average spectral efficiency is expected with increasing number of RAUs, it is important to note that some RAUs would have insignificant contribution to the total received signal. This is either due to large transmission path loss or the effect of co-channel MTs getting very close to RAUs located on the reference floor as shown in Figure 4.1(c)-(e). These RAUs could be discarded to avoid interference and to save a considerable amount of the receiver's signalling overhead. In conventional 2D outdoor DAS in cellular networks, the RAUs with the shortest distance to the MT would be selected for combining [17]; however, selecting such RAUs for uplink transmission of 3D inter-floor communication may not enhance the performance of the system if a co-channel MT is located on a floor directly above (or below) the selected RAU. Therefore, a selection strategy which determines the appropriate RAUs to select for combining based on specific location of MTs is proposed. For example, if both the

(a) Scenario I:- Single Line Configuration

(b) Scenario II:- Square Configuration

(c)

(d) – Best Case

(e) – Worst Case

(f) MT Location

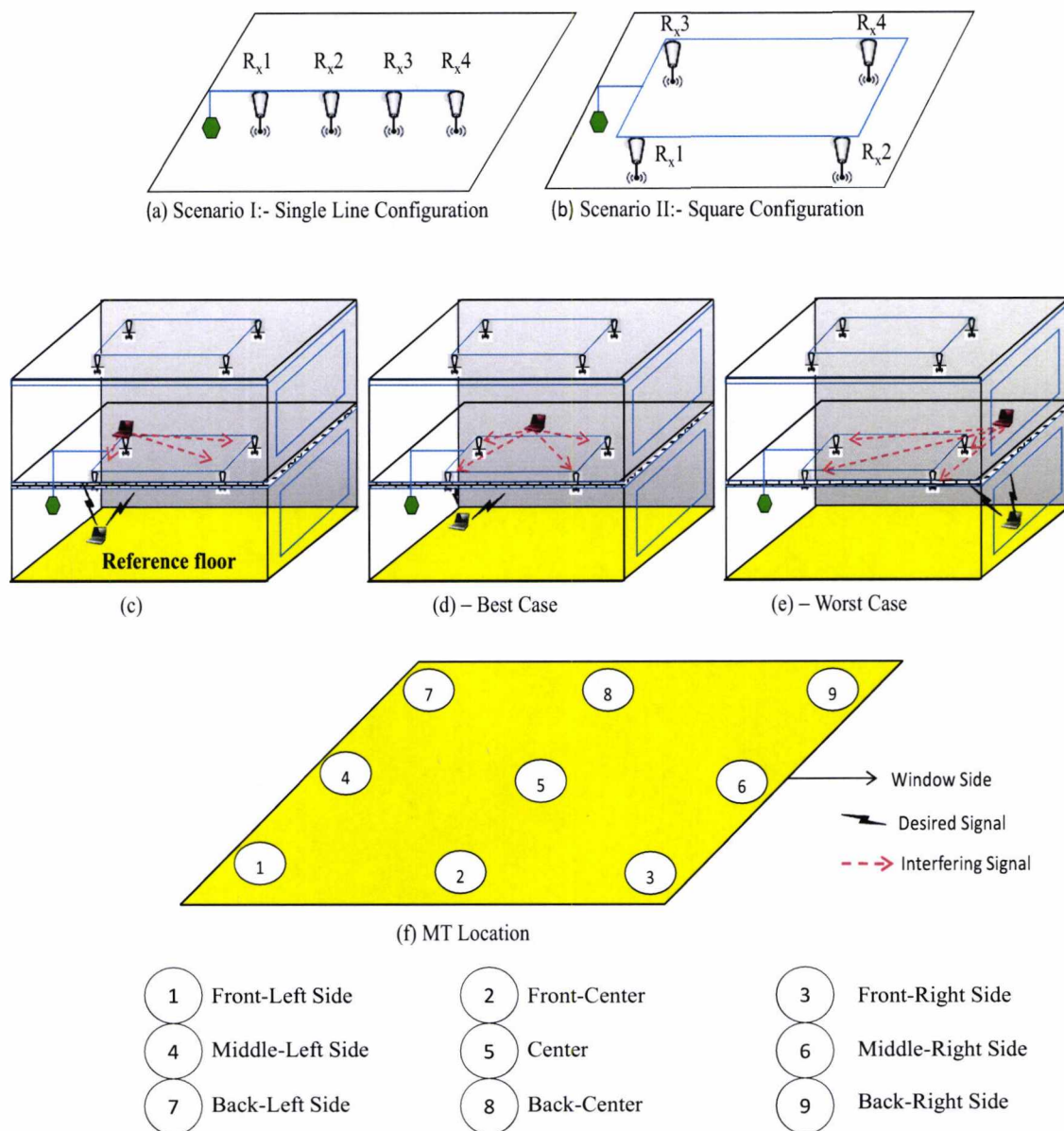| | | | | | |
|---|---|---|---|---|---|
| 1 | Front-Left Side | 2 | Front-Center | 3 | Front-Right Side |
| 4 | Middle-Left Side | 5 | Center | 6 | Middle-Right Side |
| 7 | Back-Left Side | 8 | Back-Center | 9 | Back-Right Side |

Figure 4.1: RAU locations and MT geometrical arrangements.

desired and co-channel MT are located at the center of the floor, all $N$ RAUs can be selected for combining, however, when both MTs are located at the window side of the floor, selecting just two RAUs may in fact be sufficient. This way, the receiver would only combine RAUs with significant SINRs at any location across the entire floor before taking detection decision. This insight is validated by simulation in Section 4.2.2 through Figure 4.6, where the achievable spectral efficiency is shown as a function of the parameter SNR for different values of $N'$ at specific locations of MTs.

## 4.2.2   Numerical Results

In this section, a range of results for illustrating the achievable spectral efficiency of the exemplified DAS in high-rise buildings is presented.

In order to analyse the system numerically, the analytic formulas derived in Chapter 3 are evaluated for the multi-storey building structure shown in Figure 3.1 in an uplink scenario. A summary of parameters used in evaluating the performance of the system is listed in Table 4.1, unless specified otherwise.

### Performance Comparisons - Two RAU Deployment Options

RAU deployment is a factor that can cause significant variations in the achievable spectral efficiency. Consequently, the analysis for the two RAU layout scenarios have been considered.

Figure 4.1 shows the two RAU deployment scenarios and various possible MT location combinations across the entire floor. In Scenario I, there are 4 ceiling mounted RAUs aligned horizontally and evenly spaced across the center of the floor as shown in Figure 4.1(a) (single line configuration). Scenario II is identical to Scenario I except that RAU positions are transposed to opposite sides of the floor as shown in Figure 4.1(b), a square configuration which results in 2 RAUs on all sides of

Table 4.1: Summary of Parameters

| Parameters | Value |
|---|---|
| Number of floors in the building, $U$ | 7 |
| Inter-floor spacing, $F$ | 4m |
| Floor dimension, $(x, y)$ | 40m X 40m |
| MT located across the floor at height, $v$ | 1m |
| Number of RAUs on each floor, $N$ | 4 |
| Path loss exponent, $\lambda$ | 2.5 |
| Penetration loss, $\varphi$ | 13dB |
| Reflection loss, $\hat{\varphi}$ | 8dB |
| Transmission loss through a glass window, $\ddot{\varphi}$ | 0.13dB |
| Distance between the reference and the adjacent building, $\hat{d}_{u,n}$ | 10m |
| Nakagami fading value, $m$ | $1.8, 1.5, 1.25, 1.0$ |
| Threshold value, $T$ | 0.6 |
| Transmit SNR, $E_s/N_0$ | 30dB |
| Target BER, $\hat{P}_0$ | $10^{-3}$ |

the floor. Note that when the positions $(x_u, y_u)$ and $(x_n, y_n)$ are given, the distances from MTs to RAUs can be calculated. Consequently, the SINRs can be obtained and the achievable spectral efficiency can be evaluated using the analytics results in Chapter 3. Thus, for various MT location combinations, the achievable spectral efficiency is compared for both scenarios as shown in Table 4.2. Clearly, for Scenario II, the achievable spectral efficiency is considerably better than that of Scenario I, especially at the floor sides/boundaries owing to the short distances between the desired MT and the RAUs in this configuration. For example, for Scenario II, it is observed that 25.9% of location combinations show high spectral efficiency values greater than 5.0 bits/sec/Hz, a value close to the best case, while for Scenario I, high

71

Table 4.2: Achievable Spectral Efficiency for Two RAU Deployment Scenarios and Various MT Location Combinations

| Co-channel MT Location | Scenario I | Scenario II | Scenario I | Scenario II | Scenario I | Scenario II |
|---|---|---|---|---|---|---|
| - | Desired MT Location = ① | | Desired MT Location = ② | | Desired MT Location = ③ | |
| ① | 3.1148 | 1.8744 | 3.3960 | 2.4348 | 3.2852 | 5.7363 |
| ② | 3.1290 | 5.4714 | 3.2388 | 3.2352 | 3.0378 | 5.3594 |
| ③ | 3.2236 | 5.7231 | 3.2502 | 2.4759 | 2.8823 | 1.7823 |
| ④ | 2.3175 | 5.5106 | 2.8431 | 3.4340 | 2.9911 | 5.8831 |
| ⑤ | 2.5475 | 5.7319 | 2.5027 | 3.3939 | 2.4563 | 5.6138 |
| ⑥ | 2.9747 | 5.8583 | 2.7753 | 3.3007 | 2.2088 | 5.2299 |
| ⑦ | 3.1148 | 5.8156 | 3.3960 | 3.4773 | 3.2852 | 5.9062 |
| ⑧ | 3.1290 | 5.9167 | 3.2388 | 3.5409 | 3.0378 | 5.7991 |
| ⑨ | 3.2236 | 5.8803 | 3.2502 | 3.3139 | 2.8823 | 5.5093 |
| - | Desired MT Location = ④ | | Desired MT Location = ⑤ | | Desired MT Location = ⑥ | |
| ① | 5.5293 | 2.4784 | 5.8215 | 2.8446 | 5.8322 | 3.4419 |
| ② | 5.6251 | 3.4234 | 5.5926 | 3.1666 | 5.4708 | 3.3333 |
| ③ | 5.8024 | 3.3981 | 5.6507 | 2.7303 | 5.1987 | 2.3714 |
| ④ | 4.3626 | 3.2877 | 5.1475 | 3.2208 | 5.6142 | 3.5742 |
| ⑤ | 4.9258 | 3.4385 | 4.5152 | 3.1810 | 4.7744 | 3.3489 |
| ⑥ | 5.6123 | 3.5213 | 5.0553 | 3.0906 | 4.1922 | 3.0660 |
| ⑦ | 5.5293 | 2.4784 | 5.8215 | 2.8446 | 5.8322 | 3.4419 |
| ⑧ | 5.6251 | 3.4234 | 5.5926 | 3.1666 | 5.4708 | 3.3333 |
| ⑨ | 5.8024 | 3.3981 | 5.6507 | 2.7303 | 5.1987 | 2.3714 |
| - | Desired MT Location = ⑦ | | Desired MT Location = ⑧ | | Desired MT Location = ⑨ | |
| ① | 3.1148 | 5.8156 | 3.3960 | 3.4773 | 3.2852 | 5.9062 |
| ② | 3.1290 | 5.9167 | 3.2388 | 3.5409 | 3.0378 | 5.7991 |
| ③ | 3.2236 | 5.8803 | 3.2502 | 3.3139 | 2.8823 | 5.5093 |
| ④ | 2.3175 | 5.5106 | 2.8431 | 3.4340 | 2.9911 | 5.8831 |
| ⑤ | 2.5475 | 5.7319 | 2.5027 | 3.3939 | 2.4563 | 5.6138 |
| ⑥ | 2.3175 | 5.8583 | 2.7753 | 3.3007 | 2.2088 | 5.2299 |
| ⑦ | 3.1148 | 1.8744 | 3.3960 | 2.5348 | 3.2852 | 5.7363 |
| ⑧ | 3.1290 | 5.4714 | 3.2388 | 3.2352 | 3.0378 | 5.3594 |
| ⑨ | 3.2236 | 5.7231 | 3.2502 | 2.4759 | 2.8823 | 1.7823 |
| Overall Average | Scenario I = 3.7784 | | | Scenario II = 4.0817 | | |

spectral efficiency values greater than 5.0 bits/sec/Hz occur only when the desired MT is located at the middle-left, center and middle-right sides of the floor. However, it is important to note that low spectral efficiency (near the worst case value) associated with the likelihood of co-channel MTs getting very close to RAUs located on the reference floor, are not likely to occur very often when RAUs are deployed in a single line. For example, for Scenario I, it is observed that only 4.1% of MT location combinations show spectral efficiency lower than 2.5 bits/sec/Hz, while for Scenario II, 8.9% of MT location combinations show low spectral efficiency close to the worst case value. The average of these spectral efficiencies over a very large number of uniformly distributed MT locations on the floor, shows that RAU deployment according to Scenario II is more preferable. (This indicates that RAU positions is important in the design of in-building wireless system for high data rates). Scenario II will be assumed from hereon except specified otherwise.

Figures 4.2(a)-(d) show the location-specific achievable spectral efficiency over a range of possible locations of the desired MT across the reference floor. In Figures 4.2(a)-(c), RAUs are deployed according to Scenario II (Figure 4.1(b)) and co-channel MTs are located at the back-left, center and back-right side of the co-channel floor respectively. In these figures, the position $(40, x_u)$ corresponds to the window side of the building. In Figure 4.2(d), RAUs are deployed according to Scenario I (Figure 4.1(a)) and co-channel MTs are located at the center of the co-channel floor. It is observed that the performance varies significantly and is strongly dependent on the specific location of the desired and the co-channel MTs. The achievable spectral efficiency shows four peaks at the location of the 4 RAUs; however, when the desired and the co-channel MTs are aligned at a RAU location, the performance degrades at that location as shown in Figures 4.2(a) and (c), reaching values as low as 1.7 bits/sec/Hz. These effects are caused by the relative distance of the desired MT and the interfering MT to the target RAUs on the reference floor. In floor regions where the spectral efficiency is low, signals received from adjacent floors are substantially
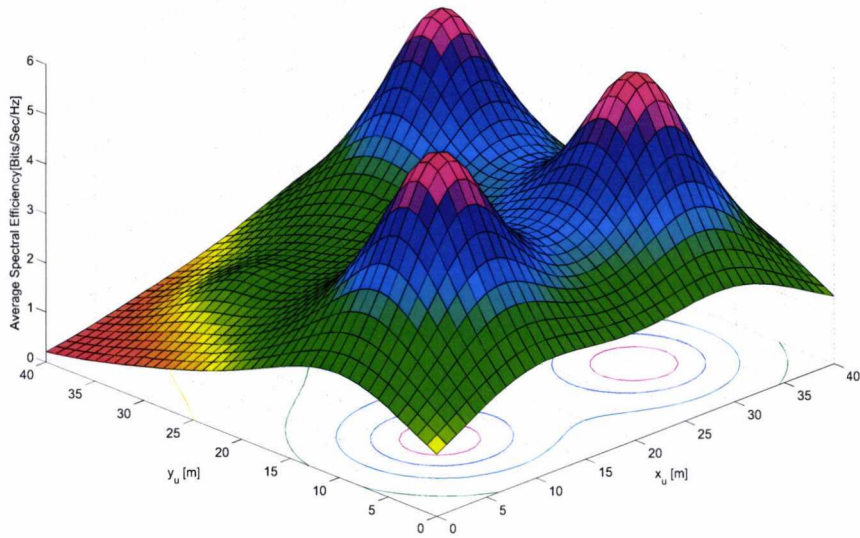
(a) Co-channel MT located at the back-left side of the floor, a position corresponding to one RAU location

Figure 4.2. Location-specific achievable spectral efficiency
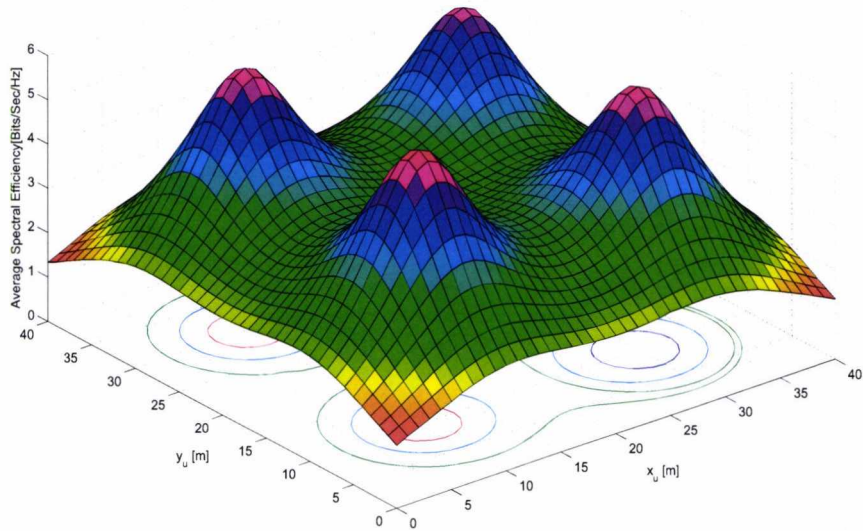


(b) Co-channel MT located at the floor center

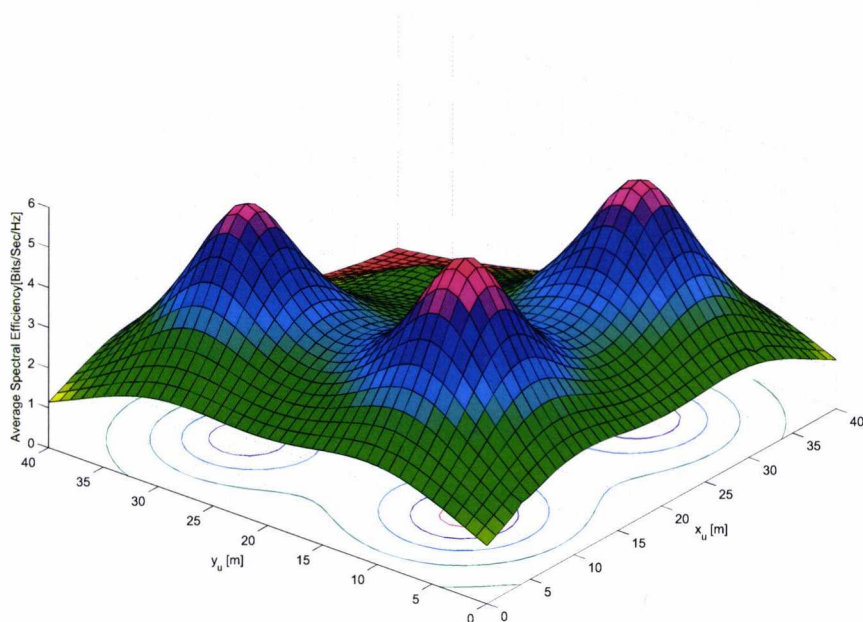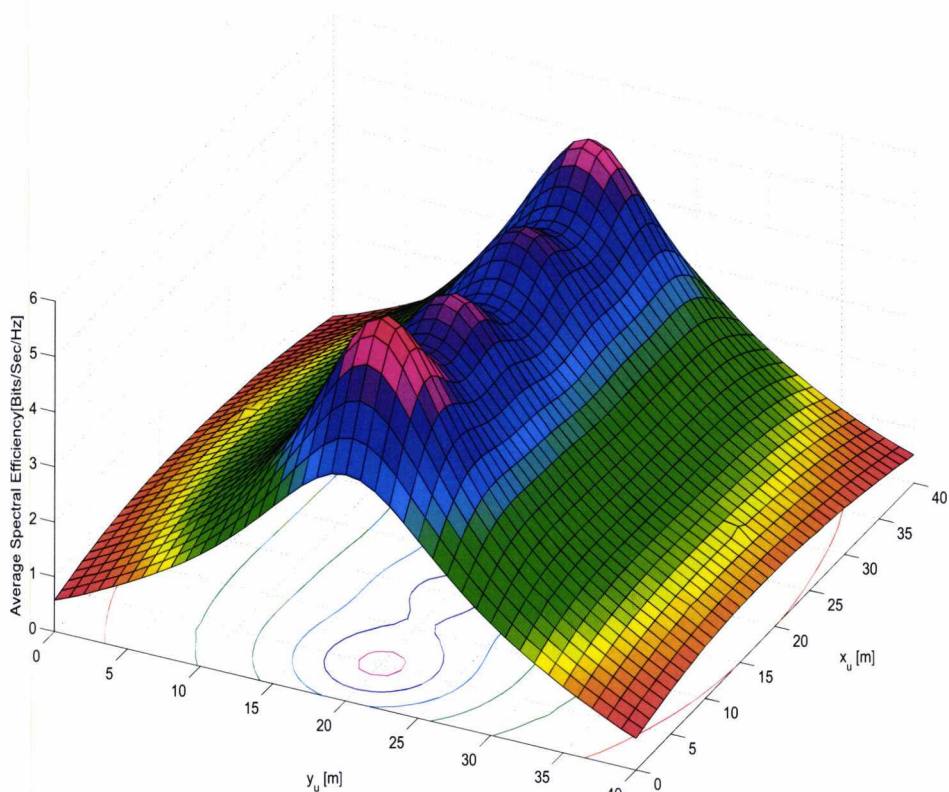Figure 4.2. Location-specific achievable spectral efficiency

(c) Co-channel MT located at the back-right side of the floor, a position corresponding to one RAU location

Figure 4.2. Location-specific achievable spectral efficiency

stronger due to increased proximity to RAUs on the reference floor, and consequently are comparable in magnitude (despite the 13 dB floor attenuation) to signals propagating through the floor. Another observation to note from Figures 4.2(a)-(c) is the difference in achievable spectral efficiency as the co-channel MT moves closer to the right side (window side) of the floor. This difference is due to significant contribution from reflected paths through the window as the co-channel MT moves closer to the window, which consequently reduces the achievable spectral efficiency. The worst-case spectral efficiency is observed when the desired MT and the co-channel MT are located at the window side as shown in Figure 4.2(c). At this location, the distances between desired MT and the RAUs are no smaller than any other location across the floor. Furthermore, the distances between co-channel MTs and the neighbouring building are shortest at this location. In Figure 4.2(d), it is found that the performance of the system is lower at the floor boundaries as observed in Table II. This is due to increased path loss of the desired signal which is significantly greater

75

(d) Co-channel MT located at the floor center

Figure 4.2. Location-specific achievable spectral efficiency for Scenario I

in the RAU deployment in Scenario I, Figure 4.1(b).

The advantage of the above analysis is that, it not only takes into account the performance of the system associated with fading and the effect of co-channel interference, but it also takes into account the likelihood of MTs being in certain locations across the floor. Thus, based on the analysis of location-specific spectral efficiency, resource allocation can be done efficiently through intelligent channel reuse in a multi-user environment. For example, an MT can be assigned the same channel if a co-channel MT is not vertically aligned at the same location on immediate adjacent floors of the building.

Figures 4.3(a)-(c) provide the achievable spectral efficiency associated with a

range of geographical arrangements of MTs, as a function of the parameter SNR. Specifically, the performance of the system is evaluated when both the desired at the co-channel MT are located in different positions within the building as shown in Figure 4.1(f). These figures clearly demonstrate that the performance of in-building systems is strongly dependent of the specific location of both the desired and the co-channel MTs across the floor. These results have been obtained by considering RAU deployment according to scenario II. Similar to results in Figures 4.2, it is evident from Figures 4.3(a)-(c) that when the desired MT and the co-channel MT are aligned, the achievable spectral efficiency degrades at that location due to similar distances of the desired MT and the strongest co-channel MT to the receiving RAUs. In Figure 4.3(a), spectral efficiency grows linearly at low SNR region; however, at SNR larger than 35dB, the performance of the system varies. The difference in performance lies in the variability of inter-floor interference. When the co-channel MTs are located
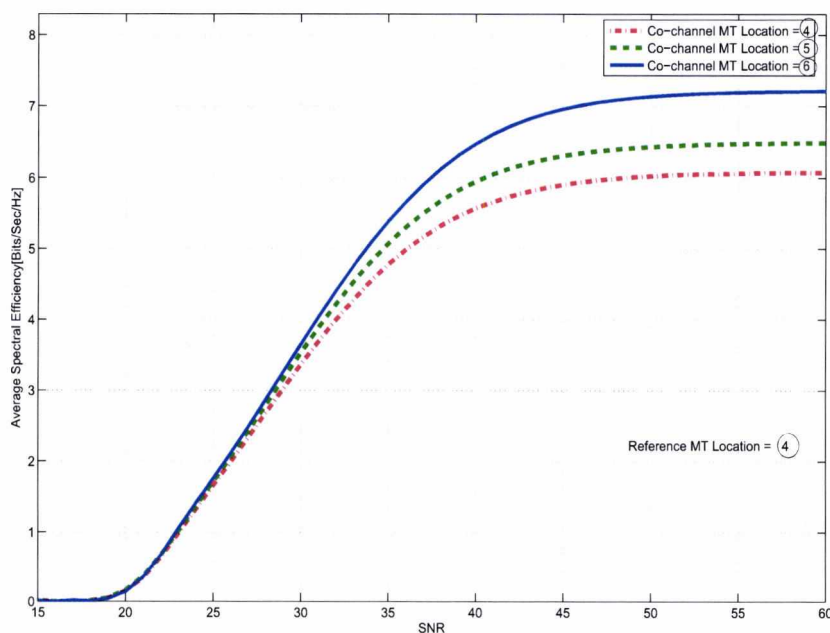


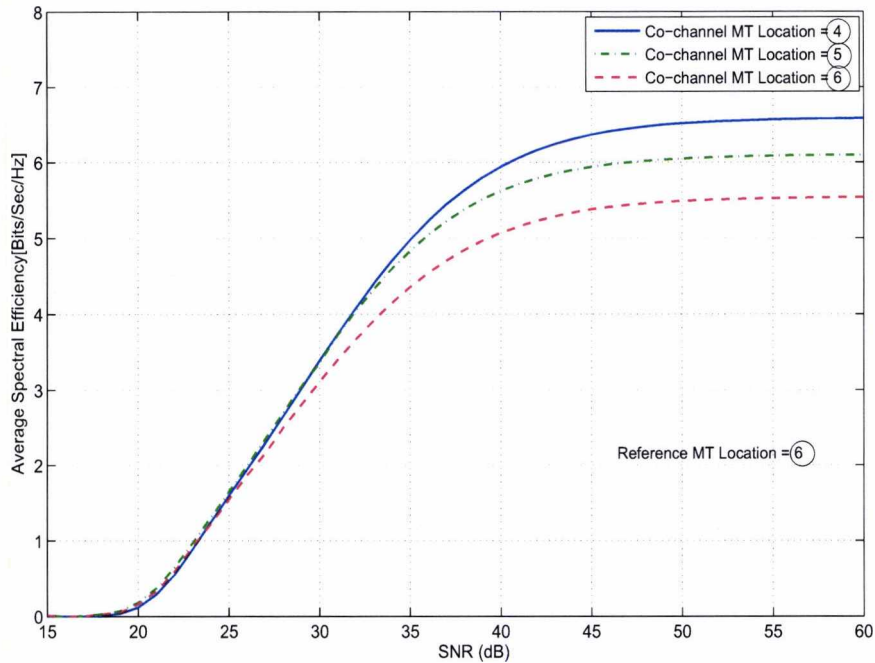(a) Reference MT at the middle-left side of the floor

Figure 4.3. Location-specific achievable spectral efficiency as a function of SNR
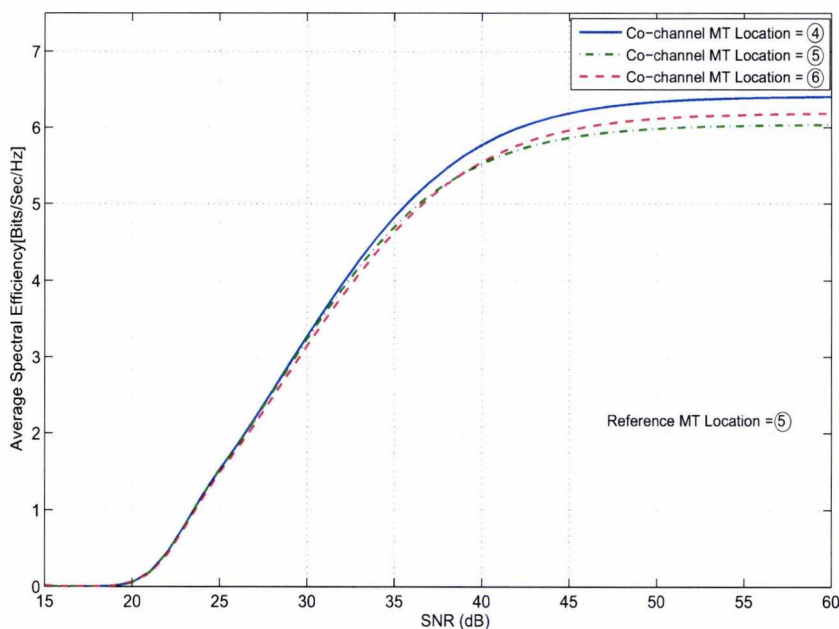
(b) Reference MT at the center of the floor

Figure 4.3. Location-specific achievable spectral efficiency as a function of SNR

at larger distances to the receiving RAU, the performance increases due to larger transmission path loss and lower level of received co-channel interference. From the result in Figure 4.3(b), the achievable spectral efficiency does not change significantly when the desired MT is located at the floor center and co-channel MTs are moved within the building. This is because the desired MT is closest to all 4 RAUS at this location than any other location, thus the received power by all 4 RAUs dominates the performance of the system. Although the achievable spectral efficiency is lower than that achievable in other locations of the desired MT, the effect of co-channel interference is minimal. The result in Figure 4.3(c) was evaluated when the desired MT is located at the window side of the floor as seen in Figure 4.1(e). In general, it is observed that the achievable spectral efficiency varies significantly as the co-channel MT is moved from the left side to the right side of the floor. When the co-channel MT is located far from the window, the co-channel signal emanating via the direct paths is most dominant, thus spectral efficiency grows linearly due

(c) Reference MT at the middle-right side of the floor

Figure 4.3. Location-specific achievable spectral efficiency as a function of SNR

to the 13 dB floor attenuation of the dominant path. However, as the co-channel MT moves closer to the window, the contributions from the reflected paths through the window becomes increasingly important, especially at high SNR region, thus achievable spectral efficiency tends to be flat. This statement is further validated in Figure 4.4.

Figure 4.4 compares the achievable spectral efficiency for a case without reflection from a neighbouring building with the case with reflection from a neighbouring building. The desired MT is located at the middle-right side of the floor, a position which is severely affected by severe reflection from the neighbouring building, i.e. position ⑥ in Figure 4.1(f). The co-channel MT is located at the middle-left, center and middle-right sides of the floor. It can be seen from the figure that, the better performance of the system without reflection is clearly evident especially at

79

high SNR region. This is due to the effect of reflection across the entire floor, on the achievable spectral efficiency. In general, it is found for both cases that the main impairment to achievable spectral efficiency is co-channel interfering signals received from direct signal transmission through the floors. However, when there is reflection from a neighbouring building, co-channel interference from reflection contributes towards the received interference power. In contrast to the case without reflection from a neighbouring building, the total co-channel interference causes the achievable spectral efficiency to gradually become flat when SNR is higher than about 35 dB. When SNR is lower than 35 dB, the noise power dominates the interference power, and it can be seen from this figure that performance for both cases are almost indistinguishable. However, the combined effect of the interference power from the direct and reflected path on the performance, dominates noise power at high SNR values when there is reflection from a neighbouring building. It is noticeable that the system achieves a better performance when the co-channel MT is located at left side
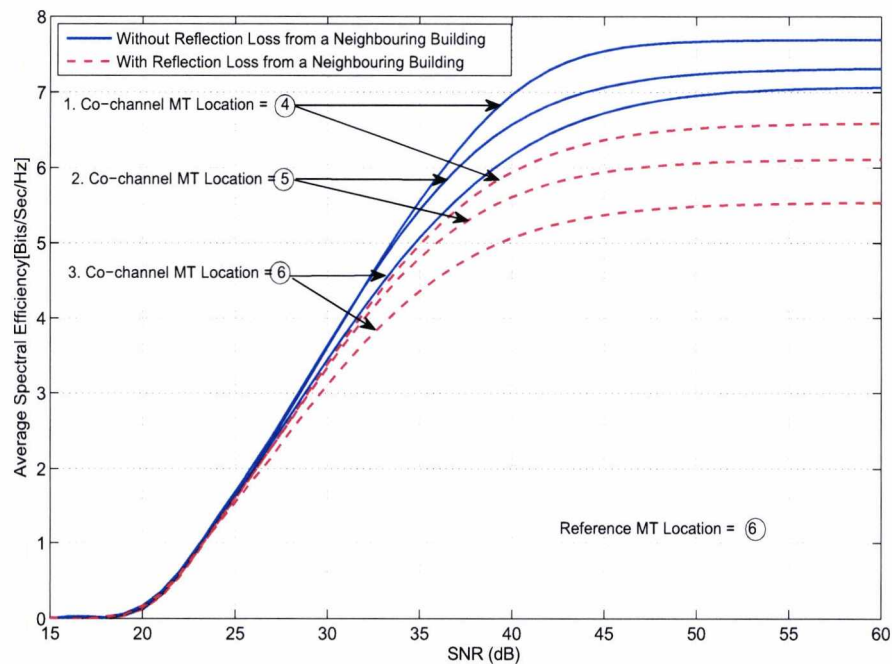


Figure 4.4. Effect of reflection loss on achievable spectral efficiency

of the co-channel floor than at the right side. This is because, at the right side, the co-channel MT is closer to the neighboring building than at the left. Thus, significant power is carried along the reflected path because the reflected signal experiences a lower transmission path loss at this location. This lowers the received SINR and thereby reduces the system performance.

Figure 4.5 shows the achievable spectral efficiency as a function of penetration loss when different values of SNR are considered. Physically, this can be interpreted as floors with different construction materials. Depending on the composition of the floors inside the building, a significant reduction in the total received co-channel interference power is due to floor penetration. If floors are made with corrugated steel panels of about 20dB penetration loss for example, an evaluation of the potential spectral efficiency can be made. It can be seen from the figure that such a system achieves the highest spectral efficiency with increasing penetration loss, owing to greater isolation from co-channel MTs. High inter-floor isolation ensures high SINR;
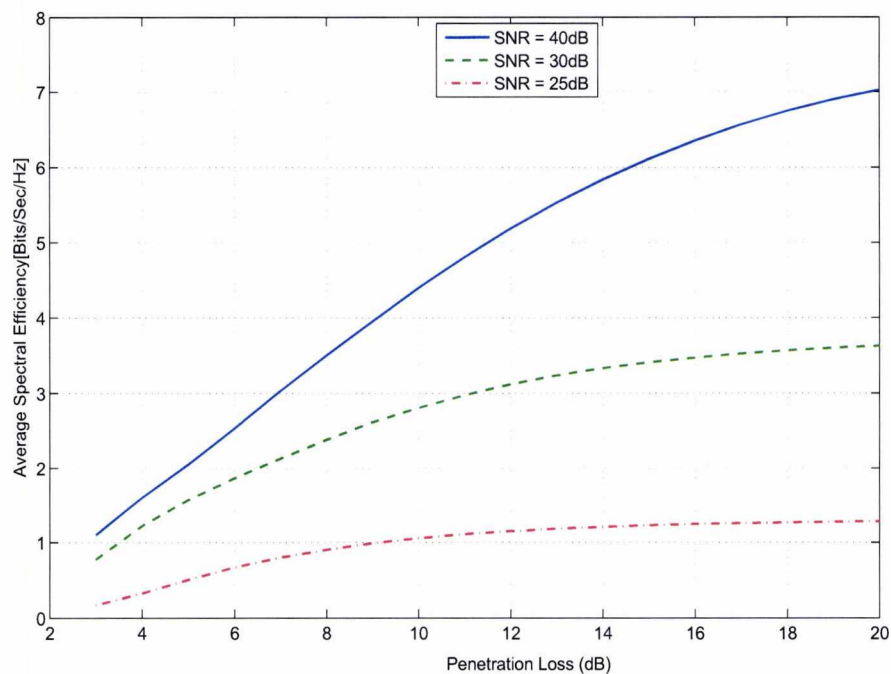


Figure 4.5. Effect of penetration loss on achievable spectral efficiency

and high spectral efficiency across the floor. Moreover, it is evident from this figure that when SNR = 25 dB, the achievable spectral efficiency increases linearly and saturates rapidly when penetration loss is larger than 8 dB. The reason is that the effect of noise on achievable spectral efficiency dominates the co-channel interference effect. Thus, the effect of co-channel interference becomes negligible with increasing penetration loss values. On the other hand, the system benefits from the increase in SNR, thus when SNR = 40dB, the achievable spectral efficiency grows linearly and then tends to be flat as penetration loss increase to about 16dB due to the co-channel interference effect on achievable spectral efficiency performance which is now larger than noise effect.

Figure 4.6 shows the achievable spectral efficiency as a function of the parameter SNR for different values of the number of selected RAU $N'$ at specific locations of MTs. These results have been obtained by considering 4 RAUs and comparing the



Figure 4.6. Comparing achievable spectral efficiency at specific MT locations when the strongest RAUs are selected

performance when the strongest RAUs are selected. The desired and co-channel MTs are located at the left side, center and right side of the floor respectively. It is seen from this figure that for the s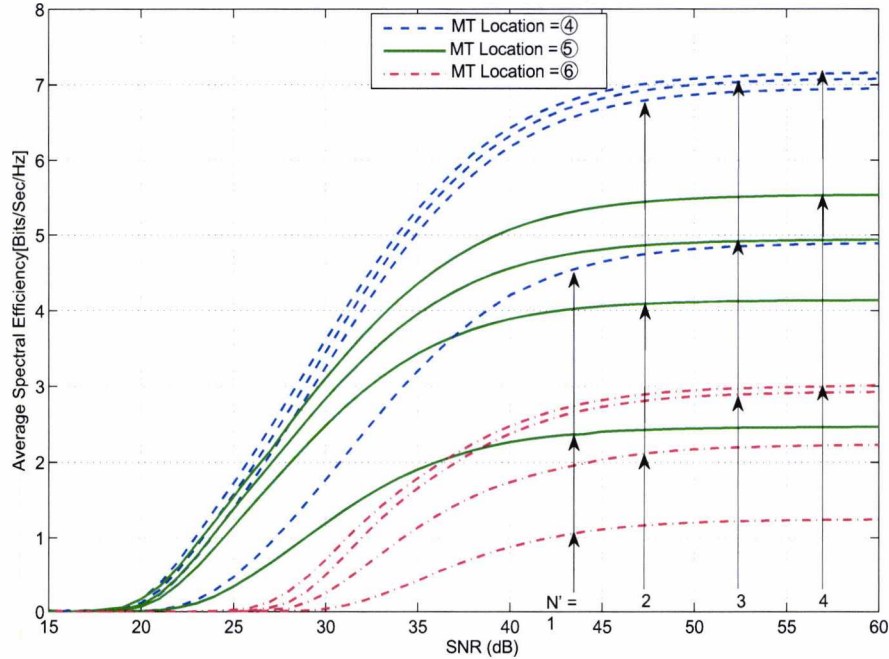ystem model under consideration, when the MTs are located on the left side of the floor, the system performance for $N' = 4$, $N' = 3$ and $N' = 2$ is very close. At this location, selecting $R_x1$ and $R_x3$ (Figure 4.1(b)) for combining, out of the 4 RAUs, achieve a spectral efficiency that is almost at optimal level. $R_x2$ and $R_x4$ only contribute weak signals due to large transmission path loss. However, when MTs are located at the center of the floor, all RAUs should be selected. A similar performance behaviour to the left side is observed at the right side of the floor, where the 3 strongest RAUs, $R_x1$, $R_x2$ and $R_x3$ are the useful diversity branches that can appreciably contribute to the received signal without any redundancy. $R_x4$ could be be discarded due to strong co-channel interference. The discarded RAU represents no loss in appreciable received signal. This way, the requirement for phase and amplitude estimation on each RAU can be reduced.

Figure 4.7 illustrates the achievable spectral efficiency of the system in a LOS and a NLOS environment. An arbitrary vector of Nakagami-$m$ fading parameters $m = [1.8, 1.5, 1.25, 1.0]$ and one that all paths undergo identical Rayleigh fading (i.e. $m = [1.0, 1.0, 1.0, 1.0]$) is considered in this figure. From this figure, the effect of the number of RAUs on the system performance is also shown. For both fading cases, RAUs are deployed according to Scenario I in Figure 4.1(a). It can be seen from the figure that the spectral efficiency of the system improves significantly with dual antenna diversity than with a single antenna. This is due to the increased SINR as more receive antennas are used for the detection. The DAS coupled with penetration loss has significantly mitigated the interference imposed by co-channel MTs having relatively weak signals on the RAUs on the reference floor. In addition, when the fading is less severe, i.e., when the value of the fading parameter $m$ increases, the spectral efficiency improves explicitly. The performance difference is due to the LOS path in Nakagami channel which improves the performance. Conversely, as more

RAUs are used for the detection, the benefit of the higher initial values of the $m$ parameter, which improves the system performance, becomes reduced. This is due to the increased co-channel interference as more RAUs are used. Note that, the noise power becomes dominant when interference is weak, thus, at low SNR region (below 35dB), spectral efficiency increases linearly. However, at high SNR region more than about 35dB, the curves tend to be flat because the co-channel interference effect on performance dominates channel noise.
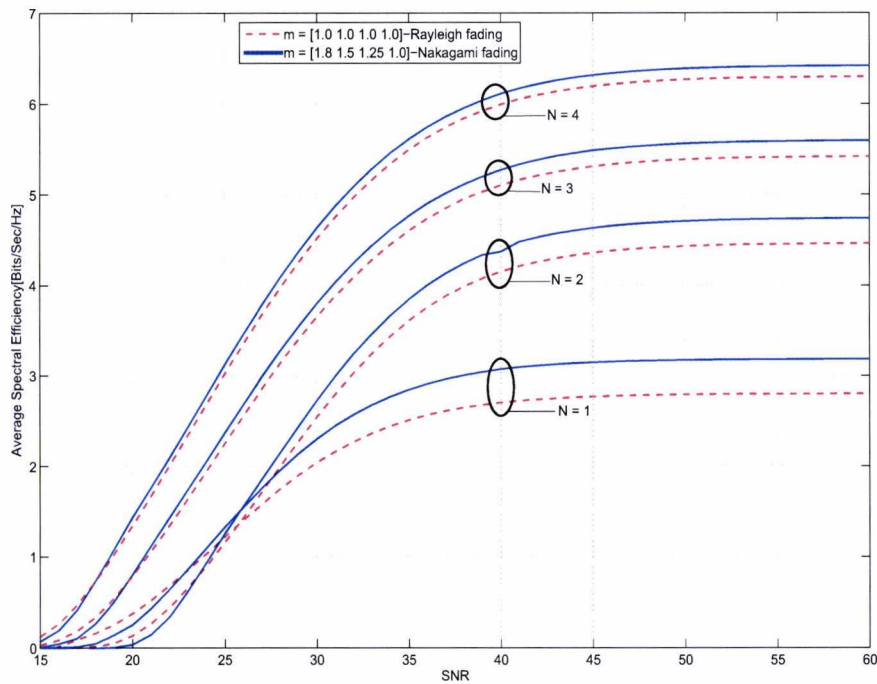


Figure 4.7. Achievable spectral efficiency in a LOS and NLOS environment

## 4.3 Summary

This chapter has investigated and discussed the performance of in-building DAS in terms of spectral efficiency achievable at various locations across the entire floor. By using an array of distributed antennas across the floor of a multi-storey building,

84

the system performance is improved. Both the location of RAUs, and the specific locations of MTs are observed to influence the performance of the system. Regions directly above/below the interfering MTs are observed to have significantly lower levels of spectral efficiency compared to rest of the floor, while the highest spectral efficiency occurs in regions directly below the desired RAU if a co-channel MT is not vertically aligned at the RAU location. It should be noted that although the figures show significant variation at various locations of MTs, the achievable spectral efficiency will change for different floor material interfaces.

It is observed that reflections from neighbouring buildings can significantly decrease the achievable spectral efficiency on adjacent floors compared to the case when no neighbouring buildings are present.

Based on analysis of location-specific spectral efficiency, RAUs with weak signal can be eliminated and the requirement for phase and amplitude estimation on each RAU can be reduced. The discarded RAUs represent no loss in appreciable spectral efficiency. Furthermore, RAU deployment should be determined to maximize spectral efficiency.

Note that an analytical approach to performance analysis is preferred in this chapter due to lower computational requirements; however, BER performance analysis in Chapter 5 shows that the analytical approach agrees with the results from Monte Carlo simulation approach. This suggests that these two techniques can substitute for each other in the performance analysis.

# Chapter 5

# Achievable BER Performance of In-Building DAS

## Contents

## 5.1 Introduction

In the previous chapter, a set of system models were presented to evaluate the achievable spectral efficiency of an in-building DAS in the presence of co-channel interference. Radio channel propagation characteristics in indoor high-rise buildings, with full frequency reuse among floors, and the resulting impact on system performance were investigated. Performance evaluation for two RAU deployment options were

also presented. The performance of the system was analysed under a specified BER constraint. This chapter presents the performance analysis of the system in terms of achievable BER, which is evaluated over possible locations of the MT across the floor. Various in-building propagation characteristics and system parameters are considered. A list of assumptions used in the analysis of the BER performance is outlined in Section 5.2. Sections 5.3 discusses the system models and BER performance evaluation techniques for the in-building DAS. The chapter is summarised in Section 5.4.

## 5.2   System Model Assumptions

A system model similar to that used in Chapter 3 has been adopted to represent the in-building DAS. It is assumed that each floor of the building is regarded as a cell and the same frequency channels are reused on every floor. Co-channel interference is composed of interference from MTs on other floors of the building which propagate via direct penetration through the floors and via reflection from a neighbouring building (Chapter 3, Figure 3.1). The binary phase-shift keying (BPSK) modulation has been assumed. The specification for the system model is listed below unless specified otherwise.

- A 7-storey building is considered.

- 3 RAUs are deployed on the ceiling of each floor for simple analysis.

- The dimension of each floor is 40m x 40m.

- The height of each floor is 4m

- MTs are uniformly located across the floor at height $v$ of 1m above the floor surface

- The path loss exponent $\lambda$ is 2.5

- The Penetration loss $\varphi$ in log-units is 13dB per floor, which is consistent with the result reported by Rappaport et al. [54] for penetration loss of about 10 to 15dB for concrete floors.

- The distance between the reference and the adjacent building $\hat{d}_{u,n}$ is 10m.

- The reflection loss $\hat{\varphi}$ at the adjacent building surface and the transmission loss $\ddot{\varphi}$ through the glass windows is 8dB and 0.13dB, respectively.

- Nakagami fading is assumed for the desired MT while co-channel MTs are subjected to Raleigh fading. Nakagami fading values $\{m_1, m_2, m_3\} = \{2.0, 1.5, 1.0\}$ are used.

- $SNR_0$ per bit of $E_s/N_0 = 20$dB used in the figures represents the transmit SNR per symbol at the MT location.

## 5.3 BER Performance Analysis

Based on the assumptions outlined in Section 5.2, theoretical analysis has been developed for the evaluation of BER performance of the in-building DAS. The BER defined in terms of the probability that an error occurs in transmission of a bit is investigated via analytical and Monte Carlo simulation techniques. Nakagami/Rayleigh fading channel models have been considered. The results from the analytical approach have been found to agree with the results from Monte Carlo simulation approach. The average BER over the MT's locations for various system parameters quantifies the system performance.

### 5.3.1 Analytical Technique

The analytical technique used in this thesis assumes that the signals from both desired and interfering MT undergo independent fading as they propagate within

the building [78]. The propagation channel between the desired MT and any of the RAUs within its floor is modelled by a Nakagami-$m$ distribution. The propagation channel between the co-channel MT and any of the RAUs on the reference floor is modelled as a Rayleigh distribution since a LOS condition does not exist in both the direct signal propagation through the floors, and the reflected paths.

Similar to the system analysis in Chapter 3, assuming the receiver of the reference MT has the precise information of path delay and the phase of the desired signal, the demodulated signal can be expressed as

$$Z_n = Re\left\{\frac{1}{T_s}\int_0^{T_s} r_{u,n}(t)\cdot e^{-j2\pi f_c t}\cdot e^{-j\theta_{u',n}}\ dt\right\} = Re\left[S_n + \sum_{u\neq u'}^{U} I_{u,n}\right] + \eta_n \quad (5.1)$$

where $S_n$, $I_{u,n}$ and $\eta_n$ follows the same definition as Equations 3.10-3.13 in Chapter 3. By applying the MMSEC, the instantaneous SINR at the receiver, given the user location $(x_u, y_y)$, can be expressed as

$$\gamma(x_u, y_u) = \sum_{n=1}^{N} \gamma_n(x_u, y_u) = \frac{\left(\sum_{n=1}^{N} W_n S_n\right)^2}{\sum_{n=1}^{N} W_n^2 \sigma_{I_u}^2 + \sum_{n=1}^{N} W_n^2 \sigma_\eta^2} = \sum_{n=1}^{N} \frac{A_n^2}{\rho_n}\alpha_{u',n}^2 \quad (5.2)$$

where $\gamma_n(x_u, y_u)$ is the SINR per RAU and $A_n^2 = P_s(d_{u',n})^{-\lambda}$. The average SINR, defined as the ratio of the average received desired signal power to the average received interfering signal power plus noise power, is given by

$$\bar{\gamma}(x_u, y_u) = \sum_{n=1}^{N} \frac{P_s \cdot (d_{u',n})^{-\lambda}}{\frac{P_s}{3}\sum_{u=1,u\neq u'}^{U}[D_u + R_u] + \frac{N_0}{2T_s}}\cdot E[\alpha_{u',n}^2]$$

$$= \sum_{n=1}^{N} \frac{\frac{2E_s}{N_0}\cdot (d_{u',n})^{-\lambda}}{\frac{2}{3}\cdot\frac{E_s}{N_0}\sum_{u=1,u\neq u'}^{U}[D_u + R_u] + 1}\cdot\Omega_n \quad (5.3)$$

where $D_u = (d_{u,n})^{-\lambda}\varphi_{u,n}^k$ and $R_u = (\hat{d}_{u,n})^{-\lambda}\hat{\varphi}_{u,n}\ddot{\varphi}_{u,n}^2$. $\frac{E_s}{N_0}$ is the ratio of the transmit symbol energy to noise power density at the MT, where $E_s$ is expressed as

$$E_s = P_s \cdot T_s \quad (5.4)$$

Since $\alpha_{u',n}^2$ is Gamma distributed, the pdf of the instantaneous SINR, $\gamma(x_u, y_u)$, in (5.2), for arbitrary values of the Nakagami fading parameters is then obtained by

89

computing the product of the moment generating function (MGF) of the SINR at each RAU, followed by the evaluation of the inverse transform. The MGF for the $\gamma(x_u, y_u)$ defined as $M_{\gamma(x_u,y_u)} = E\left[\exp(-s\gamma_n(x_u, y_u))\right]$ can be expressed as [79]

$$M_{\gamma(x_u,y_u)}(s) = \prod_{n=1}^{N} M_{\gamma_n(x_u,y_u)}(s) = \prod_{n=1}^{N} \left(1 + \frac{s\gamma_n(x_u, y_u)}{m_n}\right)^{-m_n} \tag{5.5}$$

where $M_{\gamma_n(x_u,y_u)}(s)$ denotes the MGF of the SINR at each RAU. It is assumed that the number of all interfering signals is sufficiently large for the instantaneous interference of the received signal at receiver to be Gaussian distributed [70].

The BER of the received signal at the CU can then be evaluated for its instantaneous SINR $\gamma(x_u, y_u)$ using the Gaussian approximation. Thus, assuming a coherently detected BPSK modulation, the expression for the conditional BER for coherent binary signal with fixed $\gamma(x_u, y_u)$ can be written as [80]

$$P_e(\gamma) = Q\left(\sqrt{2t\gamma(x_u, y_u)}\right), \tag{5.6}$$

where $t = 1$ is for coherent BPSK and $Q(\cdot)$ is the Gaussian Q function, given by

$$Q(x) = \frac{1}{\sqrt{2\pi}} \int_x^{\infty} e^{-t^2/2} dt \tag{5.7}$$

Therefore, the performance of the system in terms of user's average BER with random parameters $\gamma(x_u, y_u)$ over the Nakagami fading channel can be obtained by averaging $P_e(\gamma)$ over the PDF of $\gamma(x_u, y_u)$. This can be written as

$$\hat{P}_e(x_u, y_u) = \int_0^{\infty} Q\left(\sqrt{2\gamma(x_u, y_u)}\right) p_{\gamma(x_u,y_u)}(\gamma) dy \tag{5.8}$$

Following the derivations in [81] and using the alternative representation of the $Q$ function and the product form representation of the conditional BER as used in [82], the average BER can be obtained directly from the MGF in (5.5) and can be written as

$$\hat{P}_e(x_u, y_u) = \frac{1}{2} \sum_{i=1}^{k} \prod_{n=1}^{N} \left[1 + \frac{\sec^2(\theta_i)}{\beta_n}\right]^{-m_n} \tag{5.9}$$

where $k$ is a positive integer, $\sec^2(\theta_i) = 1/\cos^2(\theta_i)$, $\theta_i = (2i - 1)\pi/4k$ and $\beta_n = m_n/\bar{\gamma}_n(x_u, y_u)$

## 5.3.2 Monte Carlo Simulation Technique

The Monte Carlo simulation technique explicitly models the channel fading coefficient of the received signals. By generating random samples of the desired and interfering signals, and noise, it evaluates the instantaneous SINR for specified system parameters, and the BER of the system can then be evaluated. The overall simulation process is summarised in Figure 5.1. The instantaneous samples of the received signals from the desired and interfering MT can be obtained using their distributions. The simulation assumes a Nakagami distribution and a Rayleigh dis-
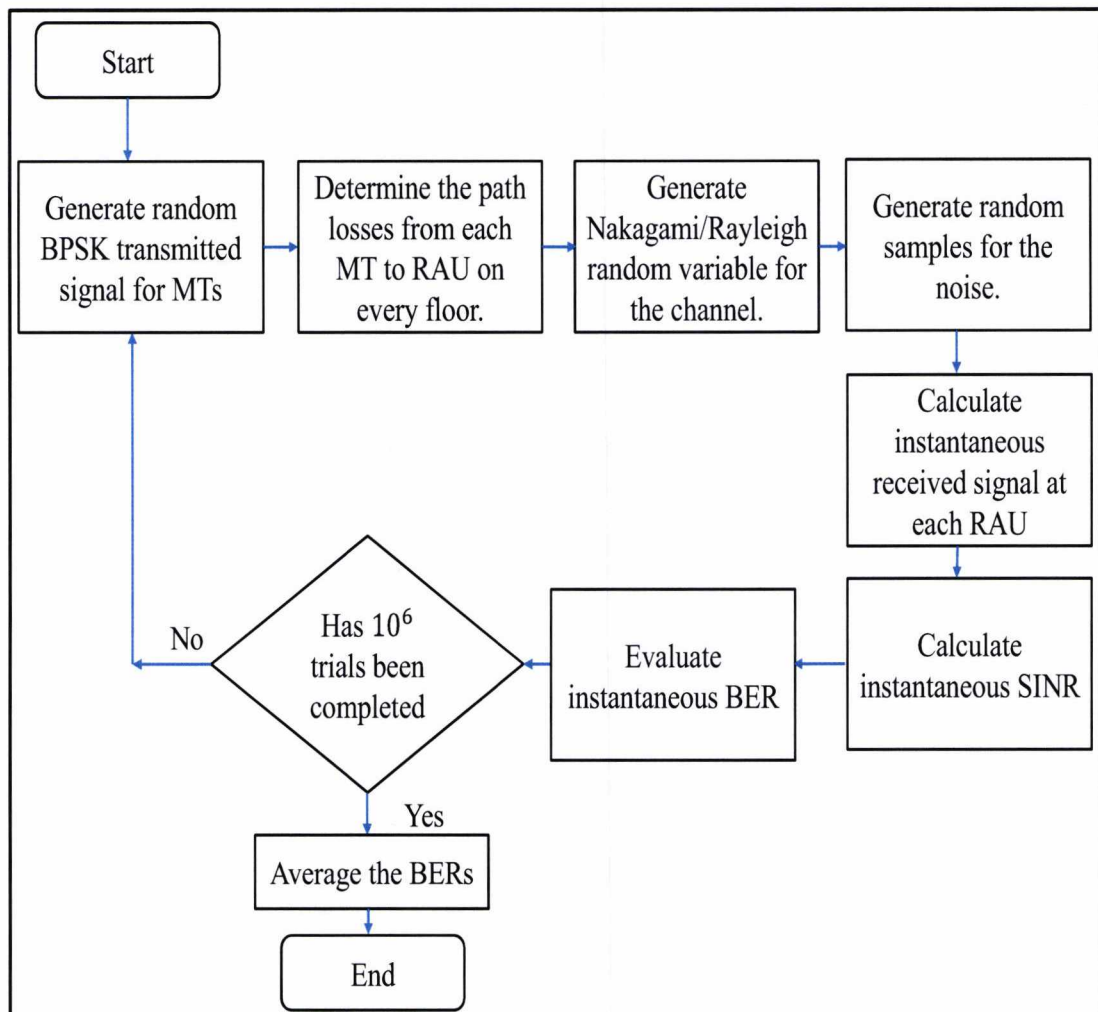


Figure 5.1: Flow chart of the Monte Carlo simulation technique.

tribution for the received envelopes for the channel responses from the desired MT and the co-channel MTs respectively. A total of $10^6$ iterations of the simulation are performed to evaluate the average BER of the system. In each iteration of the simulation, a sample is obtained from a Nakagami and Rayleigh random variable for each of received envelopes from the desired and interfering MTs. A detailed discussion of the algorithms for estimation of Nakagami/Rayleigh parameters and the generation of Nakagami/Rayleigh random variables is presented in Appendix B.

### 5.3.3   Simulation and Numerical Results

In this section, a range of results for illustrating the achievable BER of the exemplified DAS in high-rise buildings is presented.

In order to analyse the performance of the system, the analytic formulas derived in Section 5.3.1 are evaluated and compared with Monte Carlo simulation approach for the multi-storey building structure shown in the Chapter 3, (Figure 3.1) in an uplink scenario. Using an identical deployment of RAUs (scenario I, Figure 4.1(a)) and propagation characteristics as in Chapter 4, the effects of the building geometry, the number of RAUs per floor, and channel parameters on the achievable average BER are investigated for the system operating in a Nakagami-$m$ fading channel with real and arbitrary parameters for BPSK modulation.

Figure 5.2 provides the achievable BER performance of the system in a LOS and a NLOS environment. An arbitrary vector of Nakagami-$m$ fading parameters $m = [2.0, 1.5, 1.0]$ and one that all paths undergo identical Rayleigh fading (i.e. $m = [1.0, 1.0, 1.0]$) is considered in this figure. For both fading cases, $N = 3$. It is observed that when the fading is less severe, i.e., when the value of the fading parameter $m$ increases, the average BER improves explicitly. The performance difference is due to the LOS path in Nakagami channel which improves the link performance. Note that, channel noise becomes dominant when interference is weak, thus, at low
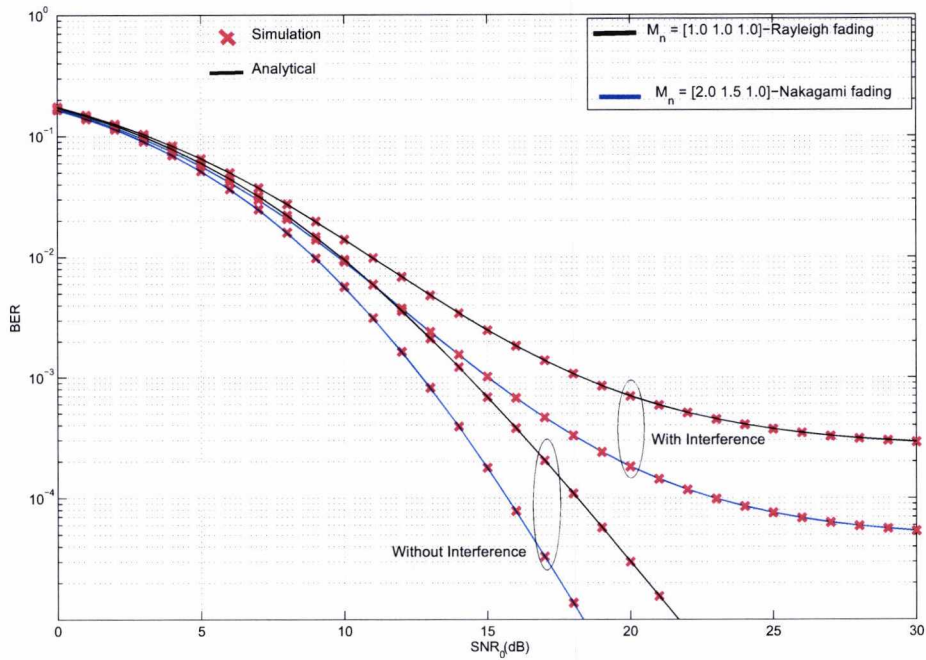
Figure 5.2: Effect of Nakagami parameter on achievable BER performance.

SNR region (below 15 dB), the average BER reduces linearly. However, at high SNR region more than about 15 dB, the curves tend to be flat because co-channel interference dominates channel noise. The BER obtained in the system with no co-channel interference is also shown in Figure 5.2 for comparison purposes. Compared with the no interference case, the BER achievable in the system with co-channel interference is higher due the presence of co-channel MTs. To validate the analysis, we have compared our theory with the results obtained with simulations. It is observed that both performance evaluation techniques show a similar trend as a function of the parameter SNR. A higher SNR gives a lower BER. This suggests that these two techniques can substitute for each other in the system performance analysis. However, the use of the analytical technique is preferred due to its lower computational

93

requirements.

Figure 5.3 compares the performance of the system for different numbers of RAUs per floor. The average BER was shown as a function of the parameter SNR assuming the user is located at the floor center and boundary. It is observed that the addition of a second RAU offers considerable improvement on the system performance by reducing the path loss. Increasing the number of antennas per floor from 1 to N decrease the propagation distance from a mobile terminal to the nearest RAU and causes the received signal power to increase. It is clearly shown that the system with 3 RAUs offers the lowest BER, which is over one order of magnitude lower than that of the single antenna branch. As expected, when the user is close to the RAU (at
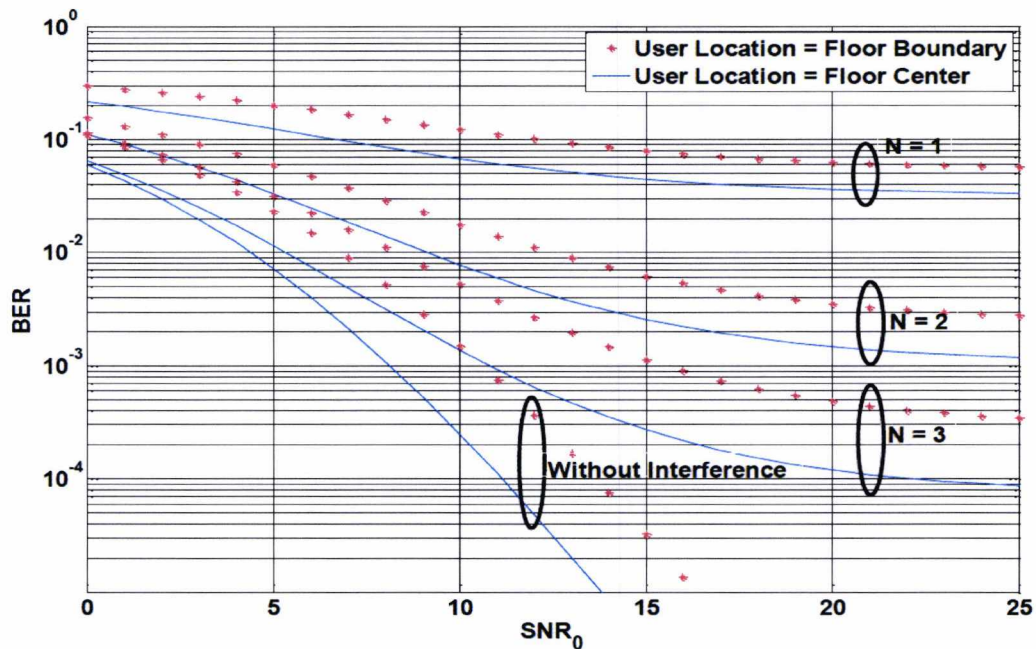


Figure 5.3: Effect of number of RAUs per floor on achievable BER performance.

the center of the floor), the received power by the RAU will dominate the achievable BER performance of the system and the resultant BER is lower than that achieved when the user is at the floor boundary. The BER obtained in the no interference case is also shown for comparison purposes.

Figure 5.4 shows the achievable BER performance with and without a neighbouring building. The system with no co-channel interference is also shown for comparison purposes. Compared with the case with no reflection loss from a neighbouring building, the BER performance of the system with reflection loss from a neighboring building deteriorates considerably as SNR increases. This can be attributed to co-channel interference received from the direct path and the reflections from the neighbouring building. The combined effect on BER performance dominates noise at high SNR range. Similar to performance behaviour in Figure 5.3, it is noticeable that at low SNR less than 8 dB, the BER performance of the system with and without a neighboring building, and the no interference case is almost indistinguishable. However, at higher SNR values the BER of the system with co-channel interference slows and gradually becomes flat. The reason is that the co-channel interference dominates the noise when SNR is large. We can predict that the benefit from the SNR increase will be getting smaller when SNR is higher than 30 dB.
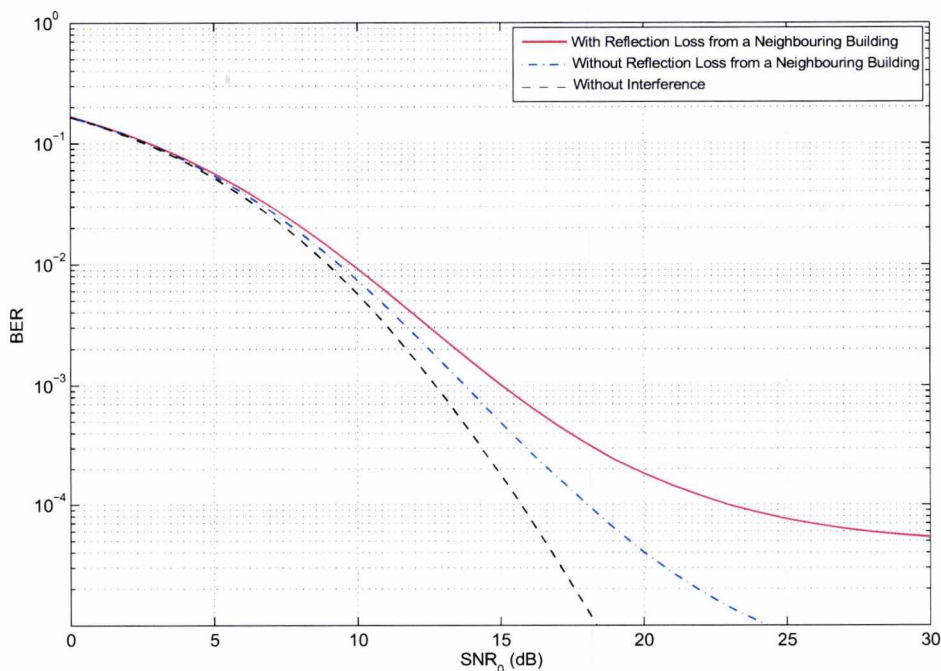


Figure 5.4: Effect of reflection loss on achievable BER performance.

In contrast, it can be seen from both figures that the system with no interference provides better performance especially at high SNR.

Figure 5.5 provides the performance of the system for different values of penetration loss. Physically, this can be interpreted as scenarios with different building materials. Depending on the composition of the floors inside the building, a significant reduction in the total received co-channel interference power is due to floor penetration. Measured penetration loss introduced by common building materials used in the construction of multi-storey buildings is listed in Table 5.1 [83]. Poured concrete over metal lathing is a popular modern construction technique which provides less RF attenuation than does solid steel planks which were used to separate floors in older buildings. Thus an evaluation of the achievable BER performance of the system in such buildings can be made. The interfering signals from adjacent floors made of concrete experience approximately 13 dB attenuation passing through the floors. The high inter-floor isolation ensures high SINR; and low BER
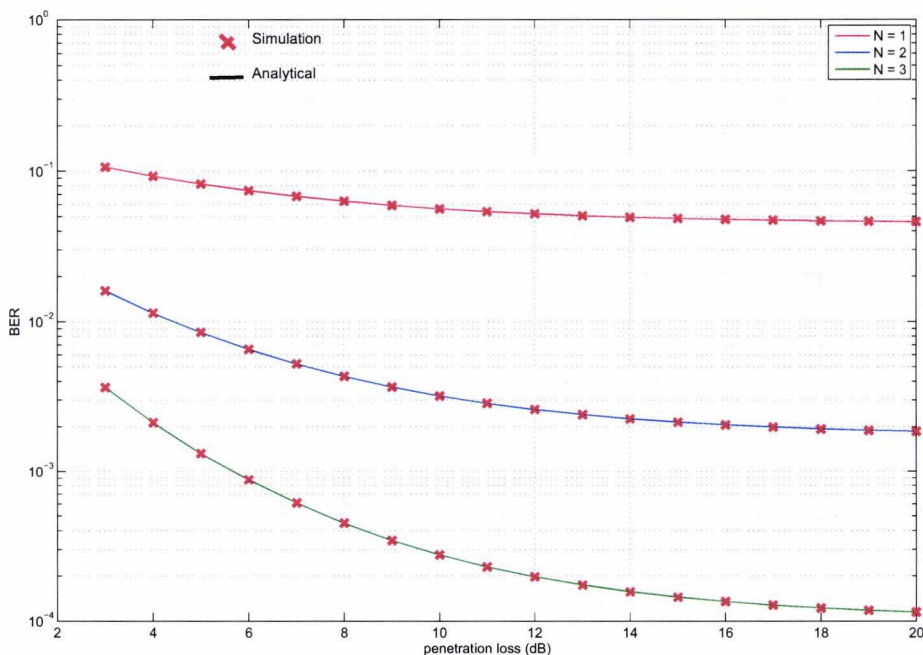


Figure 5.5: Effect of Penetration Loss on Achievable BER performance.

Table 5.1: Experimental values of penetration loss introduced by common building materials [83].

| Building material | Penetration loss(dB) |
|---|:---:|
| Concrete floors | 10-15 |
| Precast concrete slab floors | 13 |
| Corrugated steel panels | 26 |
| Aluminium siding | 20.4 |
| Light textile inventory | 3-5 |
| Foil Insulation | 3.9 |
| Metals | 26 |

across the floor is observed. An important thing to note is the significant difference in performance improvements when the number of RAUs increases. The difference is particularly pronounced when $N = 3$ where there is more than an order of magnitude difference in the BER. If we consider an acceptable BER to be $10^{-3}$, at least 3 RAUs are required for propagation in a building with this geometry. The performance of the system shows some non-linearity as the penetration loss increases because the reflected paths also contribute towards the received power. Thus the effect of the combined co-channel interference from the direct and the reflected path on BER performance is larger than noise effect when penetration loss is large. A good agreement between analytical and simulation results is again evident in this figure. Thus the analytical technique has been selected for the subsequent system performance analysis in this thesis.

## 5.4 Summary

In this chapter, it has been shown that the in-building DAS has the potential to provide high quality wireless signals to indoor users by reducing the fading effects and suppressing the effect of interference. The uplink system performance of the in-building DAS is quantified in terms of BER with the consideration of an in-building channel model that takes into account that the propagation between different floors can occur via direct paths through the floors and reflected paths from a nearby building. The major assumptions for the system models include a sufficiently large number of co-channel interference sources, which are independent of each other. This enables performance evaluation based on Gaussian approximation. A number of system models have been considered including analytical and simulation techniques, and the consideration of Nakagami fading model for the desired user, and Rayleigh fading for the interfering user. The simulation technique gives identical performance results to the analytical technique but requires significantly more computation time. The analytical and simulation results have shown performance gains when multiple RAUs are used, compared with a system with a single antenna per floor. The amount of gain becomes substantial under the effects of floor penetration and more RAUs are desirable when penetration loss increases. It is also shown that with DAS having up to 3 RAUs per floor, several floors of the building considered can reuse the same frequency without degraded performance. Furthermore, when the fading is less severe, i.e., when the value of the fading parameter $m$ increases, the BER performance improves explicitly due to the LOS path in Nakagami channel which improves the performance.

# Chapter 6

# Co-channel Interference Cancellation

## Contents

## 6.1 Introduction

As discussed in Chapter 1, the increasing demand for various wireless services often necessitates reuse of the frequency spectrum. However, interference from co-channel users will form the single most important factor limiting the system performance. In indoor wireless communication, the indoor system is likely to be in dense urban environments, where many indoor cells exist in a small region and a great portion of the coverage of the indoor cell is overlapped by that of other indoor cells, as in the case of high-rise buildings. Thus, performance is impaired by co-channel interference created due to the need to reuse the limited available spectrum in nearby floors. In

Chapters 3 and 4, a set of system models was presented to evaluate the performance of the in-building DAS in the presence of co-channel interference, and the achievable BER was investigated. However, without any scheme to reduce the effect of co-channel interference, performance gains obtained through DAS and higher reuse could be limited.

This chapter investigates the implementation of an interference cancellation strategy in which co-channel signals from neighbouring floors, received at different CUs, are separated through joint processing. A literature review of some interference management strategies is presented in Section 6.2, and system models to evaluate the performance of interference cancellation technique in the in-building DAS are outlined in Section 6.3. The impact of interference cancellation on the performance of the system is compared with that with no interference cancellation technique in Section 6.4. Finally, a summary of the findings in this chapter is presented in Section 6.5.

## 6.2    A Survey of Interference Management Techniques

Attempted solutions to the interference problem fall into two categories [84-86]: The interference mitigation and interference cancellation. Interference mitigation approach regards the interference signal as noise and attempts to suppress it. Some studies have attempted to mitigate interference by means of the transmitter or receiver design [87, 88]. However, most works on interference mitigation attempt to solve the problem by radio resource management (RRM), which smartly manages the radio resources of multiple cells. A representative RRM research divides the spectrum according to a frequency reuse factor and allocates the divided resources so as to avoid co-channel interference. Frequency reuse schemes proposed in early times managed frequency reuse factor statistically [89]. Later, the Fractional Frequency Reuse (FFR) concept was proposed, in which the strategy of frequency reuse varies

according to the cell region [90]. However, in such schemes, only a fraction of the total frequency resource is utilized.

Cell sectoring is another technique used to reduce the average interference at the edge of a cell [91, 92]. Cell sectoring employs directive antennas at the tower to restrict radiation at the BS. In contrast to FFR, sectoring improves the average SINR and improves spectral efficiency since frequencies can be reused in each sector. However, cell sectoring, which is highly effective in current cellular systems, has the potential shortcoming of reducing the multipath diversity in the channel, which in the absence of sufficient local scattering, results in the benefits of using multiple antennas at the BS being reduced. Furthermore, small sectors can result in unbalanced numbers of users per sector, limiting the capacity per user in the highly populated sectors, whilst wasting capacity in the less populated sectors [93]. Regardless, sectoring is more attractive than large frequency reuse since it does not entail as large a reuse penalty.

Another interference mitigation approach in cellular systems is to attempt to average the interference levels using spread spectrum techniques, by either direct sequence code division multiple access (DS-CDMA) or slow frequency hopping in the global system for mobile communications (GSM). In these systems co-channel interference is mitigated by adjusting the traffic load in each cell to significantly below what would be acceptable in a single-cell system. It is evident that this acceptable load drops further in dense urban environments with high concentration of potential users, due to its susceptibility to interference [94].

On the other hand, when using interference cancellation schemes, a receiver subtracts an interference signal from the received signal so that it can decode its data signal precisely. Joint detection of the received signal among co-channel receivers has drawn considerable attention in recent years due to its enormous benefits from an interference cancellation point of view. In [95, 96], a BS cooperation technique was studied in which BSs at different locations communicate detected bits

iteratively while performing separate detection and decoding of their received data streams. The performance of such an arrangement reduces the transmit power and also significantly improves the received SINR but at the cost of a backhaul traffic which can be more than ten times the actual transmitted data. The long time delay introduced by multiple exchange of information between all adjacent interfering BSs leads to excessive traffic on the communication link between the cooperating BSs in macro cellular systems. Related work [97] discusses a low backhaul distributed multiuser detection through joint scheduling of users onto resources in order to permit sequential processing of the received signal.

Another strategic interference cancellation approach implemented in this thesis is the use of DAS that performs interference cancellation through joint signal processing between CUs. This method has the potential to reduce the excessive traffic by employing multiple RAUs connected to each CU. Thus, BS coordination is not likely to be an issue in an in-building environment, since the difference in propagation times between CUs is small. The CU on each floor of the building detects and decodes the received signals and makes available at its output the transmitted data from each MT. An iterative interference cancellation process is applied where hard information bits or reliability information at the output of the CU are repeatedly exchanged with an improving estimate in each iteration.

## 6.3 Propagation and System Analysis

In order to analyse the performance of the in-building DAS with interference cancellation, the uplink transmission model in a multi-storey building is considered (Figure 6.1). In the building geometry considered (isolated building), two propagation paths are possible:

1. transmission through the floors which includes the direct and multiple reflection paths, which are entirely contained within the building perimeter; and
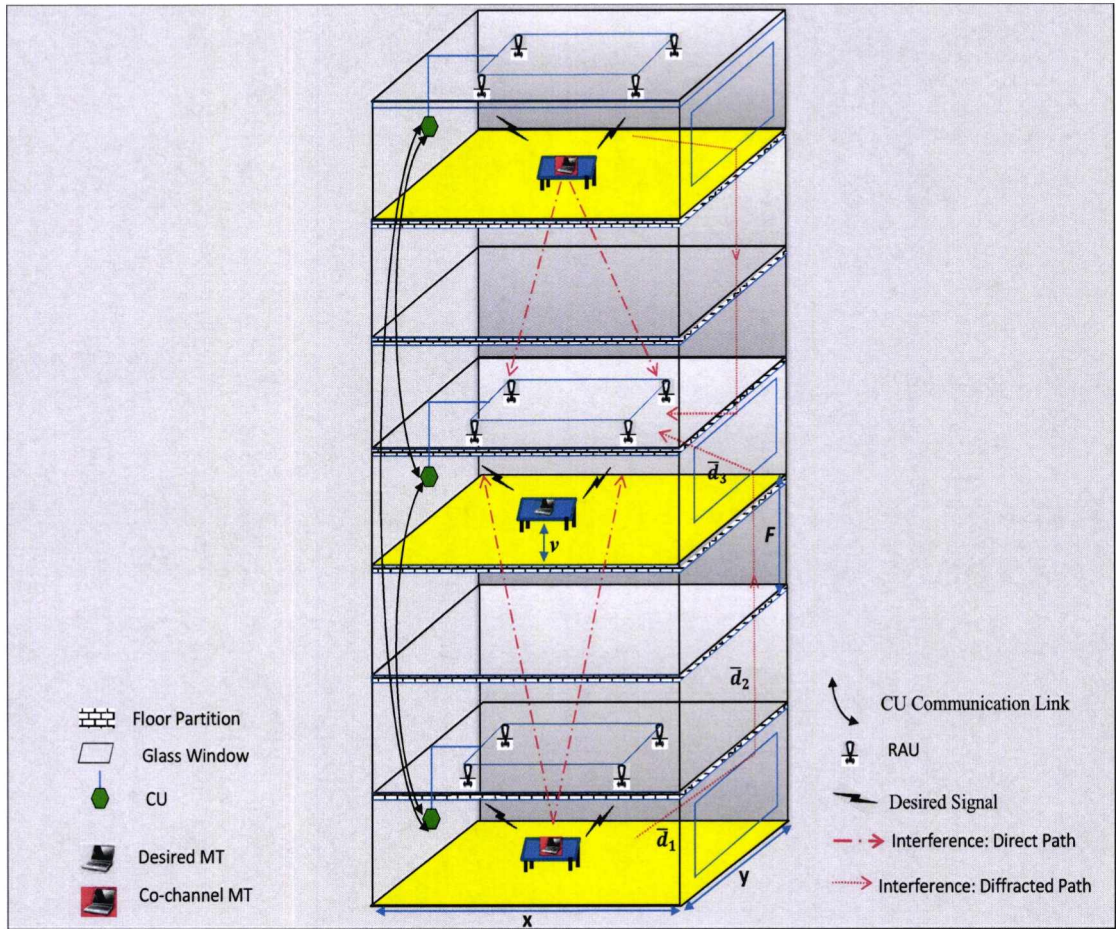
Figure 6.1: An illustration of an isolated building employing DAS with full frequency reuse on every floor.

2. transmission via paths external to the building, e.g. diffraction at the window frames down the outside face of the building.

This is consistent with findings in [24] where it is observed that diffraction along exterior building walls of an isolated building can have significant contributions to the mean received power when the transmitter and receiver are separated by several floors. The power of the penetrating component decreases by a fixed amount per floor, in addition to distance dependent loss, and depends on the composition of the floor [98]. On the other hand, the power of the diffracted components will be significantly lower, but relatively constant with distance and it is independent of the

103

number of floors but dependent on the attenuation due to the window material. The combined effect causes the received power to decrease linearly, until the power of the diffracted component is approximately the same as the direct, at which point the rate of decrease in received power slows, and is then dominated by the diffracted component. This is illustrated in Figure 6.2, which decomposes the total path loss into direct and diffracted components.
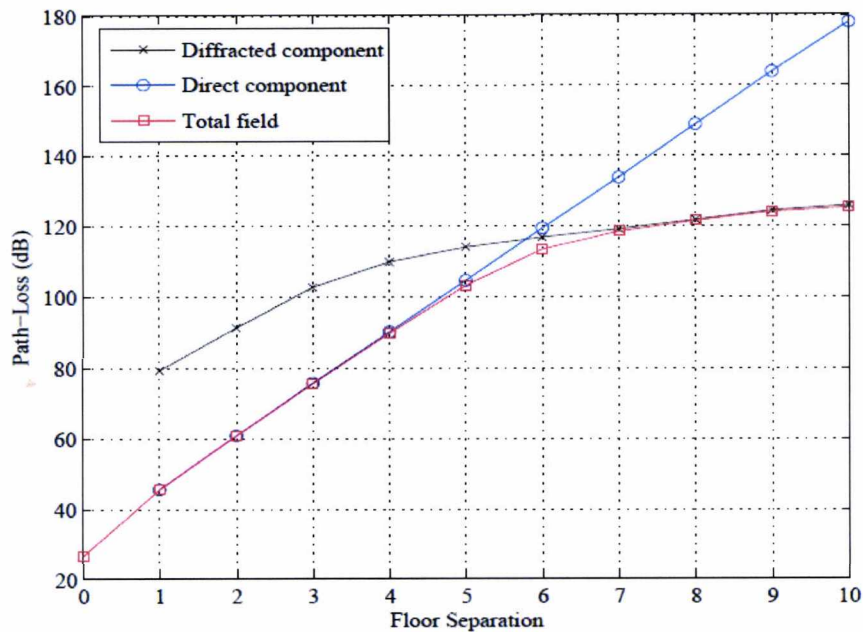


Figure 6.2: Isolating the total path loss into direct and diffracted components.

This assumption is also supported by the results in [99, 100] where it was shown that for 1-5 floor separation of an isolated building, the power decreases linearly with each additional floor, however, beyond 5-6 floor separation, the received power remains relatively constant. Thus, in the uplink transmission of the DAS considered in this chapter, the impact of co-channel interference from the direct and the diffracted paths is studied. In this case, a RAU will receive a desired signal from a MT on

the reference floor, and co-channel interfering signals from other MTs on co-channel floors via direct signal penetration through the floors and diffraction at the window frame as illustrated in Figure 6.2.

Based on these findings, the channel from MT-$u$ to the $n$-th RAU on the reference floor is modelled as the sum of low pass equivalent impulse responses of the individual paths which can be expressed as

$$h_{u,n}(t) = h'_{u,n}(t) + \bar{h}_{u,n}(t) \tag{6.1}$$

where $h'_{u,n}(t)$ and $\bar{h}_{u,n}(t)$ are the impulse response for the paths that run through the floors and the diffracted paths through the window respectively. Similar to (3.3) in Chapter 3, the complex low pass equivalent impulse response for $h'_{u,n}(t)$ can be expressed as

$$h'_{u,n}(t) = (d_{u,n})^{-\lambda/2} \cdot \varphi^{k/2}_{u,n} \cdot \alpha_{u,n} \cdot e^{j\theta_{u,n}} \cdot \delta(t - \tau_{u,n}) \tag{6.2}$$

Correspondingly, the complex low pass equivalent impulse response for $\bar{h}_{u,n}(t)$ in (6.1) can be expressed as

$$\bar{h}_{u,n}(t) = \left(\bar{d}_{u,n}\right)^{-\lambda/2} \cdot \ddot{\varphi}_{u,n} \cdot \bar{\varphi}_{u,n} \cdot \bar{\alpha}_{u,n} \cdot e^{j\bar{\theta}_{u,n}} \cdot \delta(t - \bar{\tau}_{u,n}) \tag{6.3}$$

where $\bar{d}_{u,n}$ denotes the length of the diffracted path distance between MT-$u$ and the $n$-th RAU on the reference floor when the signal is diffracted as illustrated in Figure 6.1. $\bar{d}_{u,n}$ can be approximated as

$$\bar{d}_{u,n} = \bar{d}_1 + \bar{d}_2 + \bar{d}_3 \tag{6.4}$$

where $\bar{d}_1$ is the distance between MT-$u$ and the window, $\bar{d}_2$ is the length of the diffracted path between the window of the co-channel floor and the reference floor's window, $\hat{d}_3$ is the distance between the $n$-th RAU on the reference floor and the window. In (6.3), $\ddot{\varphi}_{u,n}$ is the transmission loss through the glass windows and $\bar{\varphi}_{u,n}$ is diffraction loss at the window edge. Depending on the construction of the building and window frame, different choices may be made for this parameter. Typical values

of $\bar{\varphi}_{u,n}$ can be found in [66, p.305]. $\bar{\alpha}_{u,n}$, $\bar{\theta}_{u,n}$ and $\bar{\tau}_{u,n}$ in (6.3) are the channel fading coefficient, the path phase and the channel delay of the reflected path respectively. The distribution of $\bar{\alpha}_{u,n}$ can be approximated as a Rayleigh distribution since a LOS condition does not exist in the diffracted signal path. It is assumed that $\bar{\theta}_{u,n}$ and $\bar{\tau}_{u,n}$ are uniformly distributed over $[0, 2\pi]$ and $[0, T_s]$ respectively.

Assuming the same transmit signal model in Chapter 3, equation (3.1), the uplink received signal by the $n$-th RAU on the reference floor includes components from the desired MT-$u'$, co-channel interfering MT-$u$ from other floors of the building, and channel noise. This can be represented by its complex low-pass equivalent as

$$\bar{r}_{u,n}(t) = x_{u'}(t) \otimes h_{u',n}(t) + \sum_{u=1, u \neq u'}^{U} x_u(t) \otimes h_{u,n}(t) + \eta_n(t)$$

$$= (d_{u',n})^{-\lambda/2} \cdot \alpha_{u',n} \cdot e^{j\theta_{u',n}} \cdot x_{u'}(t - \tau_{u',n})$$

$$+ \sum_{u=1, u \neq u'}^{U} (G_d + \bar{Q}_d) \cdot x_u(t - \tau_{u,n}) + \eta_n(t) \tag{6.5}$$

where $G_d = (d_{u,n})^{-\lambda/2} \cdot \varphi_{u,n}^k \cdot \alpha_{u,n} \cdot e^{j\theta_{u,n}}$, $\bar{Q}_d = (\bar{d}_{u,n})^{-\lambda/2} \cdot \ddot{\varphi}_{u,n} \cdot \bar{\varphi}_{u,n} \cdot \bar{\alpha}_{u,n} \cdot e^{j\bar{\theta}_{u,n}}$ and $\eta_n(t)$ is the background AWGN received by the $n$-th RAU, with zero mean and a double sided power spectral density $N_0/2$.

Similar to the analysis in Chapter 3, the demodulated signal can be expressed as

$$Y_n = Re \left\{ \frac{1}{T_s} \int_0^{T_s} \bar{r}_{u,n}(t) \cdot e^{-j2\pi f_c t} \cdot e^{-j\theta_{u',n}} \, dt \right\} = Re \left[ \bar{S}_n + \sum_{u \neq u'}^{U} \bar{I}_{u,n} \right] + \eta_n \tag{6.6}$$

where the received signal component $\bar{S}_n$, is given by

$$\bar{S}_n = \frac{1}{T_s} \int_0^{T_s} (d_{u',n})^{-\lambda/2} \cdot \alpha_{u',n} \cdot e^{j\theta_{u',n}} \cdot x_{u'}(t) \cdot e^{-j\theta_{u',n}} \cdot e^{-j2\pi f_c t} dt$$

$$= \sqrt{P_s} \cdot (d_{u',n})^{-\lambda/2} \cdot b_{u'} \cdot \alpha_{u',n}$$

$$E\left[\bar{S}_n^2\right] = \sqrt{P_s} \cdot (d_{u',n})^{-\lambda/2} \cdot E[b_{u'}^2] \cdot E[\alpha_{u',n}^2] \tag{6.7}$$

where $E[\cdot]$ denotes expectation. Assuming $E[b_u^2] = 1$ and the channel fading coefficient $\alpha_{u',n}$ is Rayleigh distributed, the mean square i.e. $E[\alpha_{u',n}^2] = 1$, the received signal power is then expressed as

$$E\left[\bar{S}_n^2\right] = \sqrt{P_s} \cdot \left(d_{u',n}\right)^{-\lambda/2} \tag{6.8}$$

$\bar{I}_{u,n}$ in (6.6) is the interfering signal component received from other floors by the $n$-th RAU on the reference floor. The total co-channel interference term is written as

$$\bar{I}_u = \sum_{u=1,u\neq u'}^{U} \bar{I}_{u,n} \tag{6.9}$$

where $\bar{I}_{u,n}$ is expressed as

$$\bar{I}_{u,n} = \frac{1}{T_s} \int_0^{T_s} \left(G_d \cdot x_u(t - \tau_{u,n}) \cdot e^{-j\theta_{u,n}} + Q_r \cdot x_u(t - \hat{\bar{\tau}}_{u,n}) \cdot e^{-j\hat{\bar{\theta}}_{u,n}}\right) dt \tag{6.10}$$

The real and imaginary parts of $\bar{I}_u$ have the same variance and can be expressed as

$$\sigma_{\bar{I}_u}^2 = \frac{P_s}{3} \sum_{u\neq u'}^{U} [(d_{u,n})^{-\lambda}\varphi_{u,n}^k + (\bar{d}_{u,n})^{-\lambda}\ddot{\varphi}_{u,n}^2\bar{\varphi}_{u,n}^2] \tag{6.11}$$

According to [70], the total interference term, $\bar{I}_u$, can be approximated as a Gaussian random variable since the number of components in the sum is large.

In (6.6), $\eta_n$ is the noise component with zero mean and a variance of $\sigma_\eta^2 = N_0/(2T_s)$, which is assumed to be equal for all RAUs.

The received SINR defined as the power ratio of the desired signal to the interfering signal plus noise power without any interference cancellation can be written as

$$\begin{aligned}
\gamma &= \frac{\bar{S}_n^2}{\sigma_{\bar{I}_u}^2 + \sigma_\eta^2} \\
&= \frac{\bar{S}_n^2}{\frac{P_s}{3}\sum_{u\neq u'}^{U}[(d_{u,n})^{-\lambda}\varphi_{u,n}^k + (\bar{d}_{u,n})^{-\lambda}\ddot{\varphi}_{u,n}^2\bar{\varphi}_{u,n}^2] + \sigma_\eta^2}
\end{aligned} \tag{6.12}$$

## 6.3.1 Interference Analysis and Cancellation

By employing interference cancellation mechanism, RAUs located at different floors in the building receive uplink signals from different users and locally perform RF processing. The signals are then estimated and sent to the neighbouring CU as shown in Figure 6.1 for joint processing. The CU jointly detects and decodes the received signals, does interference cancellation and makes available at its output the transmitted data from each user. The setup for performing IC through information exchange at the CUs is as shown in Figure 6.3 considering just two co-channel floors. If the interfering user is detected and decoded first and its hard information bits (i.e. the actual bit decisions) are sent to the second CU, then at the second CU, the interference due to the interfering user is reconstructed and subtracted out of the received signal. The signal after interference cancellation is then used to detect the desired user, whose hard information bits are also sent to the first CU. An important part of the interference cancellation process is an accurate estimation of the received signal at the CU from the interfering MT on the same channel in order to cancel them to improve the detection. This estimate is subtracted from the received signal at each CU to cancel out the interference, resulting in a signal with reduced interference. The input signal of the interference estimator which represents one portion of the interfering signal part is first demodulated for all but the reference user. The interference cancellation scheme estimates a given transmitted symbol from received samples within a single symbol period. The estimator provides an estimate $\hat{b}_u(t)$ of the desired response $b_u(t)$.

During the initial information exchange of the interference cancellation step, the signal $\hat{b}_u$ is estimated based on the received signal $Y_n$, since there are no symbol estimates available. Thus, assuming equally distributed antipodal transmit symbols $\hat{b}_u \in \pm 1$, the probability that $b_u = \hat{b}_u$ is given as [80]

$$1 - \hat{P}_e(u) \tag{6.13}$$
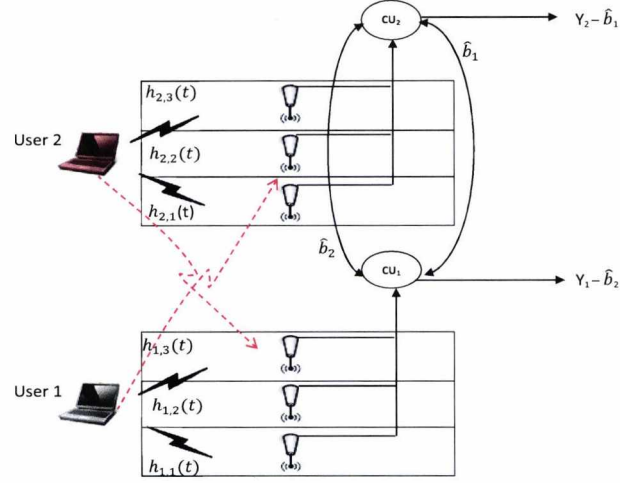
Figure 6.3: The receiver structure showing iterative interference cancellation.

where $\hat{P}_e$ is the BER before interference cancellation.

The average SINR $\bar{\gamma}$ and the BER, $\hat{P}_e$ for the first stage can be respectively written as

$$\bar{\gamma} = \frac{E\left[\bar{S}_n^2\right]}{\frac{P_s}{3}\sum_{u\neq u'}^{U}[(d_{u,n})^{-\lambda}\varphi_{u,n}^k + (\bar{d}_{u,n})^{-\lambda}\ddot{\varphi}_{u,n}^2\bar{\varphi}_{u,n}^2] + \sigma_\eta^2} \tag{6.14}$$

$$\hat{P}_e = \frac{1}{2}\left(1 - \sqrt{\frac{\bar{\gamma}}{1+\bar{\gamma}}}\right) \tag{6.15}$$

Therefore the resulting mean square error (MSE) evaluated upon the arrival of estimates from neighbouring CUs is given by

$$MSE(b_u) = E\left\{\left|\hat{b}_u - b_u\right|^2\right\} = 4\hat{P}_e(u) \tag{6.16}$$

After the arrival of estimates and the subtraction of the interference from neighbour-

109

ing CUs, the resulting signal with reduced interference is given by

$$\hat{Y}_n = Y_n -$$

$$\sum_{u \neq u'}^{U} \sqrt{P_s} \hat{b}_u \left( \frac{P_s}{3} \sum_{u \neq u'}^{U} [(d_{u,n})^{-\lambda} \varphi_{u,n}^k + (\bar{d}_{u,n})^{-\lambda} \ddot{\varphi}_{u,n}^2 \bar{\varphi}_{u,n}^2] \right)$$

$$\cdot \alpha_{u,n} e^{j(\theta_{u,n} - \theta_{u',n})} \cdot \bar{\alpha}_{u,n} e^{j(\bar{\theta}_{u,n} - \theta_{u',n})}$$

$$= \sqrt{P_s} b_{u'} \left( d_{u',n} \right)^{-\lambda/2} \cdot \alpha_{u',n} e^{j(\theta_{u',n})}$$

$$+ \sqrt{P_s} (b_u - \hat{b}_u) \cdot \Delta_I \cdot \alpha_{u,n} e^{j(\theta_{u,r} - \theta_{u',n})} \cdot \bar{\alpha}_{u,n} e^{j(\bar{\theta}_{u,r} - \theta_{u',n})} + \eta \qquad (6.17)$$

where $\Delta_I = \frac{P_s}{3} \sum_{u \neq u'}^{U} [(d_{u,n})^{-\lambda} \varphi_{u,n}^k + (\bar{d}_{u,n})^{-\lambda} \ddot{\varphi}_{u,n}^2 \bar{\varphi}_{u,n}^2]$.

By denoting

$$\Delta_{I_u} = \sqrt{P_s} (b_u - \hat{b}_u) \cdot \Delta_I \cdot \alpha_{u,n} e^{j(\theta_{u,r} - \theta_{u',n})} \cdot \bar{\alpha}_{u,n} e^{j(\bar{\theta}_{u,r} - \theta_{u',n})} \qquad (6.18)$$

as the residual interference from MT-$u$, $\hat{Y}_n$ can be rewritten as

$$\hat{Y}_n = \sqrt{P_s} b_{u',n} \left( d_{u',n} \right)^{-\lambda/2} \cdot \alpha_{u',n} e^{j(\theta_{u',n})} + \Delta_{I_u} + \eta \qquad (6.19)$$

where $\Delta_{I_u}$ is the sum of all residual interference from all co-channel users received at the $n$-th RAU on the reference floor after interference cancellation. The variance of the residual interference denoted by $\sigma_{\Delta_{I_u}}^2(u)$ may be derived as follows

$$\sigma_{\Delta_{I_u}}^2(u) = \sum_{u \neq u'}^{U} E \left\{ \left| \hat{b}_u - b_u \right|^2 \right\} \cdot E \left[ \frac{P_s}{3} \sum_{u \neq u'}^{U} [(d_{u,n})^{-\lambda} \varphi_{u,n}^k + (\bar{d}_{u,n})^{-\lambda} \ddot{\varphi}_{u,n}^2 \bar{\varphi}_{u,n}^2] \cdot \alpha_{u',n} \cdot \bar{\alpha}_{u',n} \right]$$

$$= \frac{P_s}{3} \sum_{u \neq u'}^{U} [(d_{u,n})^{-\lambda} \varphi_{u,n}^k + (\bar{d}_{u,n})^{-\lambda} \ddot{\varphi}_{u,n}^2 \bar{\varphi}_{u,n}^2] \cdot 4 \hat{P}_e(u) \qquad (6.20)$$

The received SINR after interference cancellation can now be derived as follows

$$\bar{\gamma} = \frac{E \left[ \bar{S}_n^2 \right]}{\sigma_{\Delta_{I_u}}^2(u) + \sigma_\eta^2}$$

$$= \frac{E \left[ \bar{S}_n^2 \right]}{\frac{P_s}{3} \sum_{u \neq u'}^{U} [(d_{u,n})^{-\lambda} \varphi_{u,n}^k + (\bar{d}_{u,n})^{-\lambda} \ddot{\varphi}_{u,n}^2 \bar{\varphi}_{u,n}^2] \cdot 4 \hat{P}_e(u) + \sigma_\eta^2} \qquad (6.21)$$

The BER is then evaluated using (6.15) as shown above.

## 6.4 Numerical Evaluation and Discussion

In order to evaluate the achievable performance of the in-building DAS with and without interference cancellation, the analytic formulas derived in Sections 6.3 are numerically evaluated using the 3D diagram of an isolated multi-storey building structure in Figure 6.1 in an uplink scenario for BPSK modulation (i.e. reflection/scattering paths from nearby buildings have been ignored). Equations (6.14), (6.15) and (6.21) are considered in evaluating the average BER for the performance of each method. The channel impulse response of both the desired signal and the interfering signal is assumed to be known perfectly at the CUs. Interference cancellation for a single antenna per floor has been considered for simplicity. It is important to note that no MMSEC is applied for the single antenna case. The feedback channel is assumed to be an ideal error-free channel without feedback delays. Note further that SNR per bit used in the figures of this section represent the SNR per bit at the MT transmitter location. A summary of parameters used in evaluating the performance of the system is listed in Table 6.1, unless specified otherwise.

Table 6.1: Summary of Parameters

| Parameters | Value |
|---|---|
| Number of floors in the building, $U$ | 7 |
| Floor height, $F$ | 4m |
| Floor dimension, $(x, y)$ | 40m X 40m |
| MT located across the floor at height, $v$ | 1m |
| Path loss exponent, $\lambda$ | 2.5 |
| Penetration loss, $\varphi$ | 13dB |
| Transmission loss through a glass window, $\ddot{\varphi}$ | 0.13dB |
| Diffraction loss at a window edge, $\bar{\varphi}$ | 6dB |
| Number of interference cancellation iterations | 4 |

Figure 6.4 shows the BER attained when the CUs cooperate and perform inter-ference cancellation in comparison with the system without interference cancellation. The figure shows an improvement in performance when interference cancellation is applied resulting in a lower BER, particularly at high SNR region (above 20dB). At low SNR region (below 20dB), the curves tend to converge to the no interference case. However, Figure 6.4 points out that the proposed strategy needs about 3.0 dB less than the system without interference cancellation to guarantee a BER of $10^{-1}$. It is also observed that the curve tends to be flat at high SNR region. Compared with the case without interference, the high error floor observed for the case with interference cancellation is due to transmission path loss and the fact that the co-channel MT is located right above the desired RAU. Thus, at high SNR values, the strength of the interfering signal received by this RAU is high, and may be far beyond the interference suppression capacity of the interference cancellation mechanism. We can predict that the benefit from the SNR increase and more number of interference cancellation iterations will be getting smaller when SNR is higher than 40 dB.

Figure 6.5 shows the BER as a function of the parameter SNR for a scenario for two different building geometries. Path loss exponent, $\lambda = 2.5$, represents an environment with fewer obstacles between the MT and the RAU, while $\lambda = 3.8$, represents a NLOS environment with more obstructed paths. It is seen from the figure that the two groups exhibit similar trends, however, the group with the smaller path loss exponent tends to show better performance as a result of a reduced path loss. Although a higher path loss exponent leads to greater level of isolation between co-channel floors, reducing the influence of co-channel interference, the power of the desired MT is reduced due to increased path loss leading to higher BER. The better behaviour of the system with interference cancellation with respect to the no interference cancellation case is clearly evident in this figure. This is more pronounced at high SNR region i.e. above 20dB.

Figure 6.6 shows the effect of increasing the number of floors in the building.
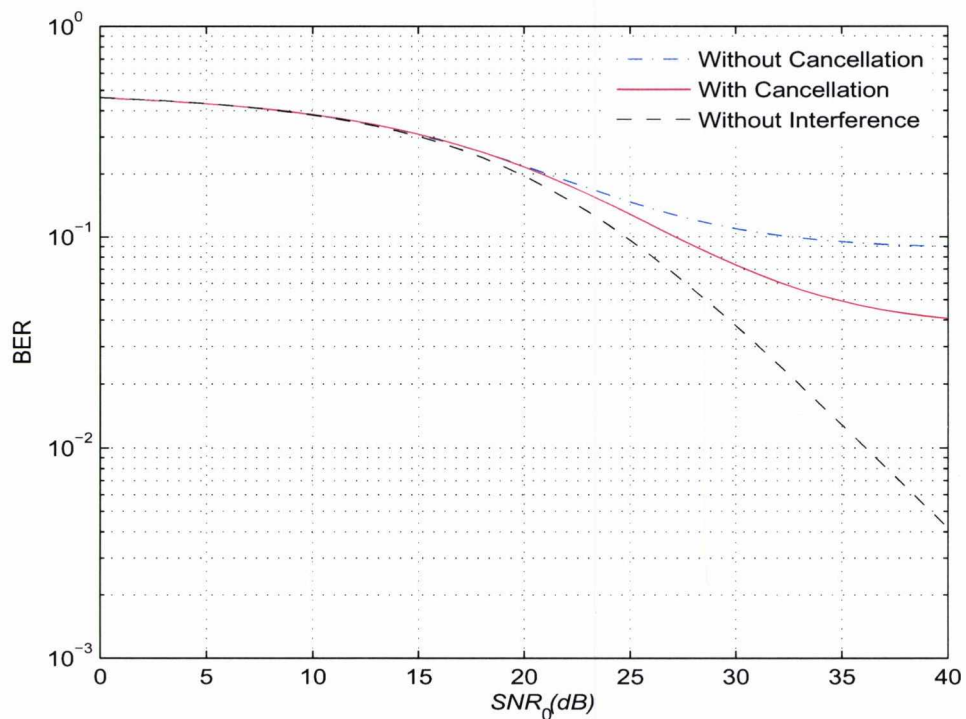
112

Figure 6.4: Effect of transmit power to noise ratio on BER.
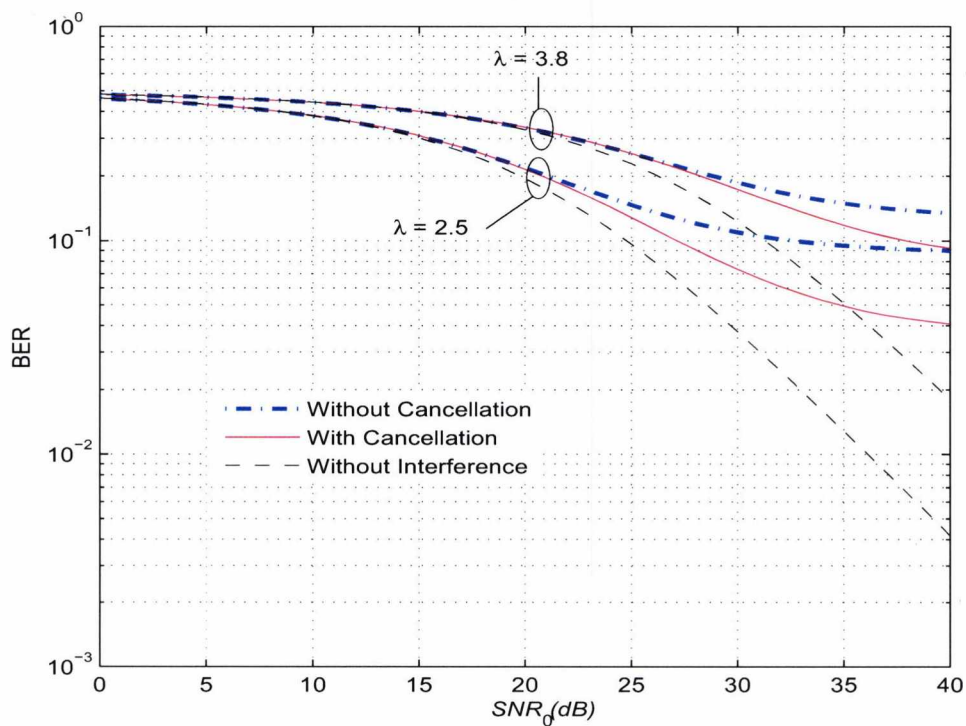


Figure 6.5: Effect of path loss exponent on BER.

Physically, this can be interpreted as increasing the number of CUs or users reusing the same frequency channels. Its is evident from this plot that, for a building with just three floors there is a large improvement in the performance with increasing SNR, when interference cancellation is employed. This is because the interference from the strongest interferers is reduced. However, the achievable gain becomes lower as the number of the interferers increases. This is largely due to the dominance of the uncancellable interference emanating from co-channel floors. It is better to perform interference cancellation and reuse the frequency within 3 tier of floors of this building. It is also observed that the curves tend to converge when SNR is below 20dB. For all investigated parameters, performance improvements are observed with the implementation of interference cancellation at the CUs in comparison with the non cooperating system.
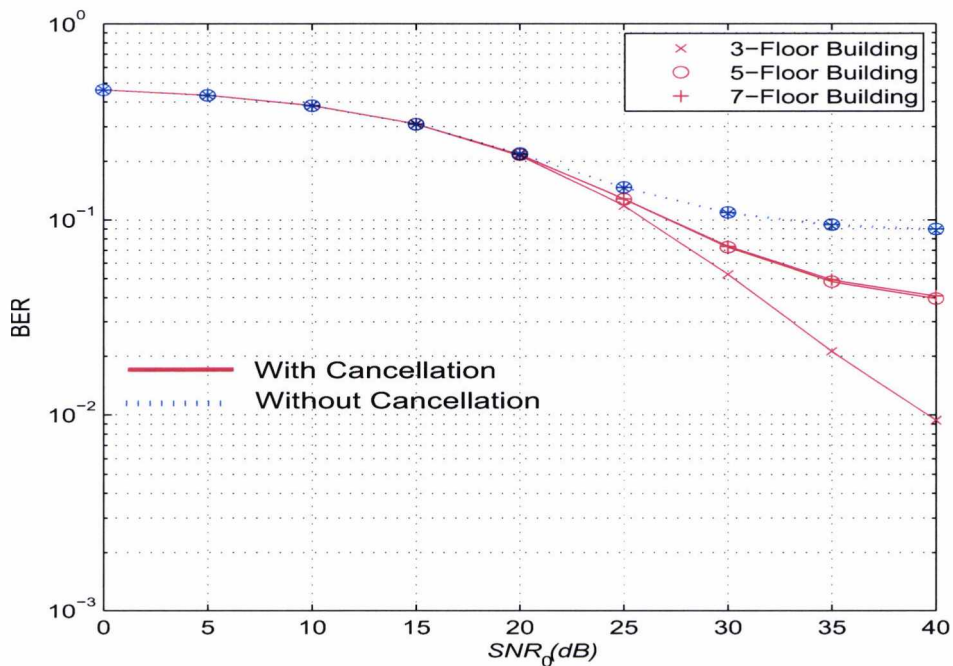


Figure 6.6: Effect of number of floors in the building on BER.

## 6.5 Summary

Co-channel interference in indoor wireless communication can be suppressed by joint processing of the received signal by co-channel receivers. A unique contribution of this thesis is that it presents a performance evaluation of interference cancellation of in-building DAS for which path loss values have been retrieved from measured results. The vast majority of the studies investigating co-channel interference cancellation strategies have been performed for systems operating in outdoor environments not in indoor or multi-floor buildings. Compared with the non cooperating case, the application of cooperation to the in-building DAS shows the potential of significantly better performance despite the degradation caused by the interference from the adjacent floors. One of the key issues with any interference cancellation technique is the complexity of implementing it in practice. The complexity is proportional to the number of cancellation stages and the number of CU. The strongest interfering floors may be chosen to be cancelled to reduce the complexity.

# Chapter 7

# Conclusions and Future Research

## Contents

The research presented in this thesis was motivated by the need to provide high data rate wireless services particularly within high-rise buildings. This is an important step towards the realization of future wireless networks which can achieve around 1Gbps data transmission with extremely low transmit power. In the conventional macrocellular system, providing high data rates for indoor users could be difficult to achieve, due to long radio transmission distance between indoor mobile users and the outdoor BSs. The path loss and shadowing loss cause a severe drop in received signal power since the transmit power is limited. Furthermore, due to limited available spectrum, system capacity needs to be improved by introducing a higher frequency reuse, but the influence of interference between co-channel users is likely to be an important issue for wireless operators.

In this thesis, in-building DAS has been proposed as one promising solution to solve the problems arising from long radio transmission distance, limited transmit

power and limited bandwidth. First, the radio propagation characteristics in indoor high-rise buildings are studied, where propagation on the same floor as the transmitter, and propagation to adjacent floors is investigated. Next, channel and system models were developed to characterise both propagation within the same floor, and to adjacent floors of a high-rise building employing DAS. This is important when considering interference, as the desired signal usually originates from a MT on the same floor, while interference typically arises from neighbouring co-channel MTs operating on immediately, or nearly, adjacent floors. Frequency reuse among floors and the resulting impact on achievable data rate is then investigated, followed by BER performance analysis of the system. The other line of this research is based on modelling in-building DAS in the context of joint processing, where CUs cooperate to reduce the interference among co-channel users.

## 7.1 Summary and Conclusions

By considering co-channel interference emanating from vertically located MTs, the performance of the system is analytically quantified in terms of location-specific spectral efficiency and BER achievable in a multi-storey building. By using a propagation channel model derived from multi-floor, in-building path loss values retrieved from measurement results, the following conclusions can be drawn:

1. Due to the range of geometric arrangements possible with MTs, the performance of the uplink does not only depend on the proximity of the desired MT to the RAUs located on the reference floor but is also very dependent on the location of the co-channel MT within the building. The highest spectral efficiency values are found in floor regions closer to the desired RAU, if a co-channel MT is not vertically aligned above the RAU location, while regions directly above/below the interfering MTs are found to have the lowest spectral efficiency values compared to rest of the floor. The worst case spectral effi-

ciency occurs when the desired MT and the co-channel MT are both located close to the window.

2. Variations in RAU location can result in significant variations in achievable spectral efficiency. The square configuration for RAU deployment outperforms the single line configuration especially at the floor sides/boundaries. However, low spectral efficiency, near the worst case value is not likely to occur in the single line configuration, due to greater isolation from co-channel MTs. Consequently, RAU location can have a major impact on system performance in high-rise buildings and as such is an important design consideration and should be determined to maximize spectral efficiency.

3. By selecting RAUs for combining based on maximum received instantaneous power at specific locations of MTs across the floor, which also reduces the effect of co-channel interference, it is found that, RAUs with weak signal can be eliminated. The discarded RAUs represent no loss in appreciable spectral efficiency.

4. Based on analysis of location-specific spectral efficiency, it is then possible to effectively allocate frequency channels to multiple users within the building, further increasing the achievable spectral efficiency.

5. Similar to the results found from the spectral efficiency analysis, when the desired MT is close to the RAU on the reference floor, the received power by this RAU will dominate the achievable BER performance of the MT, and the resultant BER is lower than that achieved when the MT is away from all the RAUs.

6. By applying cooperation to in-building DAS, the potential of significantly better performance compared to the non cooperating case is evident. It is shown

that there is a substantial gain in performance despite the degradation caused by co-interference from the surrounding floors.

The considered building is typical of many high-rise buildings supported by concrete structure and it is expected that the performance trends observed in this study will be applicable to other buildings of similar characteristics.

## 7.2 Future Research Directions

The work presented in the thesis can be extended in the following directions:

- **Investigation of location-assisted resource allocation.** In light of the results presented in this thesis, it has been demonstrated that the performance of the system is largely dependent on the location of the MTs. The effect of the user's location can be used to develop a coordinated resource allocation strategy that maximizes the spectral efficiency under certain criteria. In Chapters 4-6, it is observed that, in most circumstances, the majority of the inter-floor interference arises from MTs located on immediately adjacent floors, thus if a co-channel MT is not located on immediate adjacent floors, or not vertically aligned at the same location as the desired MT, they can be assigned the same resources. Therefore, allocation of resources based on users locations may potentially increase the achievable spectral efficiency and therefore requires further investigation.

- **Investigation of location-assisted interference cancellation.** Due to computational complexities, co-channel interference cancellation in Chapter 6 was based on a specific location of MTs. A future contribution would be to evaluate the performance for various locations of both the desired and co-channel MTs. In other words, from the knowledge of the position of MTs, an interference coordination strategy could be developed.

119

- **Investigation of optimal placement of antennas**. To optimise system performance, it would be useful to extend this study to include a variety of antenna placements including inward facing ones which could yield high capacity and efficiency. In addition, the use of more than one antenna at each RAU and the possible implications on system performance is a logical extension to this study.

With increasing demands for high data rate wireless services, wireless systems need to be enhanced to provide gigabit wireless access to MTs. In-building DASs are likely to play an important role. Thus, the results presented herein will help develop insights into their design, and guide wireless operators in the engineering of future indoor wireless communication systems.

# Appendix A

# Derivation of the Variance of

# Co-channel Interference

In this appendix, the variance of the total co-channel interference term in (3.13) is derived. From (3.12)

$$I_u = \sum_{u=1, u \neq u'}^{U} I_{u,n} \tag{A.1}$$

where $I_{u,n}$ is given in (11), then $I_u$ is rewritten as

$$I_u = \sum_{u=1, u \neq u'}^{U} \left( \frac{\hat{G}_d}{T_s} \left[ b_u[i] \cdot (\tau_{u',n}) + b_u[i+1] \cdot (T_s - \tau_{u',n}) \right] \right.$$

$$\left. + \frac{\hat{Q}_r}{T_s} \left[ b_u[i] \cdot (\hat{\tau}_{u',n}) + b_u[i+1] \cdot (T_s - \hat{\tau}_{u',n}) \right] \right) \tag{A.2}$$

The variance may be expressed as

$$\sigma_{I_u}^2 = E\left[ I_u \cdot I_u^* \right]$$

$$= E\left\{ \left[ \sum_{u=1, u \neq u'}^{U} \left( \frac{\sqrt{P_s} \cdot (d_{u,n})^{-\lambda/2} \cdot \varphi_{u,n}^k \cdot \alpha_{u,n}}{T_s} \cdot \left[ b_u(i) \cdot (\tau_{u',n}) + b_u(i+1) \cdot (T_s - \tau_{u',n}) \right] \right. \right. \right.$$

$$\left. \left. \left. + \frac{\sqrt{P_s} \cdot (\hat{d}_{u,n})^{-\lambda/2} \cdot \hat{\varphi}_{u,n}^{1/2} \cdot \ddot{\varphi}_{u,n} \cdot \hat{\alpha}_{u,n}}{T_s} \cdot \left[ b_u(i) \cdot (\hat{\tau}_{u',n}) + b_u(i+1) \cdot (T_s - \hat{\tau}_{u',n}) \right] \right) \right]^2 \right\} \tag{A.3}$$

Since $E\left[\alpha_{u,n}^2\right] = 1$, $E[b_u] = 0$, $E[b_u \cdot b_u^*] = 1$ and $E\left[\tau_{u',n}^2\right] = E\left[\left(T_s - \tau_{u',n}\right)^2\right] = \frac{T_s^2}{3}$, and likewise $E\left[\hat{\alpha}_{u,n}^2\right] = 1$, and $E\left[\hat{\tau}_{u',n}^2\right] = E\left[\left(T_s - \hat{\tau}_{u',n}\right)^2\right] = \frac{T_s^2}{3}$, the real and the imaginary parts of $I_u$ have the same variance expressed as

$$\sigma_{I_u}^2 = \frac{P_s}{3} \sum_{u \neq u'}^{U} [(d_{u,n})^{-\lambda} \varphi_{u,n}^k + (\hat{d}_{u,n})^{-\lambda} \hat{\varphi}_{u,n} \ddot{\varphi}_{u,n}^2] \tag{A.4}$$

Equation (A.4) leads to the total co-channel interference term (13) at $n$-th RAU on the reference floor.

# Appendix B

# Generation of Rayleigh and Nakagami Random Variables

This appendix discusses the generation of random variables based on Rayleigh and Nakagami distributions associated mainly with Chapter 5.

## B.1 Generation of Independent Rayleigh Random Variables

A complex Rayleigh random variable (RV) $r_v$ can be generated by combining two quadrature identical independently distributed (i.i.d.) Gaussian RVs, namely

$$r_v = R_I + jR_Q \tag{B.1}$$

where $R_I$ and $R_Q$ are independent Gaussian RVs, with a mean of zero and a standard deviation of $\sigma$. The generation of Rayleigh random variables is useful in the modelling of the received signals by each RAU. Rayleigh RVs can be generated in MATLAB using the following codes

$$rv = 1/sqrt(2) * [randn(1, N) + j * randn(1, N)] \tag{B.2}$$

where *randn* generates gaussian random variables with zero mean and variance 1. $N$ denotes the sample size. The factor $1/sqrt(2)$ normalizes the power of $rv$ to unity.

## B.2 Generation of Independent Nakagami Random Variables

In order to generate Nakagami distributed samples, it is useful to note that if a RV $r_v^n$ has a Nakagami distribution with parameters $m$ and $\Omega$, then $(r_v^n)^2$ has a gamma distribution with shape parameter $m$ and scale parameter $\Omega$ [69, pp. 52]. The algorithm adopted in this thesis is based on the Statistics Toolbox of Matlab with a modification based on [101]. The program generates Nakagami random samples based on the Nakagami-$m$ distribution as follows.

$$Y = randraw(distribName, distribParams, sampleSize); \qquad \text{(B.3)}$$

returns array Y of size = sampleSize of random variates from distribName distribution with parameters distribParams. The detailed Matlab code can be found in [102].

USAGE:

$randraw('nakagami', m, sampleSize)$ - generates sampleSize number of variates from the Nakagami distribution with shape parameter $m$ and spread parameter $\Omega = 1$;

$randraw('nakagami', [m, \Omega], sampleSize)$ - generates sampleSize number of variates from the Nakagami distribution with shape parameter $m$ and spread parameter $\Omega$;

$randraw('nakagami')$ - returns help for the Nakagami distribution.

EXAMPLES:

1. y = randraw('nakagami', 1.1, [1 1e5]);

2. y = randraw('nakagami', [0.6, 2], 1, 1e5);

3. y = randraw('nakagami', [3, 2.5], 1e5 );

The RVs are then superimposed on other in-building propagation parameters to model the received signal by each RAU as discussed in Chapter 5.

# References

[1] "Worldwide Mobile Market Forecasts: 2009-2013," Portio Research, 2009.

[2] "Cisco Visual Networking Index: Global Mobile," Data Traffic Forecast Update, 2010-2015.

[3] A. U. H. Sheikh, *Wireless Communications: Theory and Techniques*. Boston: Kluwer Academics Publishers, 2004.

[4] A. Goldsmith, *Wireless Communications*. New York: Cambridge University Press, 2005.

[5] J. Wang, *High-speed Wireless Communications*: Ultra-wideband, 3G Long Term Evolution, and 4G Mobile Systems. Cambridge University Press, 2008.

[6] C. Qunhui, "Evolution and deployment of LTE," *Huawei Coomunicate*, issue 61, pp. 51-55, Sept. 2011.

[7] J. Gozalvez, "First commercial LTE network [Mobile Radio]," *IEEE Veh. Technol. Mag.*, vol. 5, no. 2, pp. 8-16, Jun. 2010.

[8] B. O'Hara and A. Petrick, *The IEEE 802.11 handbook: a designer's companion*. New York: IEEE, 2nd edition, 2005.

[9] S. R. Saunders, S. Carlaw, A. Giustina, R. R. Bhat, V. S. Rao, and R. Siegberg, *Femtocells: Opportunities and Challenges for Business and Technology*. John Wiley and Sons Ltd, 2009.

126

[10] F. Adachi, K. Takeda, T. Yamamoto, and R. Matsukawa, "Gigabit distributed antenna network and its related wireless techniques," *proc. 7th international Wireless Commun. and Mobile Compu. Conf.*, pp. 1550-1556, August 2011.

[11] S. Scheinert. (2006) Wireless Net DesignLine - In-building cellular: Why it is a Wi-Fi alternative. [Online]. Available: http://www.wirelessnetdesignline.com/howto/wlan/192701513.

[12] H. Claussen, L. T. W. Ho, and L. G Samuel, "An overview of the femtocell concept," *Bell Labs Tech. J.*, 13:1 (2008), pp. 221 - 245.

[13] S. W. Peters and R. W. Heath, Jr., "The future of WiMAX: Multihop relaying with IEEE 802.16j," *IEEE Commun. Mag.*, vol. 47, no. 1, pp. 104-111, January 2009.

[14] Y. Liang and V. V. Veeravalli, "Cooperative relay broadcast channels," *IEEE Trans. Info. Theory.* vol. 53, no. 3, pp. 900-928, Mar.2007.

[15] B. Lin, Pin-Han Ho, L. L. Xie, and X. Shen, "Optimal relay station placement in IEEE 802.16j networks," *proc. int. conf. on Wireless Commun. and Mobile Comput..*, pp. 25-30, 2007.

[16] O. Oyman, J. N. Laneman, and S. Sandhu, "Multihop relaying for broadband wireless mesh networks: From theory to practice," *IEEE Commun. Mag.*, vol. 45, no. 11, pp. 116-122, Nov. 2007.

[17] H. Zhu, "Performance comparison between distributed antenna and microcellular systems," *IEEE J. Select Areas Commun.*, vol. 29, no. 6, pp. 1151-1163, June 2011.

[18] R. Coombs and R. Steele, "Introducing microcells into macrocellular networks: A Case Study," *IEEE Trans. Commun.*, vol. 47, no. 4, pp. 568-576, April. 1999.

[19] Chih-Lin I, L. J. Greenstein, and R. D. Gitlin, "A microcell/macrocell cellular architecture for low and high-mobility wireless users," *IEEE J. Select Areas Commun.*, vol. 11, no. 6, pp. 885-891, August 1993.

[20] M. V. Clark, V. Erceg and L. J. Greenstein, "Reuse efficiency in urban microcellular networks ," *IEEE Trans. Veh. Tech.*, vol. 46, no. 2, pp. 279-288, May 1997.

[21] W. Choi and J. G. Andrews, "Downlink performance and capacity of distributed antenna systems in a multicell environment," *IEEE Trans. Wireless Commun.*, vol. 6, no. 1, pp. 69-73, Jan. 2007.

[22] A. Saleh, A. Rustako, and R. Roman, "Distributed antennas for indoor radio communications," *IEEE Trans. Commun.*, vol. 35, no. 12, pp. 1245-1251, Dec. 1987.

[23] J. Park, E. Song, and W. Sung, "Capacity analysis for distributed antenna system using cooperative transmission schemes in fading channels," *IEEE Trans. Wireless Commun.*, vol. vol.8, no. 2, pp. 586-592, Feb. 2009.

[24] A. C. M. Austin, M. J. Neve, and G. B. Rowe, "Modelling inter-floor radio-wave propagation in office buildings," *proc. IEEE APS/URSI Int. Symp.*, 2008, pp. 392-395.

[25] V. Chandrasekhar et al., "Femtocell Networks: a Survey," *IEEE Commun. Mag.*, vol. 46, no. 9 pp. 59-67, Sept. 2008.

[26] R. Janaswamy, *Radiowave propagation and smart antennas for wireless communications*, ser. Kluwer international series in engineering and computer science; SECS 599. Boston: Kluwer Academic Publishers, 2001.

[27] R. Vaughan and J. Bach Andersen, *Channels, propagation and antennas for mobile communications*, ser. IEE electromagnetic waves; no. 50. London: Institution of Electrical Engineers, 2003.

[28] W. Stallings, *Wireless Communications and Networks*, 2nd ed. Upper Saddle River, NJ: Pearson Prentice Hall, 2005.

[29] J. Weitzen and T. Grosch, "Comparing coverage quality for femtocell and macrocell broadband data services," *IEEE Commun. Mag.*, vol. 48, no. 1, pp. 40Ũ44, Jan. 2010.

[30] J. D. Parsons, *The Mobile Radio Propagation Channel*, 2nd ed. Chichester, New York: J. Wiley, 2000.

[31] J. B. Andersen, T. S. Rappaport, and S. Yoshida, "Propagation measurements and models for wireless communications channels," *IEEE Commun. Mag.*, vol. 33, no. 1, pp. 42-49, 1995.

[32] S. Armour, A. Doufexi, B.-S. Lee, A. Nix, and D. Bull, "The impact of power limitations and adjacent residence interference on the performance of WLANs for home networking applications," *IEEE Trans. Consumer Electron.*, vol. 47, no. 3, pp. 501-511, August 2001.

[33] S. Y. Seidel and T. S. Rappaport, "Site-specific propagation prediction for wireless inbuilding personal communication system design," *IEEE Trans. Veh. Technol.*, vol. 43, no. 4, pp. 879-891, Nov. 1994.

[34] D. W. Browne, J. Medbo, H. Asplund, and J.-E. Berg, "A simple approach to site sensitive modeling of indoor radio propagation," *Proc. IEEE Veh. Technol. Soc. Conf.* (VTC '02 (Spring)), vol. 1, pp. 384-388, May 2002.

[35] R. A. Valenza, "A ray tracing approach to predicting indoor wireless transmission," in *Proc. 43rd Veh. Technol. Conf.*, pp. 214-218, 1993.

[36] T. S. Rappaport, *Wireless Communications: Principles and Practice.* Upper Saddle, River, N.J.: Prentice Hall PTR, 1996.

[37] M. Nakagami, *The m-distribution: A general formula of intensity distribution of rapid fading,* in Statistical Methods in Radio Wave Propagation, W. C. Hoffman, Ed. New York: Pergamon, 1960.

[38] R. Ganesh, K. Pahlavan, and Z. Zvonar, *Wireless Network Technologies.* Kluwer Academic Publishers, 2000.

[39] U. Dersch, J. Troger, and E. Zollinger, "Multiple reflections of radio wavs in a corridor," *IEEE Trans. Antennas Propag.*, vol. 42, no. 9, pp. 1571-1574, Sep. 1994.

[40] S. E. Alexander, "Characterising buildings for propagation at 900 MHz," *Electron. Lett.*, vol. 19, no. 20, p. 860, Sep. 1983.

[41] M. Thiel and K. Sarabandi, "3D-wave propagation analysis of indoor wireless channels utilizing hybrid methods," *IEEE Trans. Antennas Propag.*, vol. 57, no. 5, pp. 1539-1546, May 2009.

[42] D. Cox, R. Murray, and A. Norris, "800 MHz attenuation measured in and around suburban houses," AT&T Bell Laboratories Technical J., vol. 673, no. 6, pp. 921-954, 1984.

[43] H. Hashemi, "The indoor radio propagation channel," *Proc. IEEE*, vol. 81, no. 7, pp. 943-968, 1993.

[44] S.Y. Seidel and Rappaport, T.S., "Path loss prediction in multifloored buildings at 914MHz," *Electron. Lett.*, Vol. 27, No. 15, pp. 1384-1387, Jul. 1991.

[45] A. J. Motley and J. M. P. Keenan, "Personal communication radio coverage in buildings at 900 MHz and 1700 MHz," *Electron. Lett.*, vol. 24, no. 12, pp. 763-764, 9 June 1988.

[46] J. F. LaFortune and M. Lecours, "Measurement and modeling of propagation losses in a building at 900 MHz," *IEEE Trans. Veh. Technol.*, vol. 39, no. 2, pp. 101-108, May 1990.

[47] W. Honcharenko, H. L. Bertoni, and J. Dailing, "Mechanisms governing propagation between different floors in buildings," *IEEE Trans. Antennas Propag.*, vol. 41, no. 6, pp. 787-790, June 1993.

[48] H.L. Bertoni, *Radio Propagation for Modern Wireless Systems*, Prentice Hall PTR, New Jersey, 2000.

[49] S. Y. Seidel and T. S. Rappaport, "914MHz path loss prediction models for indoor wireless communications in multifloored buildings," *IEEE Trans. Antennas Propag.*, vol. 40, no. 2, pp. 207-217, Feb. 1992.

[50] M. F. Iskander and Z. Yun, "Propagation prediction models for wireless communication systems," *IEEE Trans. Microwave Theory Tech.*, vol. 50, no. 3, pp. 662-673, Mar. 2002.

[51] S. Seidel, T. S. Rappaport, J. Feuerstein, and K. L. Blackard, "The impact of surrounding buildings on propagation for wireless in-building personal communications system design," *in Proc. 42nd IEEE Veh. Technol. Conf.*, vol. 2, pp. 814-818, Denver, Colorado, USA, May 10-13, 1992.

[52] K. W. Cheung, J. H. M. Sau, and R. D. Murch, "A new empirical model for indoor propagation prediction," *IEEE Trans. Veh. Technol.*, vol. 47, no. 3, pp. 996-1001, Aug. 1998.

[53] Recom. ITU-R P.1238-6, "Propagation data and prediction methods for the planning of indoor radiocommunication systems and radio local area networks in the frequency range 900 MHz to 100 GHz," 2009.

[54] A. C. M. Austin, M. J. Neve, G. B. Rowe, and R. J. Pirkl, "Modeling the effects of nearby buildings on inter-floor radio-wave propagation," *IEEE Trans. Antennas Propag.*, vol. 57, no. 7, pp. 2155-2161, July 2009.

[55] D. Astely, E. Dahlman, A. Furuskllr, Y. Jading, M. lindstrom, and S. Parkvall, "LTE: The evolution of mobile broadband," *IEEE Commun. Mag.*, vol. 47, No. 4, pp. 44-51, April 2009.

[56] ITU, D. Astely, E. Dahlman, A. Furuskllr, Y. Jading, M. lindstrom, and S. Parkvall, "LTE: The evolution of mobile broadband," *IEEE Commun. Mag.*, vol. 47, No. 4, pp. 44-51, April 2009.

[57] F. Adachi, P. Wei, T. Obara, T. Yamamoto, R. Matsukawa, M. Nakada, "Distributed antenna network for gigabit wireless access," *IEEE 54th Inter. Midwest Symp. Circuits and Systems.*, pp. 1-4, Aug. 2011.

[58] L. Dai, S. Zhou, and Y. Yao, "Capacity analysis in CDMA distributed antenna systems," *IEEE Trans. Wireless Commun.*, vol. 4, no. 6, pp. 2613-2620, Nov. 2005.

[59] J. Zhang and J. G. Andrews, "Distributed antenna aystems with randomness," *IEEE Trans. Wireless Commun.*, vol. 7, no. 9, pp. 3636-3646, Sept. 2008.

[60] X. You et al., "Cell edge performance of cellular mobile systems," *IEEE J. Select Areas Commun*, vol. 29, no. 6, pp. 1139-1150, June 2011.

[61] A. Obaid and H. Yanikomeroglu, "Reverse-link power control in CDMA distributed antenna systems," *in Proc. of IEEE Wireless Communs and Net. Conf.*(WCNC), 2000.

[62] G. L. Stuber, *Principles of Mobile Communication*, 2nd ed. Boston: Kluwer Academic Publishers, 2001.

[63] S. Y. Tan, M. Y. Tan, and H. S. Tan, "Multipath delay measurements and modeling for interfloor wireless communications," *IEEE Trans. Veh. Technol.*, vol. 49, no. 4, pp. 1334-1341, July 2000.

[64] H. Claussen, L. T. W. Ho, and L. G. Samuel, "Self-optimization of coverage for femtocell deployments," *Proc., IEEE Wireless Telecomm. Symp.*, pp. 278-285, April 2008.

[65] T. Alade, O.Hassan, H.Zhu, J.Wang, "Performance Evaluation of In-Building DAS for High Data Rate Wireless Transmission,", *Submitted, IEEE, Trans. on Wireless Comm.*, 2011.

[66] D. M. Dobkin, *RF Engineering for Wireless Networks, Hardware, Antennas, and Propagation*, UK: Elsevier, 2005.

[67] H. Zhu and J. Wang "Chunk-based resource allocation in OFDMA systems - part I: chunk allocation," *IEEE Trans. Commun*, vol. 57, no. 9, pp. 2734-2744, Sept 2009.

[68] A.M.D. Turkmani, "Radio transmission at 1800MHz into, and within, multistory buildings," *IEEE Proc. Commun., Speech and Vision, Pt. I*, vol. 138, No. 6, pp. 577-584, Dec. 1991.

[69] J.G. Proakis, M.Salehi, *Digital Communications* Fifth Edition, McGraw-Hill International Edition, 2008.

[70] R. K. Morrow and K. S. Lehnert, "Bit-to-bit error dependence in slotted DS/SSMA packet systems with random signature sequences," *IEEE Trans. Commun.*, vol. 37, no. 10, pp. 1052-1061, 1989.

[71] M. K. Simon and M.S. Alouini, *Digital Communication Over Fading Channels*: A Unified Approach to Performance Analysis. New York: Wiley, 2000.

[72] V. Aalo and J. Zhang, "Average error probability of optimum combining with a co-channel interferer in nakagami fading," *IEEE Wireless Commun. and Netw. Conf.*, vol. 1, pp. 376-381, July 2000.

[73] G. Efthymoglou and V. Aalo, "Performance of RAKE receivers in Nakagami fading channel with arbitrary fading parameters," *IEEE Electronic Lett.*, vol.31, No.18, pp. 1610-1612, Aug. 1995.

[74] A.J. Goldsmith and S.G Chua, "Variable-Rate Variable-Power M-QAM for Fading Channels," *IEEE Trans. Commun.*, vol. 2, COM-45, pp. 1218-1230, 1997.

[75] H. Matsuoka, S.Sampei, N. Morinaga and Y. Kamio, "Adaptive Modulation System with Variable Coding Rate Concatenated Code for High Quality Multi-Media Communication Systems," *Proc. IEEE Veh. Technol. Conf. VTC '96*, Atlanta, GA, pp. 487-491, April 1996.

[76] A. Goldsmith, "Variable-Rate Coded M-QAM for Fading Channels," *Proc. Commun. Theo. Mini Conf. (CTMC-III)in conj. with IEEE Global Commun. Conf. GLOBECOM '94*, San Francisco, CA, pp. 186-190, Nov. 1994.

[77] M. S. Alouini and A. J. Goldsmith, "Adaptive modulation over Nakagami fading channels," *Wireless Pers. Commun.*, vol. 13, pp. 119-143, May 2000.

[78] J.Wang and L. B. Milstein, "Approximate interference of a microcellular spread spectrum system," *Electronics Letters*, vol. 31, no. 20, pp. 1782-1783, Sept. 1995.

[79] A. Annamalai, C. Tellambura and Vijay K. Bhargava, "A General Method for Calculating Error Probabilities Over Fading Channels," *IEEE Trans. Commun.*, vol. 53, No. 5, pp. 841-852, May 2005.

[80] M. K. Simon and M.S. Alouini, "A unified approach to the probability of error for noncoherent and differentially coherent modulations over generalized fading channels," *IEEE Trans. Commun.*, vol. 46, no. 12, pp. 1625-1638, Dec. 1998.

[81] A. Annamalai, C. Tellambura, V.K Bhargava, "A simple and accurate analysis of digital communication systems with diversity reception in different fading environments," *IEEE Inter. Sympo. Personal indoor & Mobile Com.* Sept. 1998.

[82] A. Annamalai, and V.K Bhargava, "A reduced-complexity rake receiver structure for high-speed indoor wireless communication," *Globacom Telecom. Conf.* vol. 1, pp. 253-258, 1998.

[83] R. Wilson, J. A. Crawford, "Propagation Losses Through Common Building Materials," Magis Networks, Inc., Aug. 2002.

[84] G. Boudreau, J. Panicker, N. Guo, R. Chang, N. Wang, and S. Vrzic, "Interference Coordination and Cancellation for 4G Networks," *IEEE Commun. Mag.*, vol. 47, no. 4, pp. 74-81, April 2009.

[85] J. G. Andrews. et al., "Interference cancellation for cellular systems: a contemporary overview," *IEEE Wireless Commun.*, vol. 12, no. 2, pp. 19-29, April 2005.

[86] J. G. Andrews. et al., "Overcoming Interference in Spatial Multiplexing MIMO Cellular networks," *IEEE Trans. Wireless Commun.*, vol. 14, no. 6, pp. 95-104, Dec. 2007.

[87] A. M. Rabiei and N. C. Beaulieu, "Cochannel interference mitigation using whitening receiver designs in bandlimited microcellular wireless systems," *IEEE Trans. Wireless Commun.*, vol. 8, no. 3, pp. 1284-1294, March 2009.

[88] X. Huang and H. Wu, "Robust and Efficient Intercarrier Interference Mitigation for OFDM Systems in Time-Varying Fading Channels," *IEEE Trans. Veh. Tech.*, vol. 56, no. 5, pp. 2517-2528, Sept. 2007.

[89] R. Giuliano et al. "WiMAX fractional frequency reuse for rural environments," *IEEE Wireless Commun.*, vol. 15, no. 3, pp. 60-65, June 2008.

[90] A. L. Stolyar and H. Viswanathan, "Self-Organizing Dynamic Fractional Frequency Reuse in OFDMA Systems," INFOCOM 2008. The 27th Conf. Computer Commun. IEEE, pp. 691-699, April 2008.

[91] H. Nguyen, K. Tran, N. Agoulmine, "Impact of Interference on the System Performance of WiMAX Relay 802.16j with Sectoring ," *IEEE ICC '11*, pp. 1-5, June, 2011.

[92] J. Zhang et al., "An efficient algorithm for adaptive cell sectoring in CDMA systems," *IEEE ICC '03*, vol. 2, pp. 1238-1242, May, 2003.

[93] C. U. Saraydar and A. Yener, "Adaptive cell sectorization for CDMA systems," *IEEE JSAC*, vol. 19, no. 6, pp. 1041-1051, June 2001.

[94] W. Choi and J. G. Andrews, "Spatial Multiplexing in Cellular MIMO-CDMA Systems with Linear Receivers: Outage Probability and Capacity," *IEEE Trans. Wireless Commun.*, vol. 4, no. 7, pp. 2612-2621, July 2007.

[95] S. Khattak, W. Rave and G. Fettweis, "Multiuser Turbo Detection in Distributed Antenna System," *15th IST Mobile and Wireless Comm.* Summit, Jun 2006.

[96] A. Sklavos, T. Weber, "Interference suppression in multi-user OFDM systems by antenna diversity and joint detection," *in COST 273 TD(01)020*, Bologna, Oct. 2001.

[97] S. Khattak, G. Fettweis, "Low Backhaul Distributed Detection Strategies for an Interference Limited Uplink Cellular System," *Proc. IEEE Veh. Technol. Conf. VTC Spring, '08*, pp. 693-697, May 2008.

[98] W. Honcharenko, H. L. Bertoni, J. L. Dailing, J. Qian, and H. D. Yee, "Mechanisms governing UHF propagation on single floors in modern office buildings," *IEEE Trans. Veh. Technol.*, vol. 41, no. 4, pp. 496-504, Nov. 1992.

[99] J. Andersen, T. S. Rappaport, and S. Yoshida, "Propagation Measurements and Models for Wireless Communications Channels," *IEEE Commun. Mag.*, vol. 33, no. 1, pp. 42-49, Jan. 1995.

[100] M. A. Panjwani, A. L. Abbott, and T. S. Rappaport, "Interactive computation of coverage regions for wireless communication in multifloored indoor environments," *IEEE J. Select. Areas Commun.*, vol. 14, pp. 420-430, Apr. 1996.

[101] MATLAB CENTRAL, "http://www.mathworks.com/matlabcentral/fileexchange/7309"

[102] MATLAB CENTRAL, "http://www.mathworks.com/matlabcentral/fileexchange/7309-randraw/content/randraw.m"